Nonadiabatic Quantum Molecular Dynamics

Aiichiro Nakano

Collaboratory for Advanced Computing & Simulations
Department of Computer Science
Department of Physics & Astronomy
Department of Quantitative & Computational Biology
University of Southern California

Email: anakano@usc.edu

I. NAQMD Basics

Nonadiabatic Quantum Molecular Dynamics

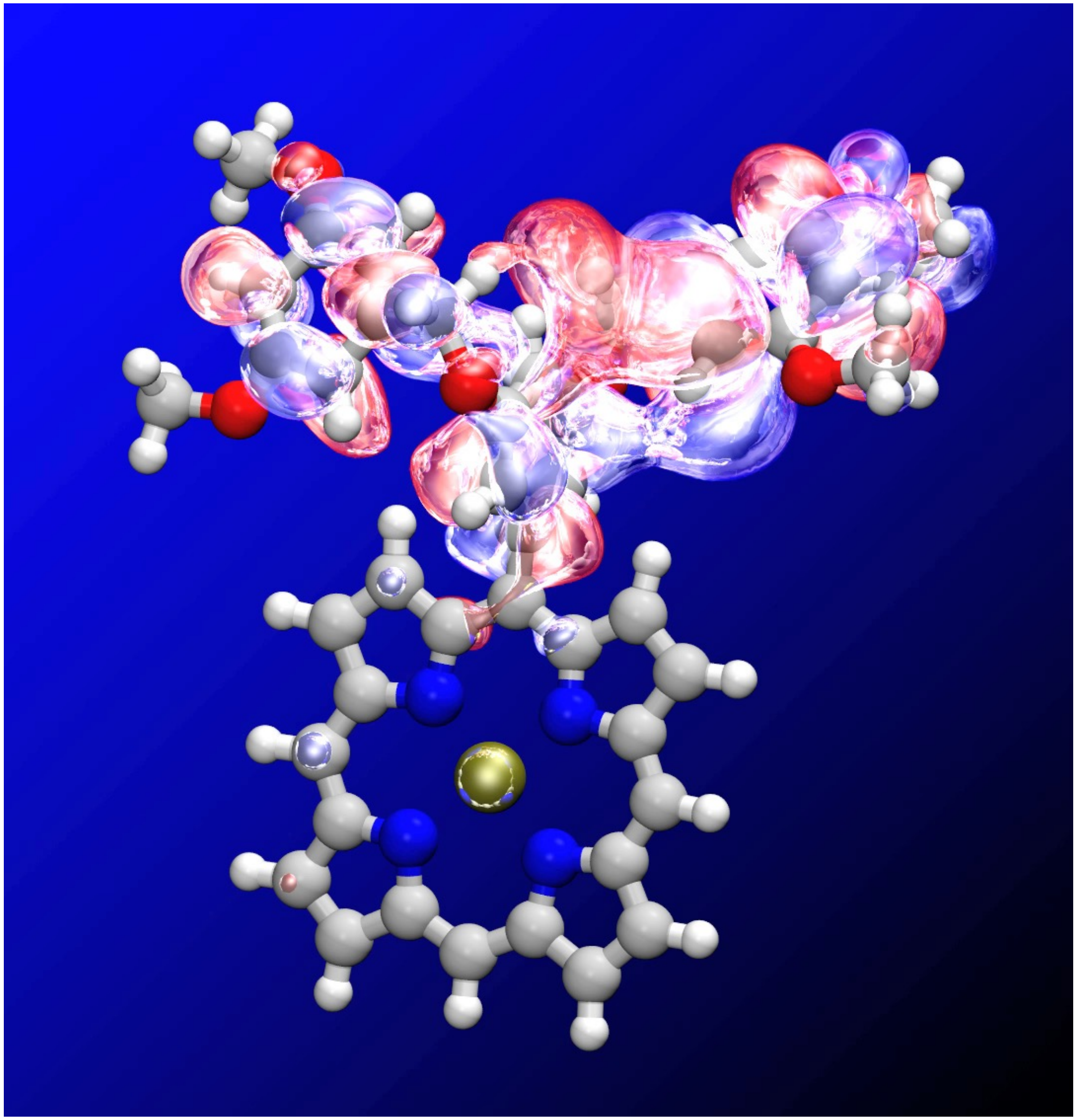

Appl. Phys. Lett. **98**, 113302 (’11); *ibid*. **100**, 203306 (’12); *ibid*. **102**, 173301 (’13); *Comput. Phys. Commun*. **184**, 1 (’13); *J. Chem. Phys*. **140**, 18A529 (’14); *IEEE Computer* **48(11)**, 33 (’15); *Sci. Rep*. **5**, 19599 (’16); *Nature Commun*. **8**, 1745 (’17); *Nano Lett*. **18**, 4653 (’18); *Nature Photon*. **13**, 425 (’19); *Science Adv*. **8**, eabk2625 (‘22)

Zn porphyrin

Rubrene/C$_{60}$

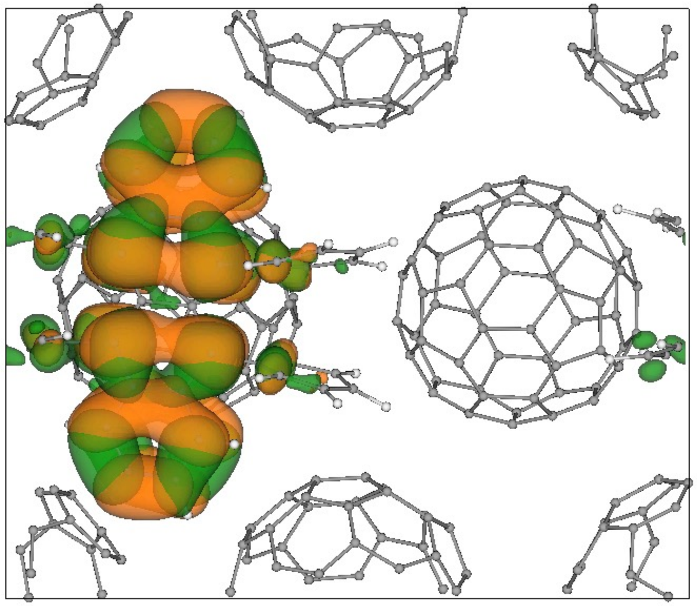

quasi-electron; quasi-hole

- **Excited states: Linear-response time-dependent density functional theory** [Casida, ’95]
- **Interstate transitions: Surface hopping** [Tully, ’90; Jaeger, Fisher & Prezhdo, ’12]

Time-Dependent Density Functional Theory

- **Invertibility theorem**

  The mapping $G: \{v(\mathbf{r},t) + c(t)\} \mapsto n(\mathbf{r},t)$ is one-to-one & therefore is invertible

  external potential　　time-dependent constant　　electron density

- **Time-dependent density-functional theory (TDDFT) theorem:**

  Every physical quantity is a functional of $n(\mathbf{r},t)$

- **Action principle:**

  Action integral is stationary at the exact density:

  $\delta A_v / \delta n(\mathbf{r},t) = 0$ at $n(\mathbf{r},t) = G[v(\mathbf{r},t)]$, where

  $A_v[n(\mathbf{r},t)] = \int dt \langle \psi(t) | i\hbar\, \partial/\partial t - T - U | \psi(t) \rangle - \int dt \int d\mathbf{r} n(\mathbf{r},t) v(\mathbf{r},t)$

  kinetic energy operator　　electron-electron interaction

Runge & Gross, *Phys. Rev. Lett*. **52**, 997 ('84); Ng. & Singwi, *ibid*. **59**, 2627 ('87)

Time-Dependent Kohn-Sham Scheme

- **Time-dependent many-body problem is equivalent to solving time-dependent Kohn-Sham (TDKS) equations**

Hartree (mean-field) potential

$$\begin{cases} \left[i\hbar\,\partial/\partial t + \hbar^2\nabla^2/2m - v(\mathbf{r},t) - \int d\mathbf{r}'\,\frac{e^2 n(\mathbf{r}',t)}{|\mathbf{r}-\mathbf{r}'|} - v_{\mathrm{xc}}(\mathbf{r},t)\right]\psi_i(\mathbf{r},t) = 0 \\ n(\mathbf{r},t) = \sum_{i=1}^{N}|\psi_i(\mathbf{r},t)|^2 \end{cases}$$

where the exchange-correlation (xc) potential is given by

$$v_{\mathrm{xc}}(\mathbf{r},t) = \delta A_{\mathrm{xc}}/\delta n(\mathbf{r},t)$$

$$A_{\mathrm{xc}}[n(\mathbf{r},t)] = -\int dt\langle\psi(t)|i\hbar\,\partial/\partial t - T - U|\psi(t)\rangle$$

$$+\int dt\langle\psi(t)|i\hbar\,\partial/\partial t - T|\psi(t)\rangle_{e=0}$$

non-interacting electrons action

$$-\frac{1}{2}\int dt\int d\mathbf{r}\int d\mathbf{r}'\frac{e^2}{|\boldsymbol{r}-\mathbf{r}'|}n(\mathbf{r},t)n(\mathbf{r}',t)$$

Hartree (mean-field) action

Runge & Gross, *Phys. Rev. Lett*. **52**, 997 ('84)

See notes on (1) TDDFT summary, (2) TDDFT fundamentals

TDDFT & Many-Body Theory

- **TDKS orbitals are used as a basis set to calculate physical properties with the help of many-body theory, *e.g.*, GW approximation for one-body** [Hybertsen & Louie, *Phys. Rev. Lett*. **55**, 1418 ('85)] **& Bethe-Salpeter equation (BSE)** [Rohlfing & Louie, *Phys. Rev. Lett*. **81**, 2312 ('98)] **for two-body properties**
- **Many-body theory provides a systematic way to approximate TDKS exchange-correlation (xc) potential** ($1 = (\mathbf{r}_1, t_1)$, *etc*.):

$$v_{\mathrm{xc}}(1) = -2i \int d2 \int d3 \int d4\, \pi^{-1}(1,2) G_0(2,3) \Sigma_{\mathrm{xc}}(3,4) G(4,2)$$

where (p denotes a closed-time path & $\bar{1}$ denotes integration over 1)

$$G(1,1') = -(i/2) \sum_\sigma \langle T_{\mathrm{p}}[\psi_\sigma(1)\psi_\sigma^\dagger(1')] \rangle$$

$$\Sigma_{\mathrm{xc}}(1,1') = -2^{-1} U(1,\bar{2}) \chi^{(2)}(\bar{3},1';\bar{2}^+,\bar{2}) G^{-1}(\bar{3},1')$$

$$U(1,2) = \frac{e^2}{|\mathbf{r}_1 - \mathbf{r}_2|} \delta_{\mathrm{p}}(t_1 - t_2)$$

$$\chi^{(\nu)}(1,1';\ldots;\nu,\nu') = \frac{\delta^{\nu-1}}{\delta\phi(1,1')\cdots\delta\phi(\nu,\nu')} \sum_\sigma \langle T_{\mathrm{p}}[\psi_\sigma(1)\psi_\sigma^\dagger(1')] \rangle$$

$$G_0^{\mathrm{r|a}}(1,1') = \mp i[\theta(t_1 - t_1')|\theta(t_1' - t_1)] \sum_i \psi_i(1)\psi_i^*(1')\,;\, G_0^{\mathrm{c}}(1,1') = -i \sum_i \psi_i(1)\psi_i^*(1')$$

$$\pi_{\mathrm{r}}(1,2) = -2i\hbar^{-1}[G_0^{\mathrm{r}}(1,2)G^{\mathrm{c}}(2,1) + G_0^{\mathrm{c}}(1,2)G^{\mathrm{a}}(2,1)]$$

See note on field-theory of xc potential

Beyond Adiabatic XC Kernel

- **Time-dependence of the exchange-correlation (xc) functional in time-dependent density functional theory (TDDFT) is commonly ignored (adiabatic xc kernel)**
- **Time-dependence like memory effects has been modeled by parametrizing higher-order dynamic correlations in dynamic mean-field theory (DMFT), also incorporating spin-flipping processes**

Acharya *et al*., *Phys. Rev. Lett*. **125**, 017202 ('20); Turkowski & Rahman, *Comput*. **10**, 77 ('22); Suzuki *et al*., *Phys. Rev. A* **101**, 050501(R) ('20)

Laser-pulse demagnetization of Ni

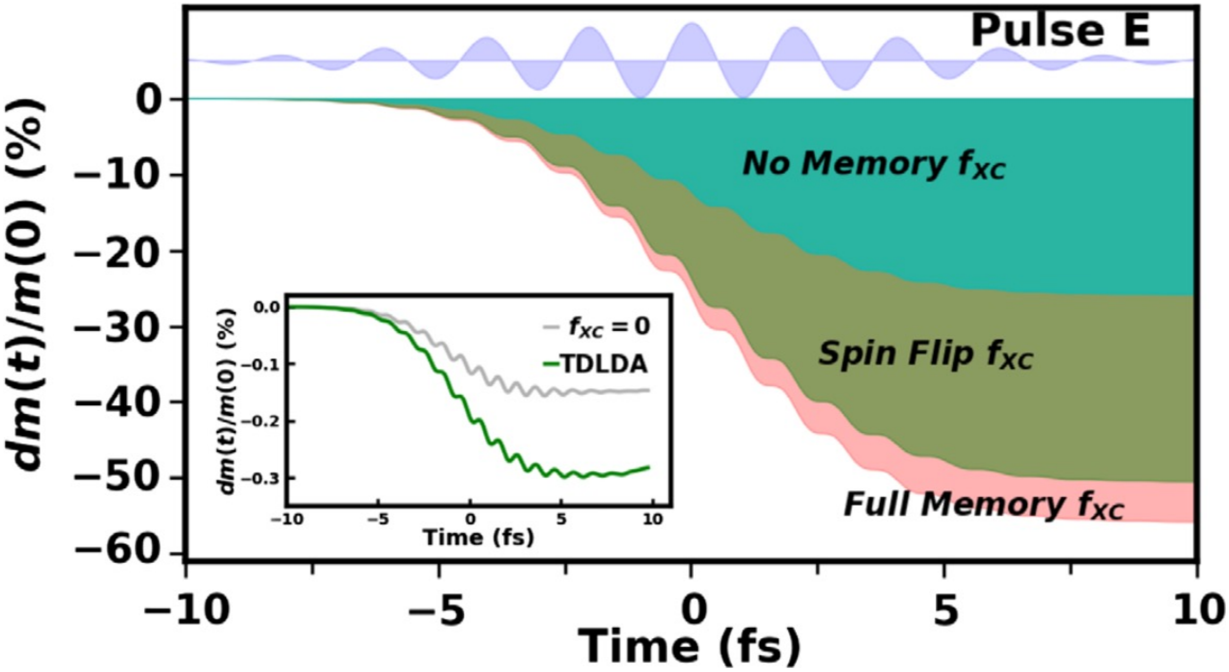

$$\int d\tau\, v_{\mathrm{xc}}(\mathbf{r}, t-\tau)\psi(\mathbf{r},\tau)$$

memory (convolution)

↕ Fourier transform

$$v_{\mathrm{xc}}(\mathbf{r},\omega)\psi(\mathbf{r},\omega)$$

Frequency-dependent product

TDDFT & Physics

- **TDKS equations, even within the random phase approximation (RPA, $v_{xc} = 0$) or static v_{xc}, describe collective effects like screening & plasma oscillation**

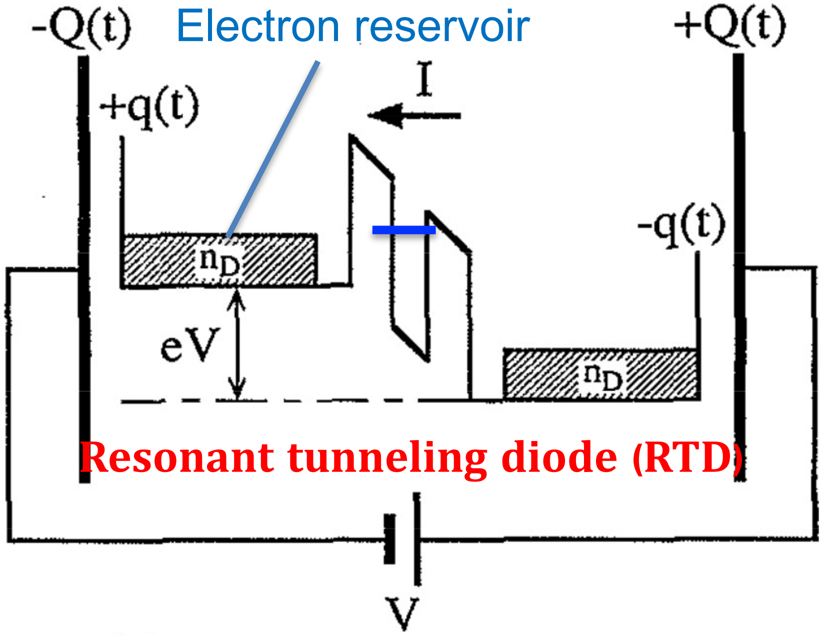
Electron reservoir

Resonant tunneling diode (RTD)

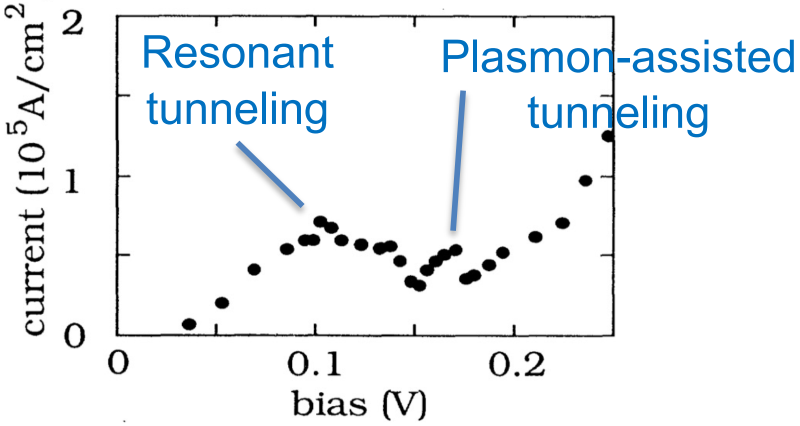
Resonant tunneling

Plasmon-assisted tunneling

Screening (no electric field within electrode)

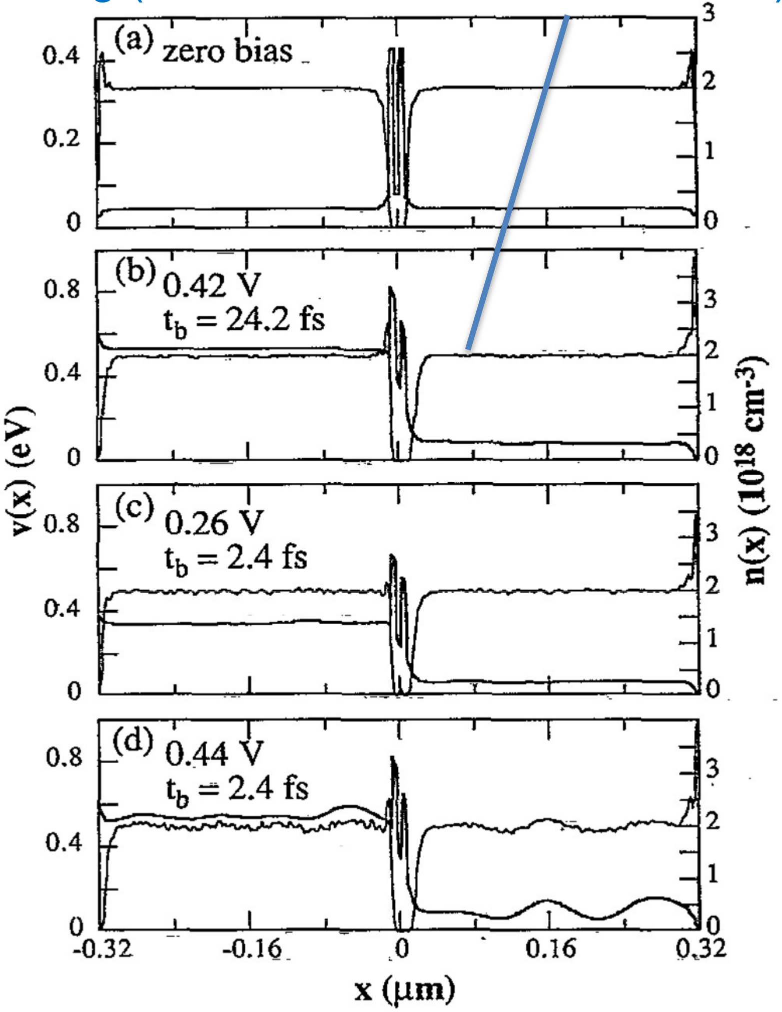

Nakano *et al.*, *Phys. Rev. B* **43**, 9066 ('91); *Appl. Phys. Lett*. **64**, 2569 ('94)

Collective Effects

- **Screening:** In electrons with average number density n, along with uniform positive charge that neutralizes the total electronic charge, the electrostatic potential $\phi(\mathbf{r})$ due to an external point charge Q is obtained (within large n & linearized approximations) as

Fermi energy

$$\phi(\mathbf{r}) = \frac{Q}{r}\exp(-k_{\mathrm{TF}} r)\,;\; k_{\mathrm{TF}} = \left(\frac{6\pi n e^2}{E_{\mathrm{F}}}\right)^{1/2}\;;\; E_{\mathrm{F}} = \frac{\hbar^2}{2m}(3\pi^2 n)^{2/3}$$

Thomas-Fermi wave number

- **Plasma oscillation:** A slab of uniform electron/positive-background can sustain an oscillation with plasma frequency

$$\omega_{\mathrm{p}} = \left(\frac{4\pi n e^2}{m}\right)^{1/2}$$

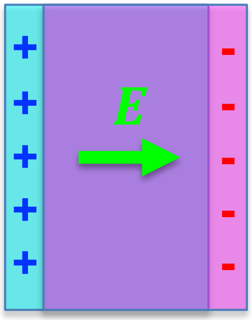

Surface-Hopping NAQMD

- **Incorporate electron transitions with the time-dependent density-functional theory (TDDFT) & surface-hopping method**

Tully, *J. Chem. Phys*. **93**, 1061 ('90), *ibid*. **129**, 044104 ('08) ; Duncan *et al*., *J. Am. Chem. Soc*. **129**, 8528 ('07)

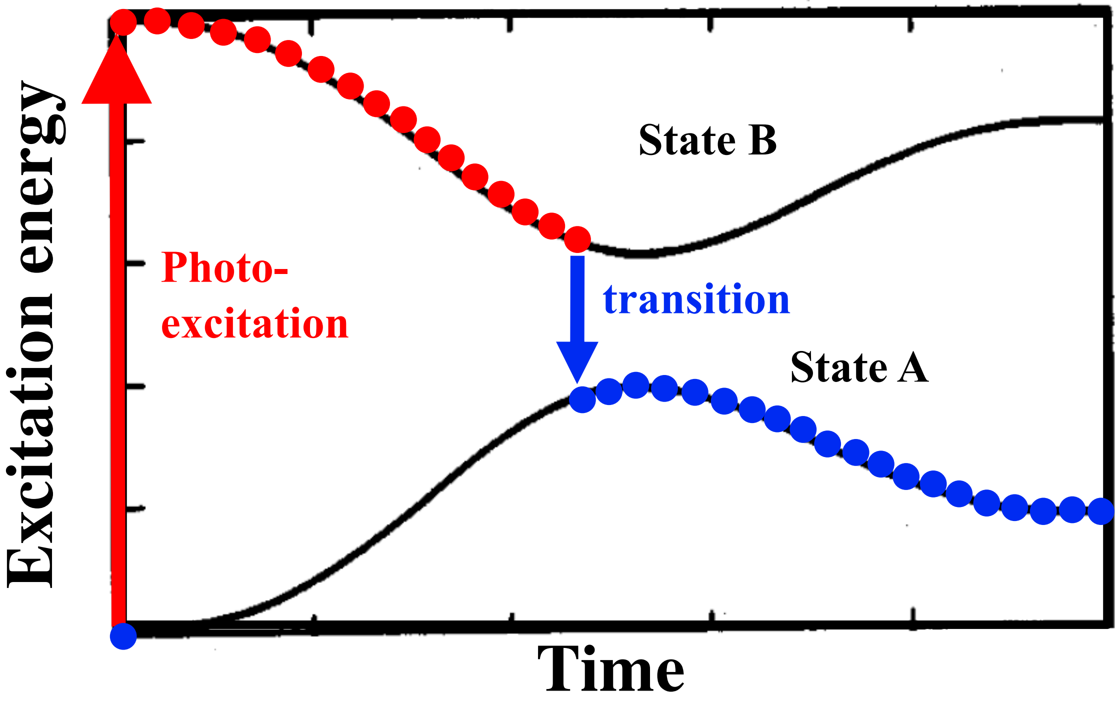

- **Electronic transitions from the current state to another occur stochastically based on the switching probability obtained by solving TDDFT equations**

$$\Psi(\mathbf{r},t) = \sum_J C_J^{(I)}(t)\Phi_J(\mathbf{r};\mathbf{R}(t)) \qquad C_J^{(I)}(0) = \delta_{I,J}$$

$$\frac{d}{dt}C_J^{(I)}(t) = -\sum_k C_k^{(I)}(t)\left(i\omega_K\delta_{JK} + \left\langle \Phi_J \middle| \frac{\partial}{\partial t} \middle| \Phi_K \right\rangle\right)$$

***K*-th excitation frequency**

***J*-th adiabatic excited state**

Electronic transition assisted by nuclei motion

Surface-Hopping Procedure

- **Density matrix $a_{kl}(t)$ & state probability $p_k(t)$**

  $$a_{kl}(t) \equiv c_k(t)c_l^*(t);\ p_k(t) \equiv a_{kk}(t) = |c_k\ (t)|^2$$

- **Probability dynamics**

  $$\frac{d}{dt}p_k(t) = \sum_{k'(\neq k)} b_{kk'}$$

  Nonadiabatic coupling

  $$b_{kk'} = 2\frac{d\mathbf{R}}{dt} \bullet \mathrm{Re}(\mathbf{d}_{kk'} \bullet a_{k'k});\ \mathbf{d}_{kk'} = \left\langle \psi_k \middle| \frac{\partial}{\partial \mathbf{R}} \middle| \psi_l \right\rangle$$

- **Fewest-switches surface hopping (FSSH) algorithm**

  During one NAQMD step (Δt), stochastically choose a state transition according to the transition probability matrix

  $$\pi_{k' \leftarrow k} = \frac{\Delta t b_{k'k}}{p_k} = 2\Delta t \boxed{\frac{d\mathbf{R}}{dt}} \bullet \frac{\mathrm{Re}(\boxed{\mathbf{d}_{kk'}} \bullet a_{k'k})}{a_{kk}}$$

- **From a swarm of independent classical trajectories toward a quantum-mechanical description of nuclei motion**

  DISH: Jaeger *et al*., *J. Chem. Phys*. **137**, 22A545 ('12) — implemented in QXMD; SQUASH: Akimov & Prezhdo, *Phys. Rev. Lett*. **113**, 153003 ('14): Liouville space hopping: Wang *et al*., *J. Phys. Chem. Lett*. **6**, 3827 ('15)

See note on fewest-switch surface hopping

Excited-State Forces

- **Electronic excitations modify the energy landscape for atoms**
- **QXMD code employs a non self-consistent, perturbative scheme inspired by the Harris-Foulkes functional** [Harris, *Phys. Rev. B* **31**, 1770 ('85); Foulkes & Haydock, *Phys. Rev. B* **39**, 12520 ('89)] **to efficiently compute excited-state forces**

Shimojo *et al*., *Comput. Phys. Commun*. **184**, 1 ('13); *J. Chem. Phys*. **140**, 18A529 ('14)

See also Torralba *et al*., *J. Chem. Theory Comput*. **5**, 1499 ('09)

II. NAQMD Applications

- Photovoltaics: photocarrier, charge transfer, charge recombination, singlet fission
- Dielectric breakdown of polymers: hot-carrier dynamics & chemistry
- Photoinduced phase transition & quantum matter
- Optoelectronics
- Laser-driven photochemistry

Example: Light Harvesting Dendrimers

Electron-hole pairs photoexcited at peripheral antennas travel to the core

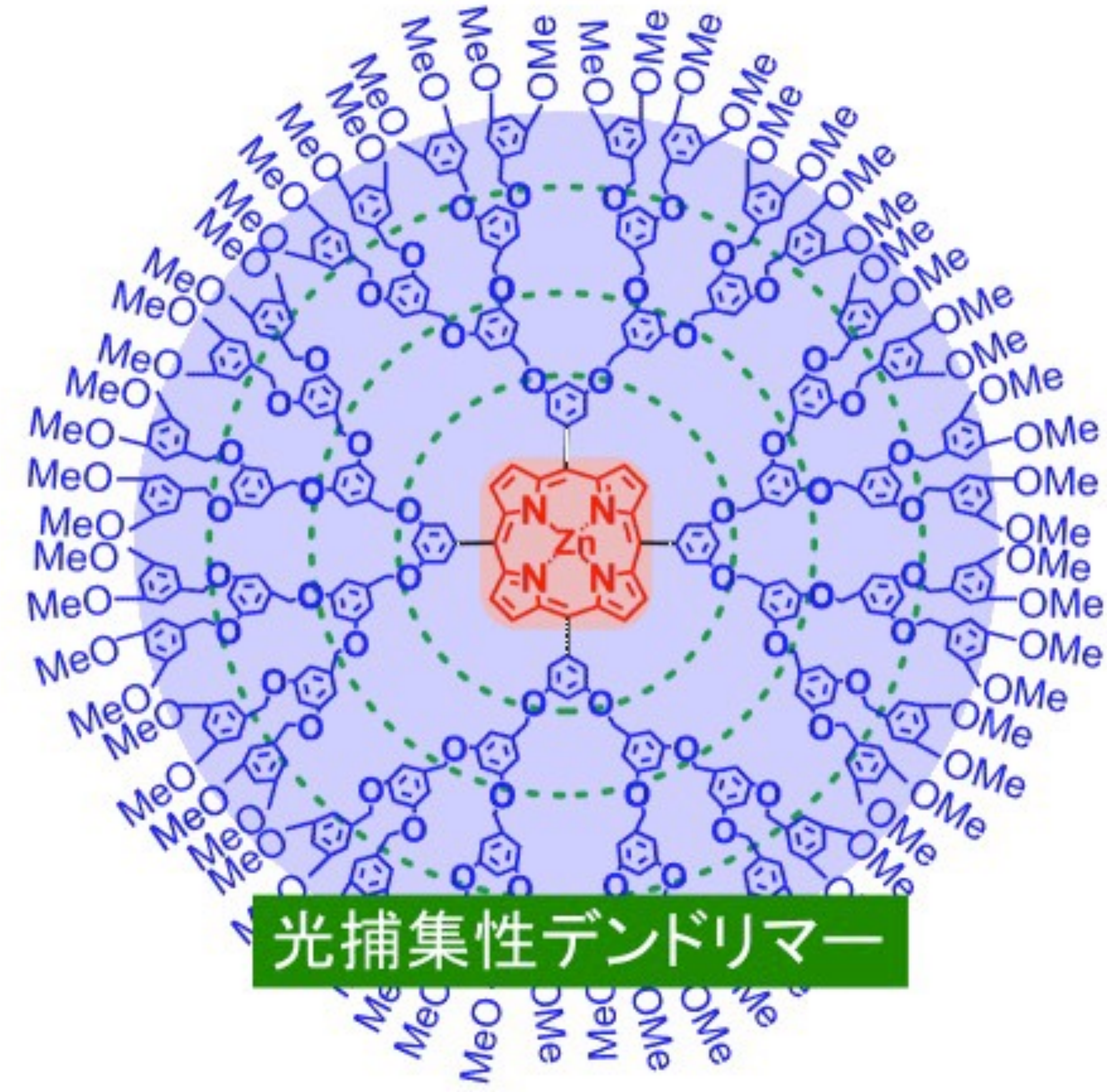

Prof. I. Akai
Kumamoto Univ.

Key: Rapid electron transfer for solar-energy applications

Electron Transfer in a Dendrimer

Nonadiabatic quantum molecular dynamics simulation with fewest-switches surface hopping [Tully, ’90] **& time-dependent density functional theory**

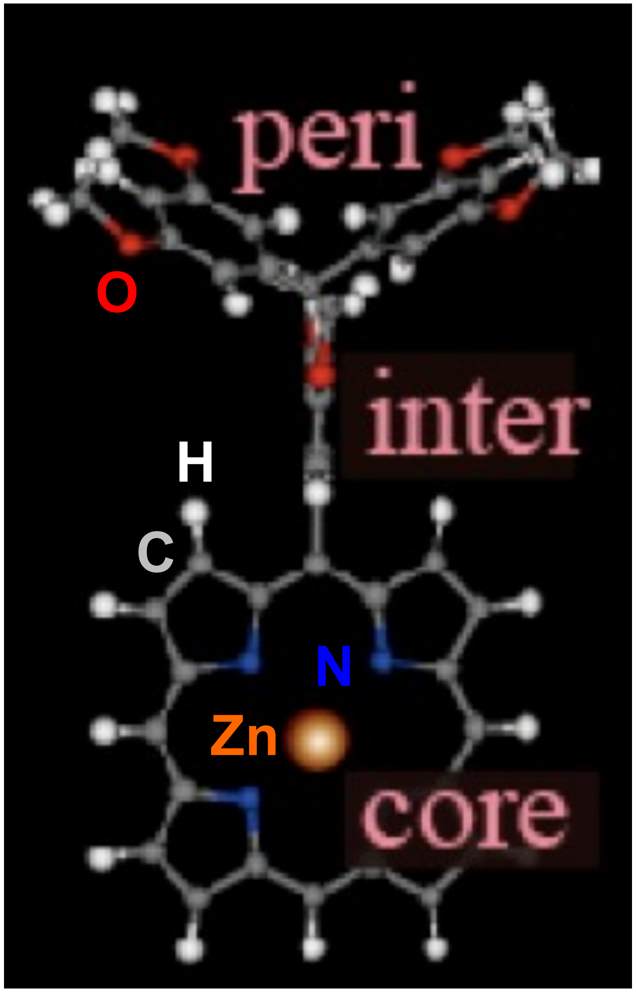

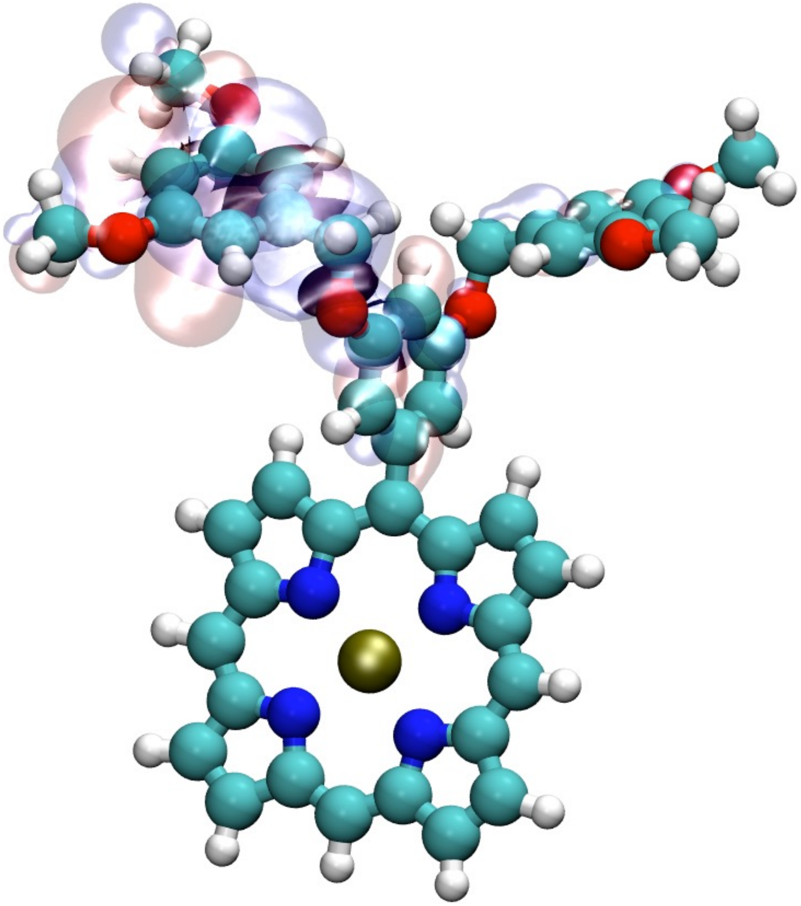

Ohmura *et al.*, *Appl. Phys. Lett*. **98**, 113302 (’11)

Photoexcitation Simulation

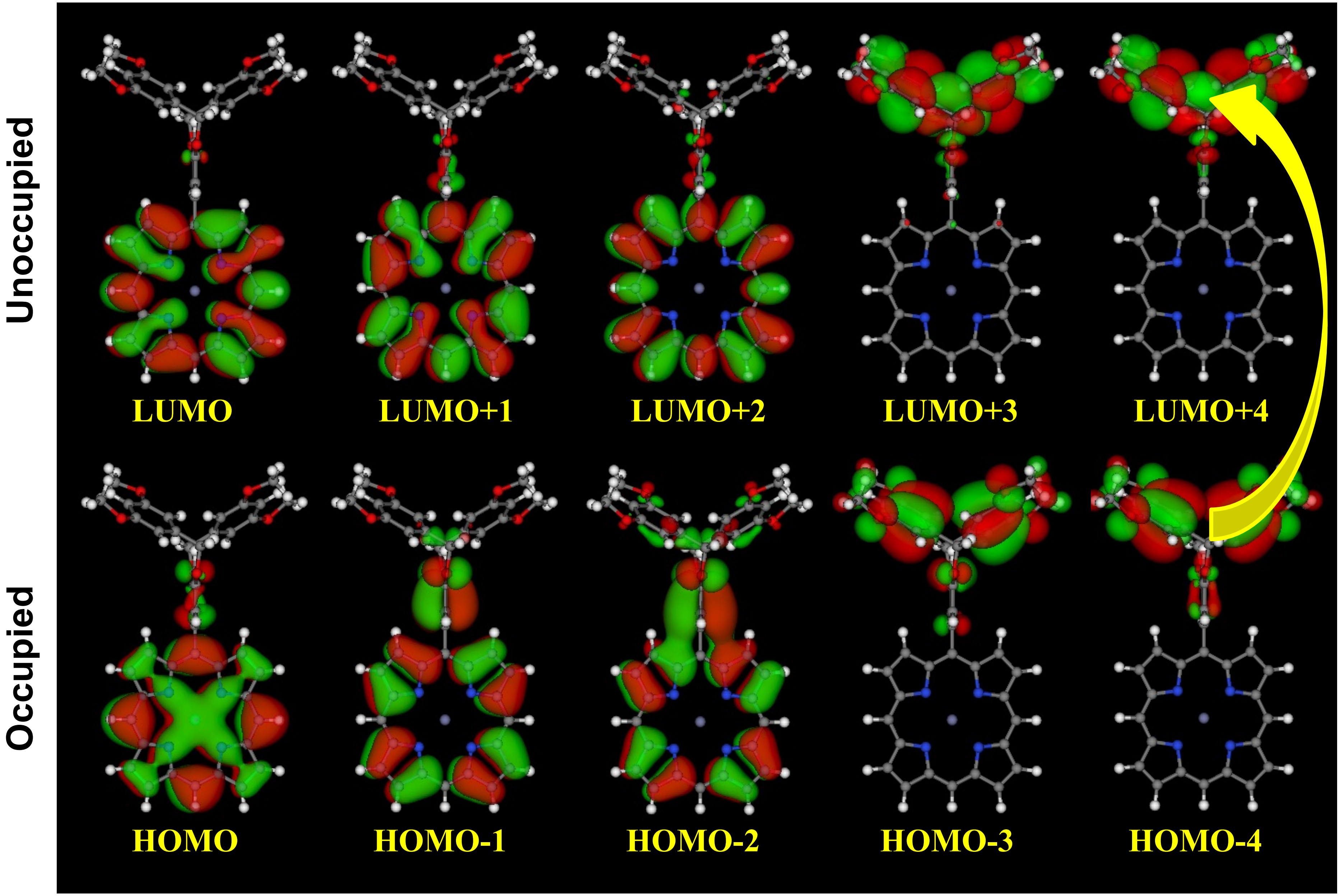

An electron in HOMO-4 is excited to LUMO+4

Optical Absorption Spectrum

- **Oscillator strength calculated by the linear-response TDDFT**

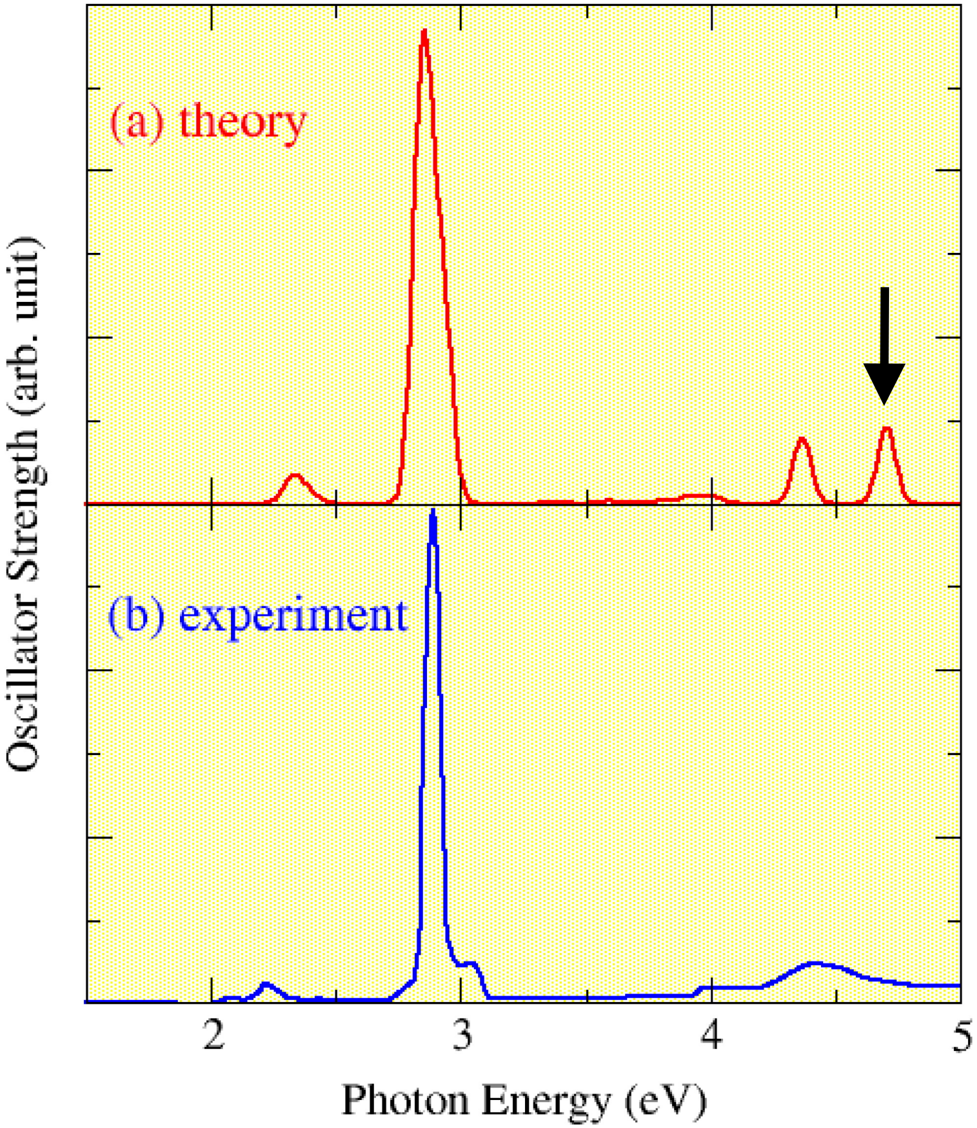

- **Excellent agreement with experimental data** [Akai *et al.*, ’06]

Effect of Exchange-Correlation Functional

- **Oscillator strength calculated by the linear-response TDDFT**

$$K_{ia\sigma,jb\tau} = \left[\psi_{i\sigma}\psi^*_{a\sigma}\middle|\psi_{j\tau}\psi^*_{b\tau}\right] - C_{\mathrm{HF}}\delta_{\sigma\tau}\left[\psi_{i\sigma}\psi^*_{j\sigma}\middle|\psi_{a\tau}\psi^*_{b\tau}\right] + (1 - C_{\mathrm{HF}})f^{\mathrm{x}}_{ia\sigma,jb\tau} + f^{\mathrm{c}}_{ia\sigma,jb\tau}$$

$$\left[g\middle|h\right] = \int d\mathbf{r}\int d\mathbf{r}'\,\frac{g(\mathbf{r})h(\mathbf{r}')}{|\mathbf{r}-\mathbf{r}'|}$$

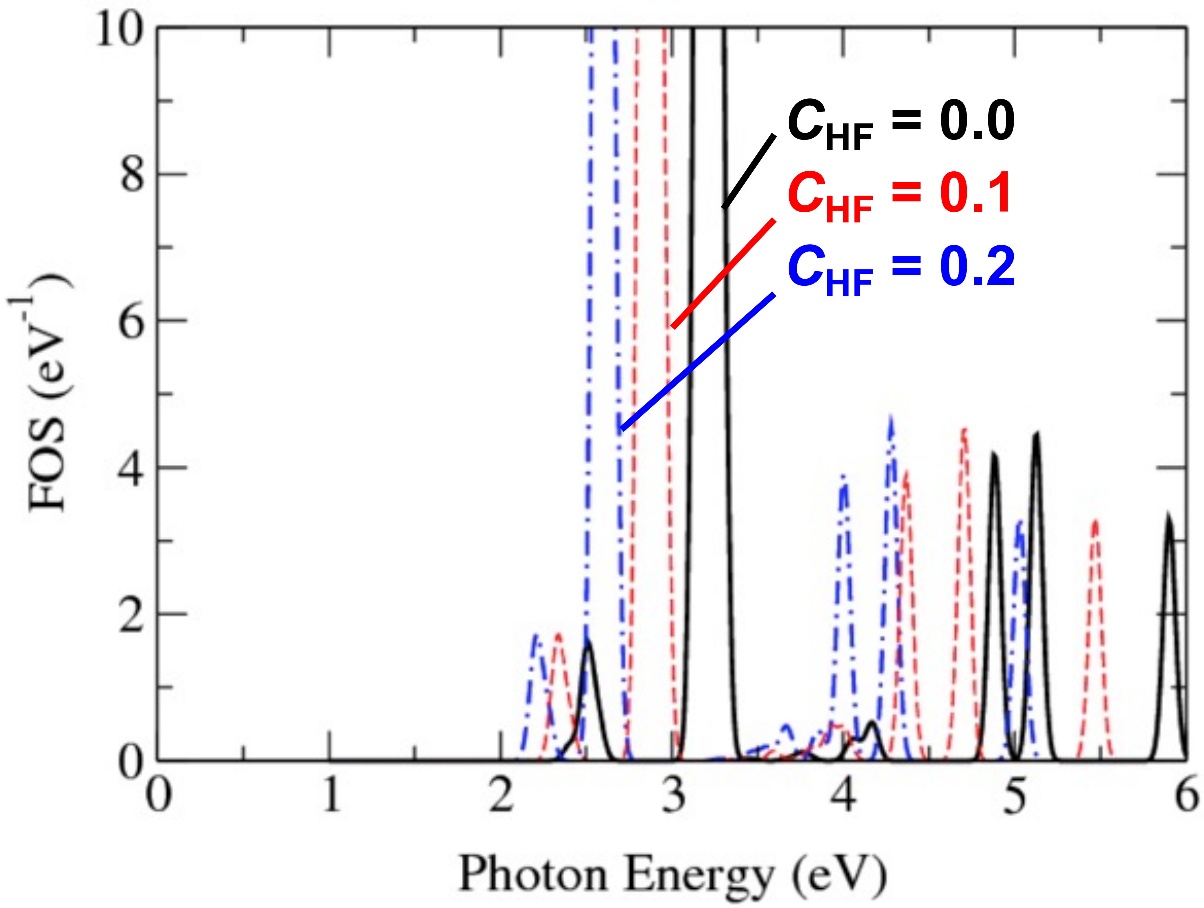

- **At most 20% difference in excitation energies by different approximations**

Electron Transfer in a Dendrimer

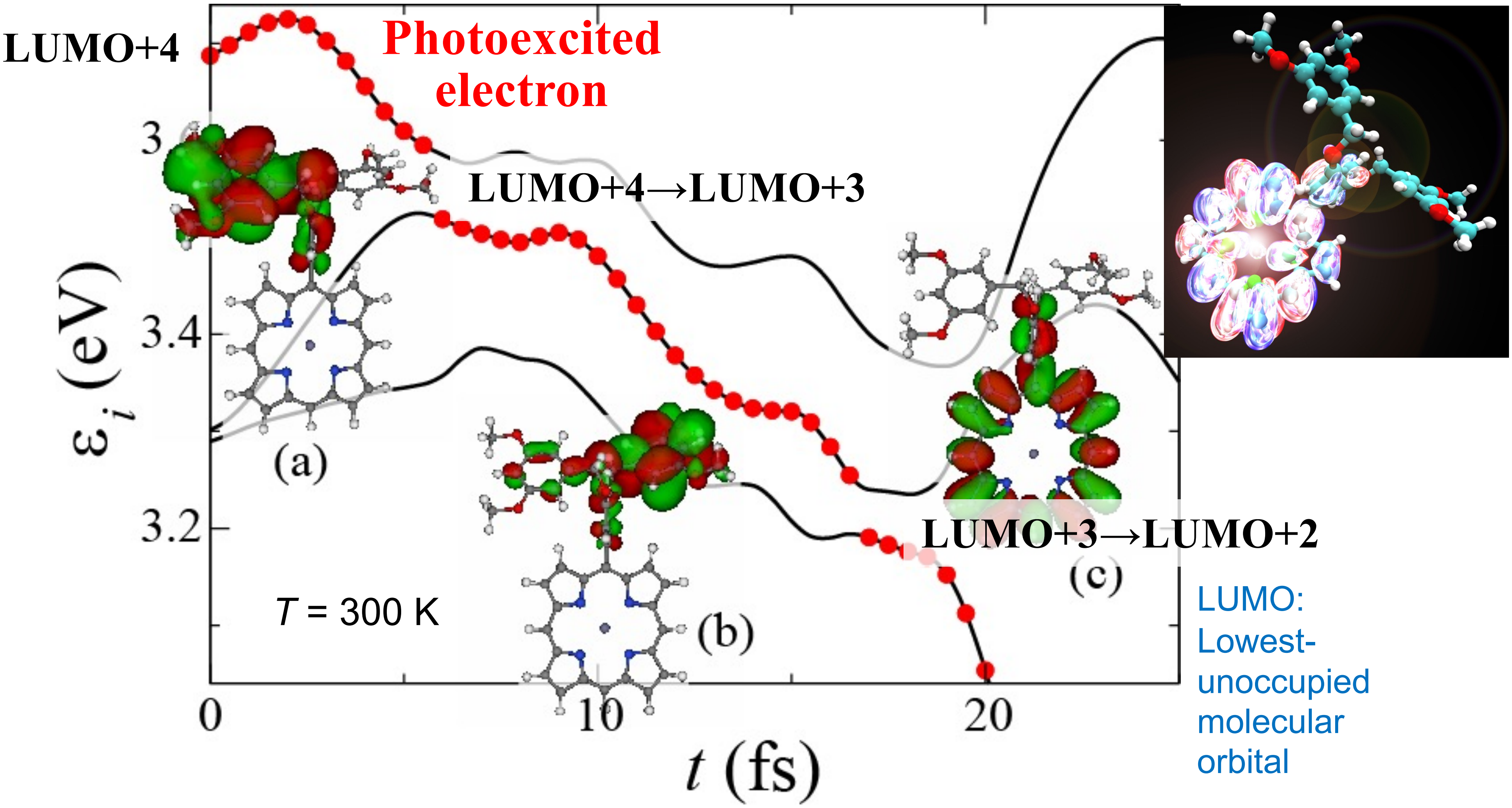

LUMO: Lowest-unoccupied molecular orbital

- **The photoexcited electron at the peripheral antenna is transferred to the core due to the energy-crossing & overlapping of orbitals assisted by thermal molecular motions**

Electron Transfer in a Light-Harvesting Dendrimer

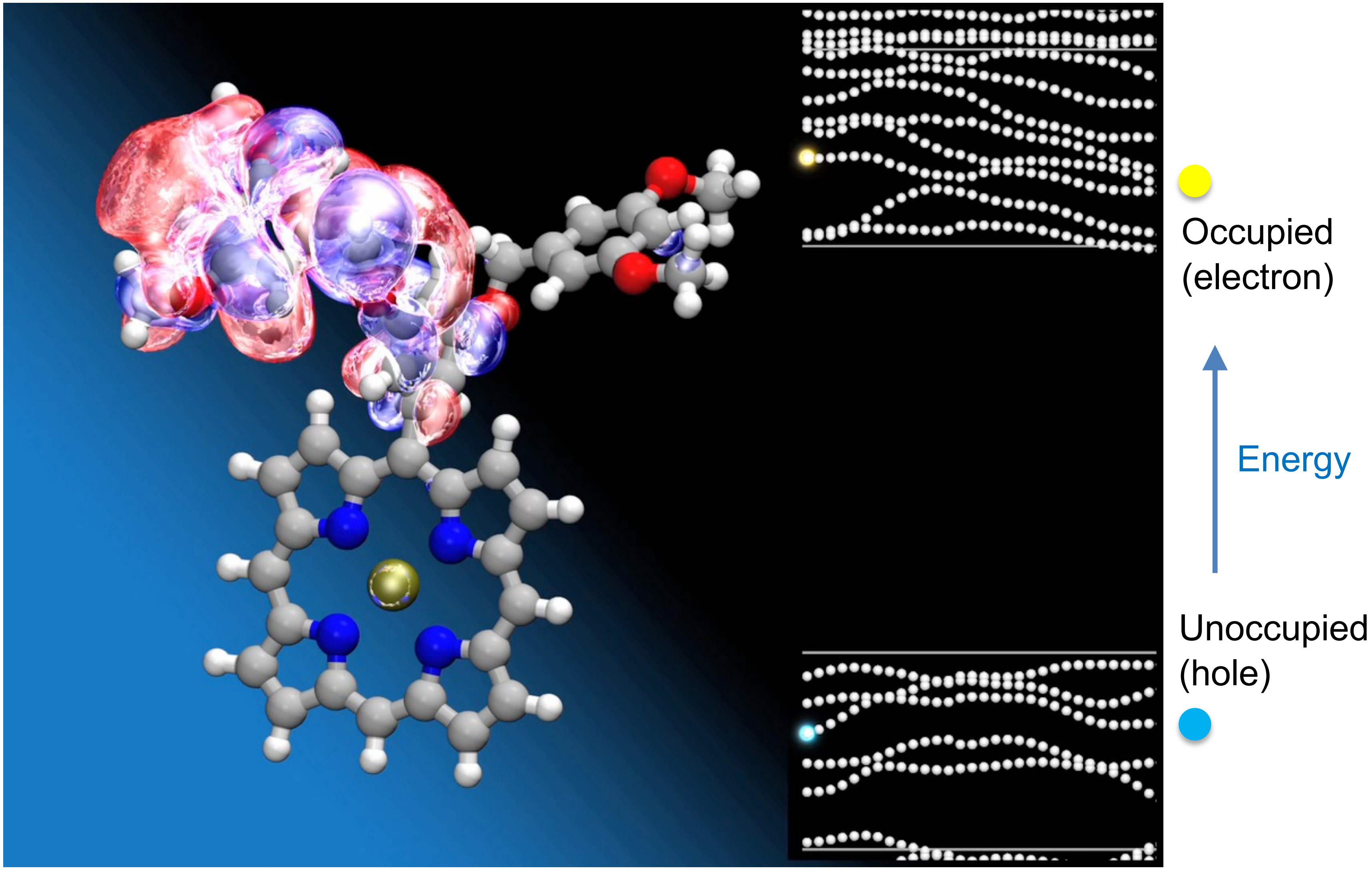

- **The photoexcited electron at the peripheral antenna is transferred to the core due to the energy-crossing & overlapping of orbitals assisted by thermal molecular motions**

Electron Transfer Mechanism

- **Probability in the antenna & core regions (averaged over 15 trajectories)**

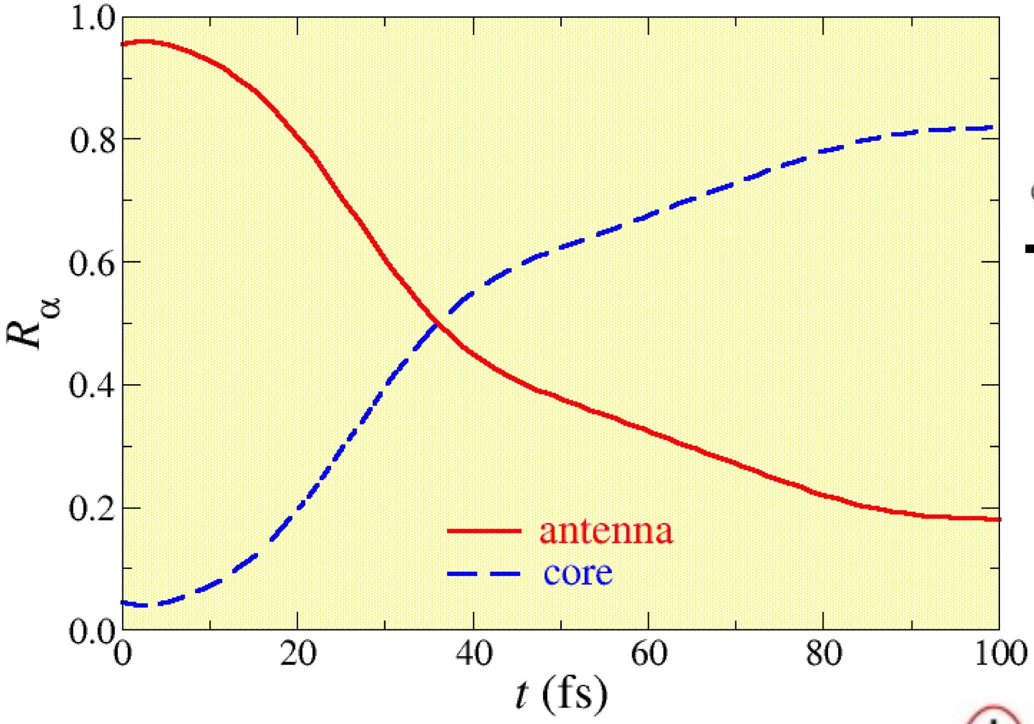

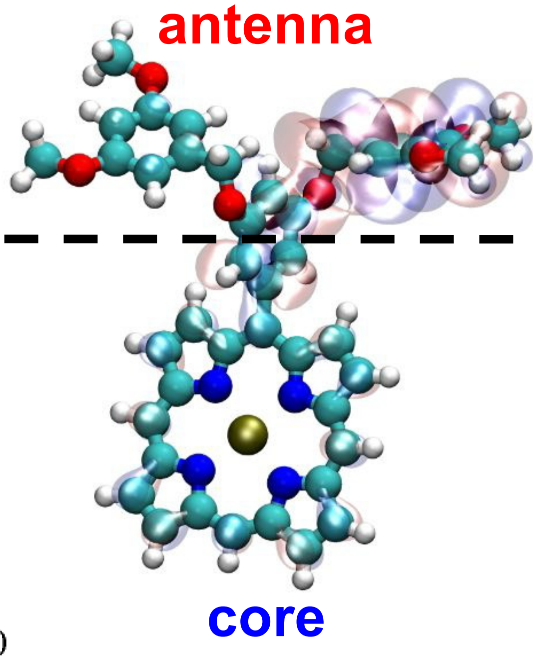

- **The resulting electron transfer rate due to the *Dexter* mechanism is much larger than that due to the *Förster* mechanism**

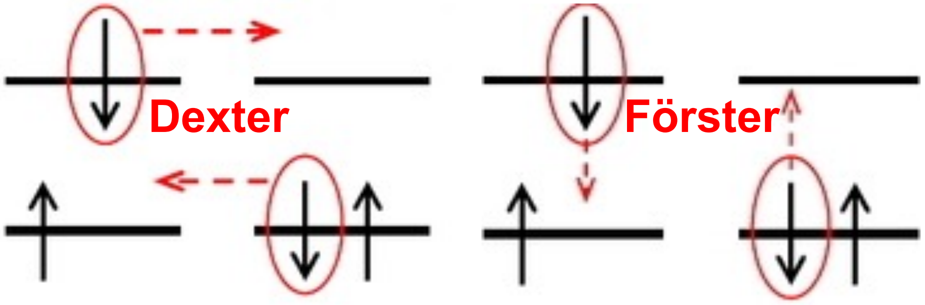

$$k_{\text{Dexter}}^{-1} = \boxed{40\text{fs}}$$

$$<< k_{\text{Forster}}^{-1} = \left[\frac{2\pi}{\hbar}\sum_{b\notin\{\text{occ}\};j\in\{\text{occ}\}} \left|K_{ia\sigma,jb\sigma}\right|^2 \times \frac{1}{\sqrt{2\pi\alpha}}\exp\left(-\frac{(\omega_{ia\sigma}-\omega_{jb\sigma})^2}{2\alpha^2}\right)\right]^{-1} = \boxed{1\text{ps}}$$

Effect of Temperature

Adiabatic MD simulation of a dendrimer at temperature 300 & 100 K

300 K

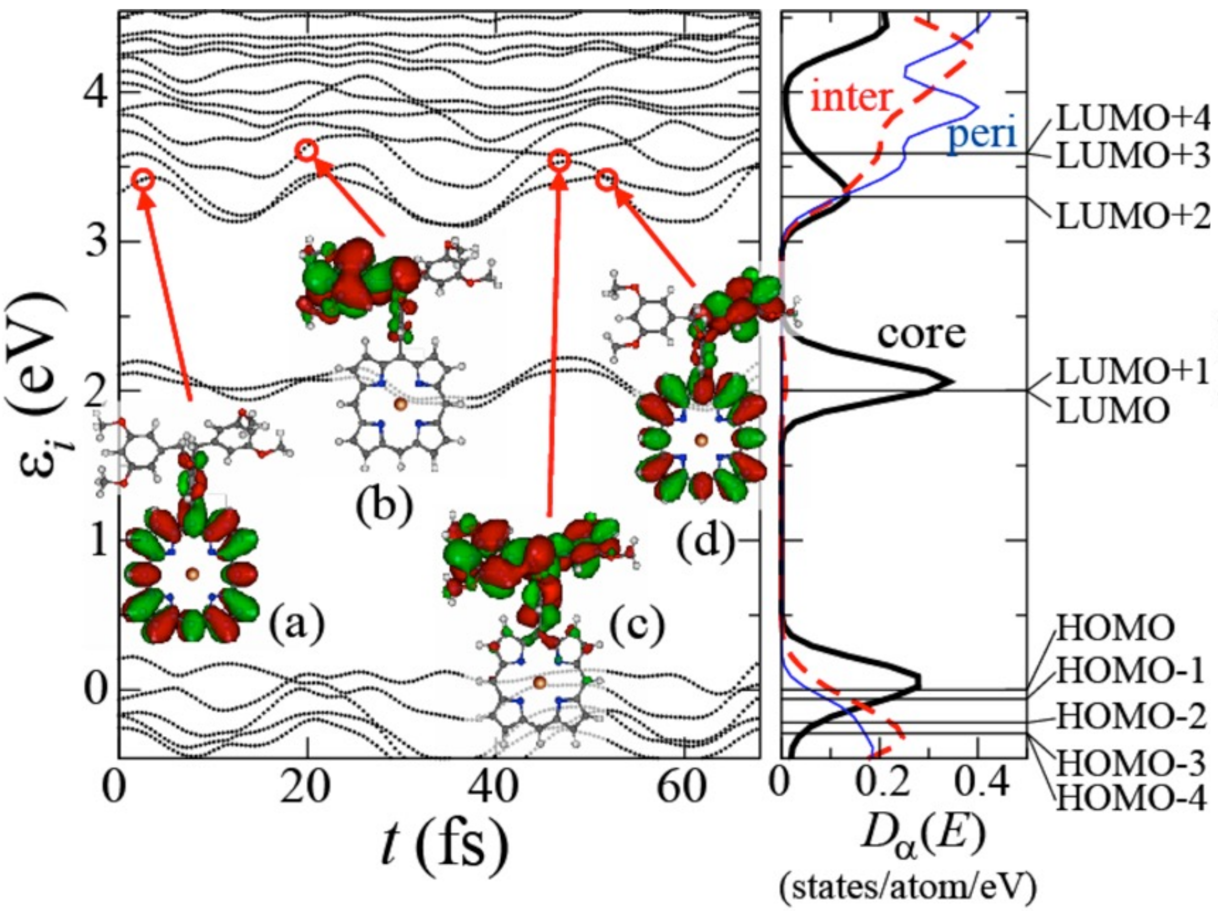

100 K

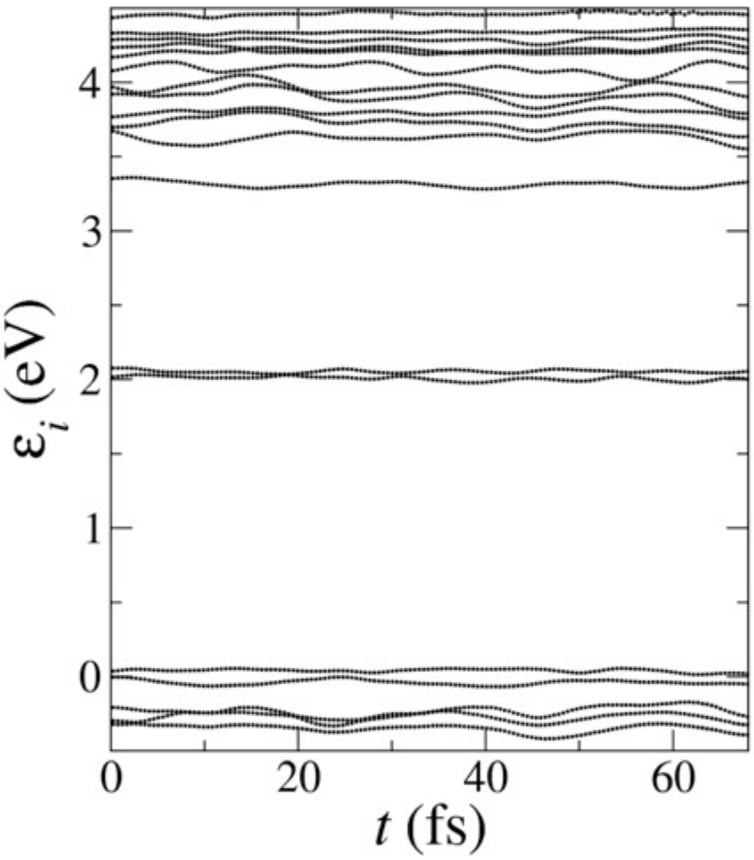

Electron transfer is suppressed at low temperatures

Effect of Solvent

Adiabatic QMD simulation of a dendrimer in solvent, tetrahydrofuran (THF), $(CH_2)_4O$, at temperature 300 K used in experiments [Akai *et al*., ’06, ’08]

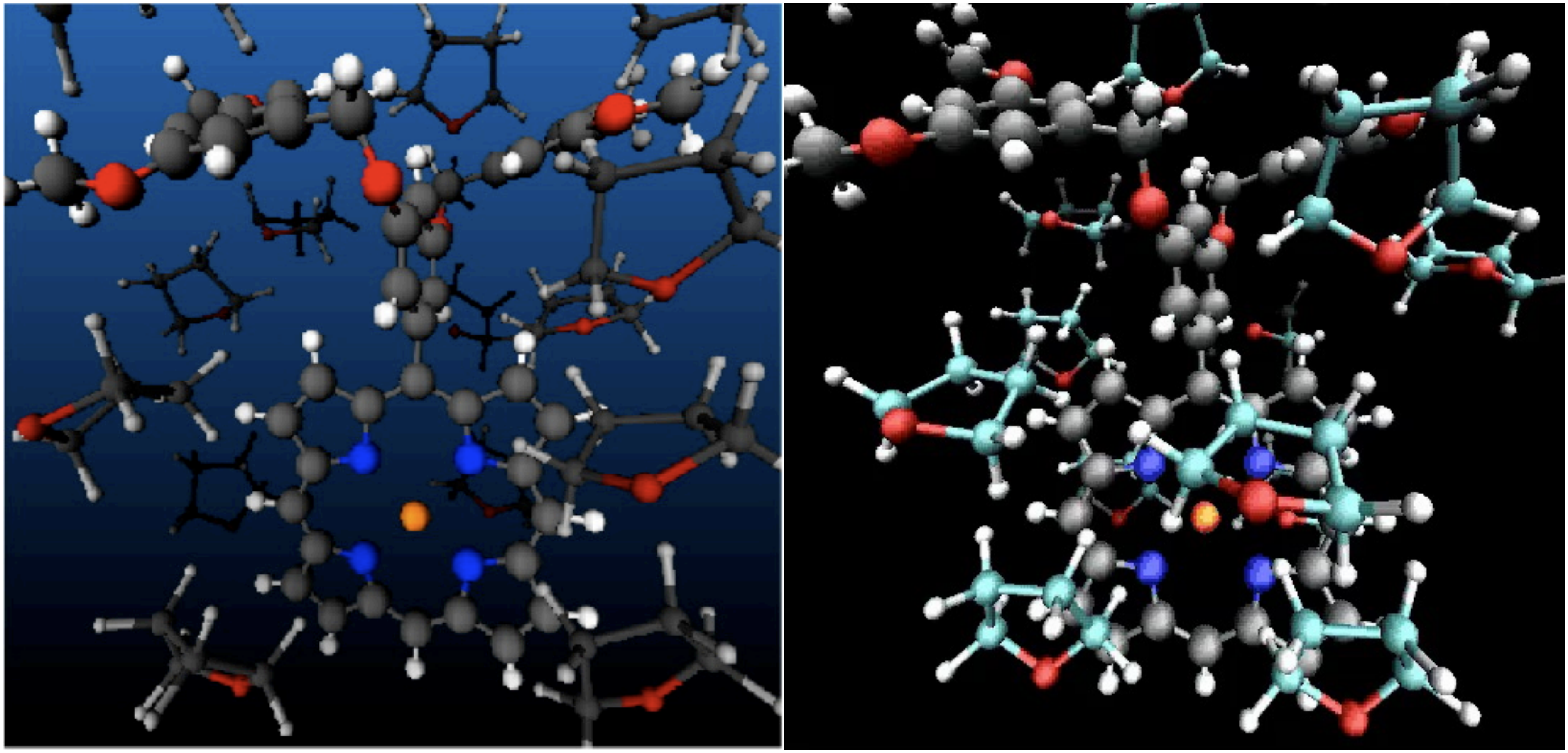

Solvent suppresses orbital energy-crossing & consequently electron transfer

Key Molecular Mechanism

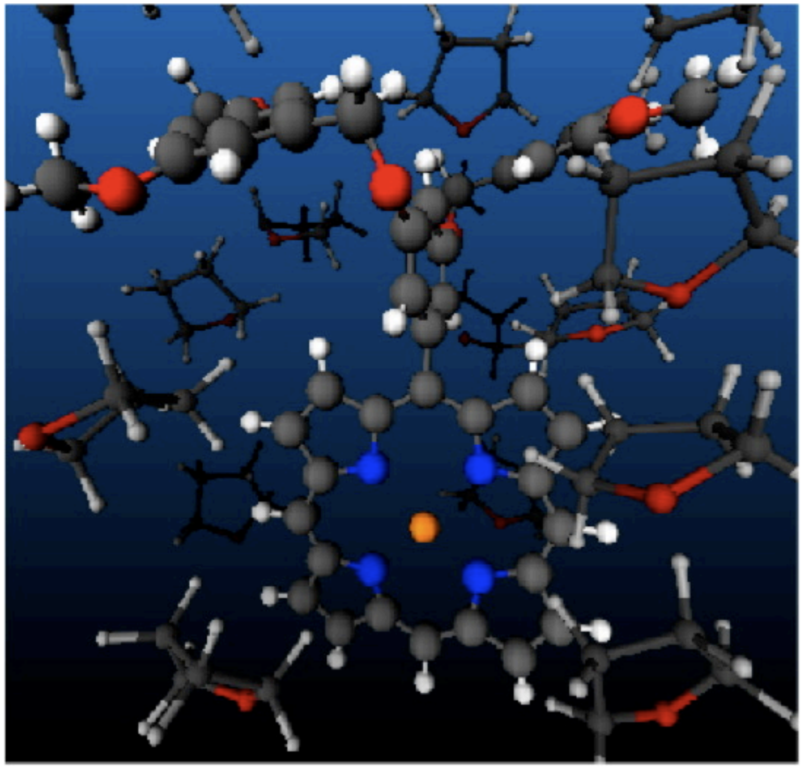

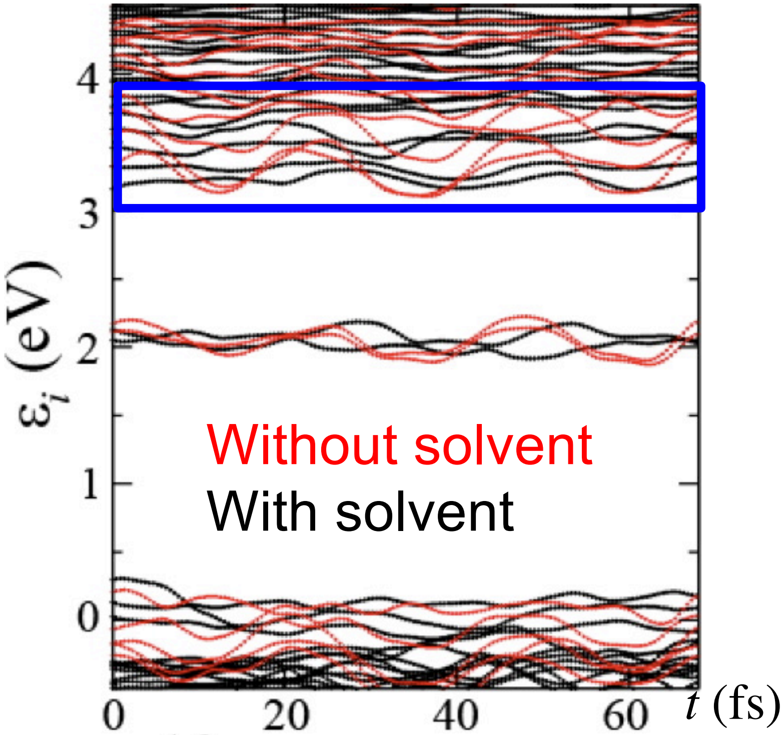

- **Solvent (tetrahydrofuran) suppresses orbital energy-crossing & electron transfer**

$$\sigma = \left\langle \varepsilon_i^2 \right\rangle - \left\langle \varepsilon_i \right\rangle^2 = 0.13\text{eV(vacuum)} \rightarrow 0.04\text{eV(THF)}$$

- **Aromatic ring motion in the periphery is the key mechanism for rapid electron transfer**

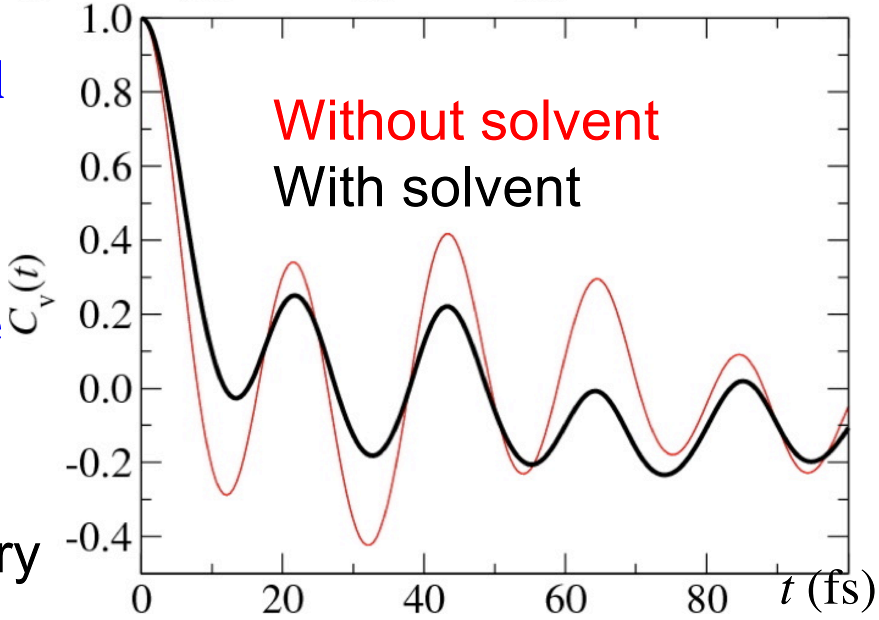

Velocity autocorrelation
in the aromatic rings in the periphery

Organic Photovoltaics (OPV)

- Exciton dynamics

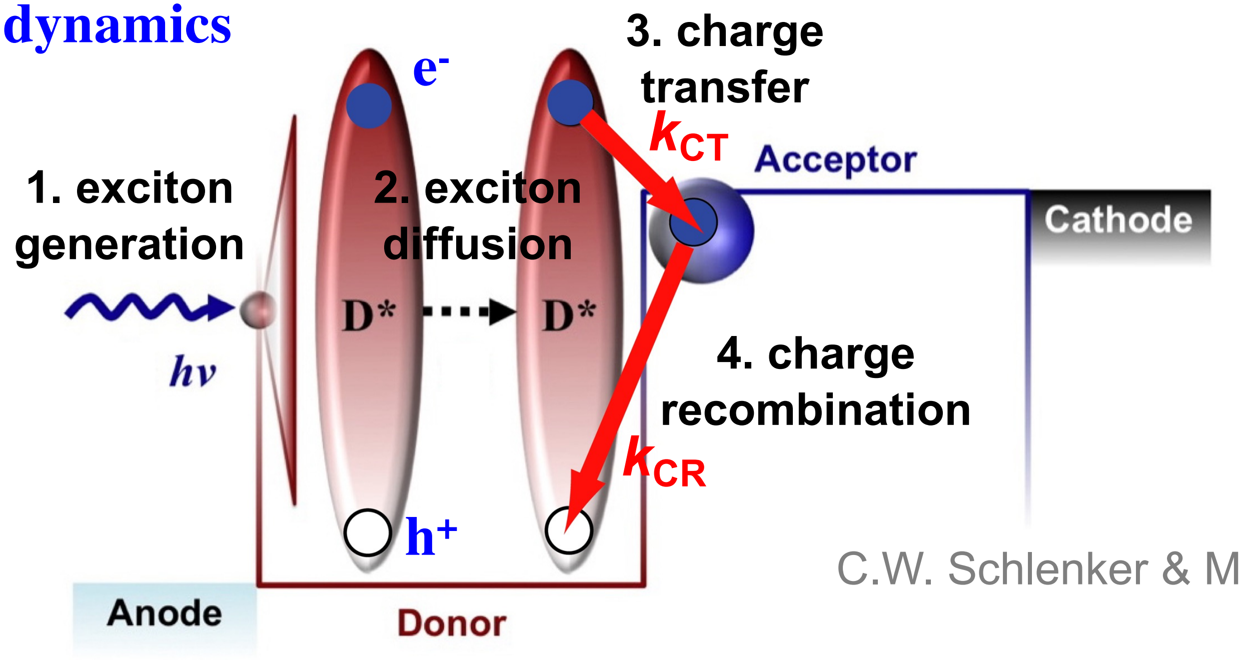

C.W. Schlenker & M. E. Thompson ('11)

- Open-circuit voltage is sensitive to the interfacial structure

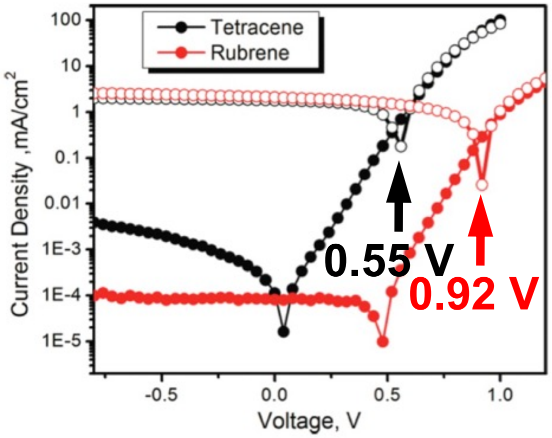

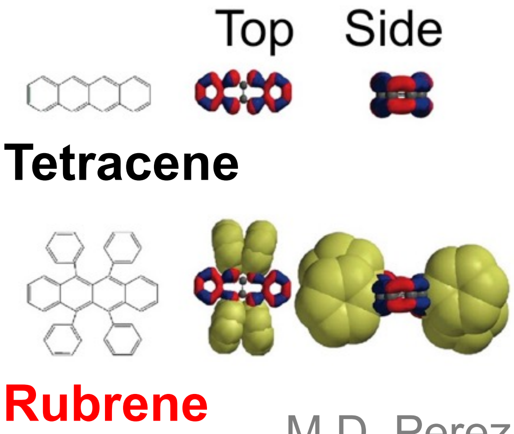

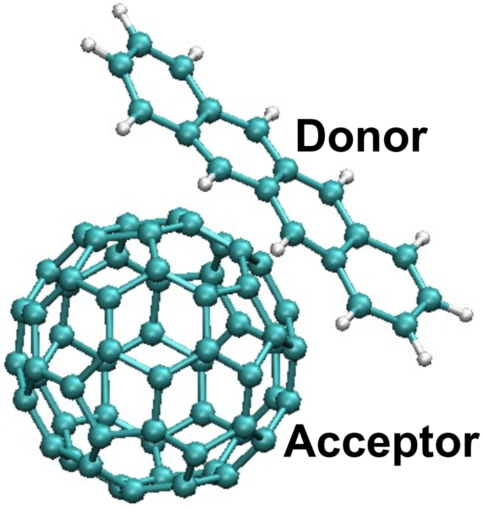

M.D. Perez *et al.*, *JACS* **131**, 9281 ('09)

Tetracene or Rubrene/Fullerene

LUMO: Tetracene/C_{60}

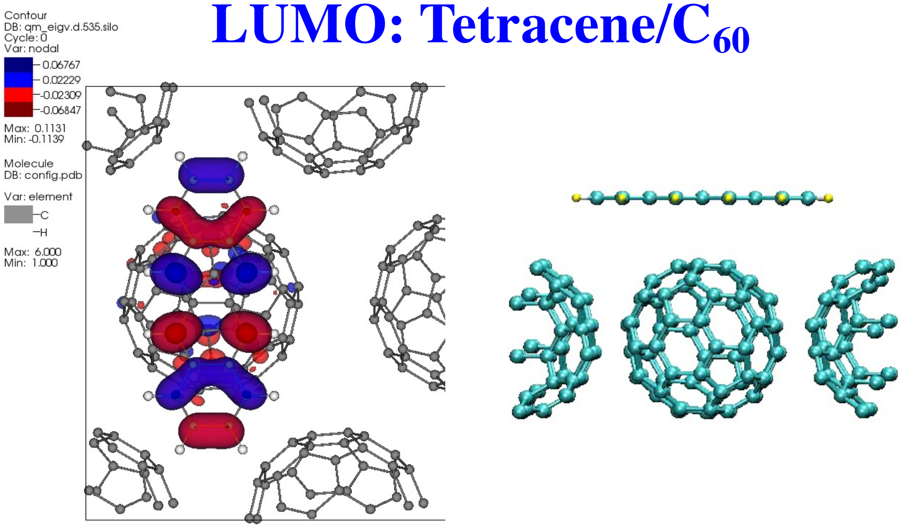

LUMO: Rubrene/C_{60}

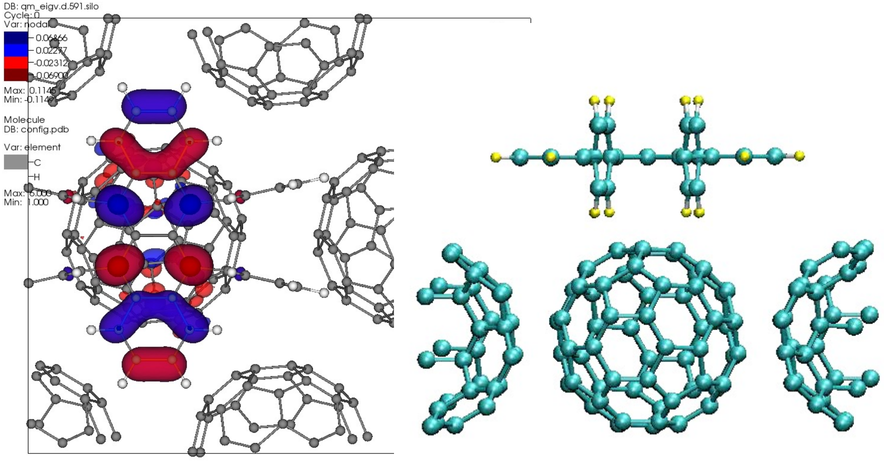

Small level fluctuation → small charge transfer

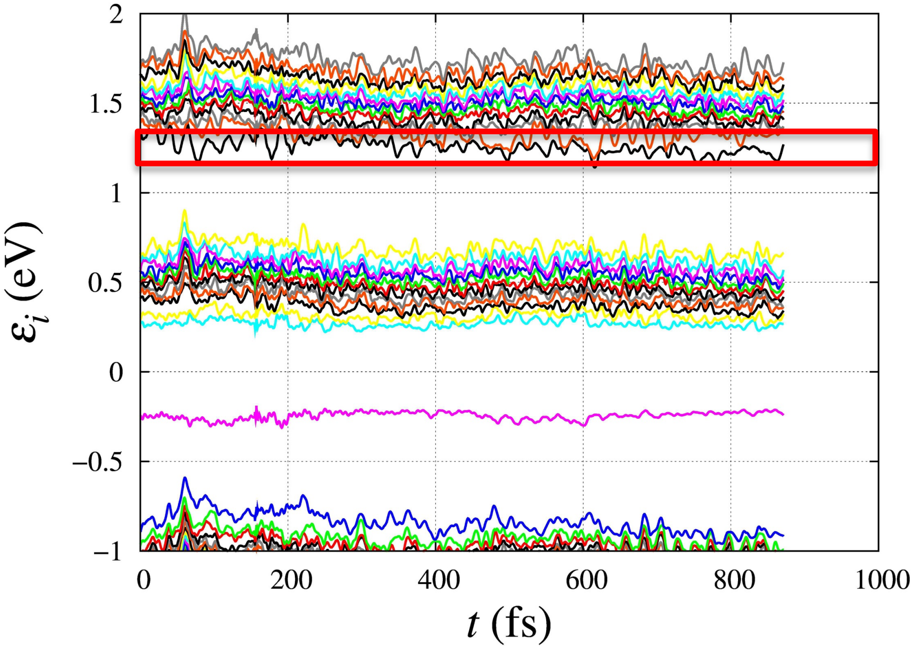

Large level fluctuation → large charge transfer

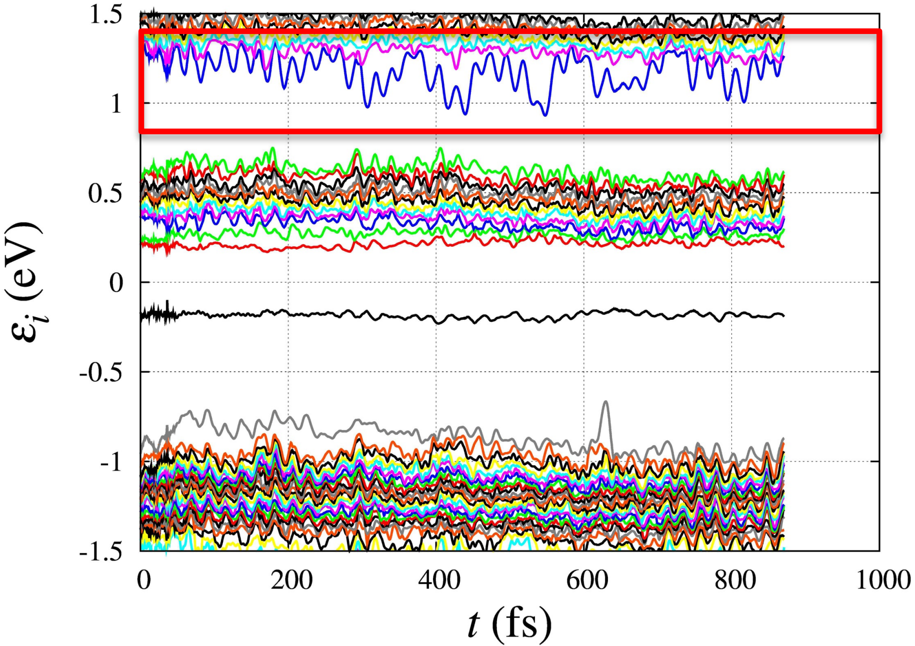

Mou *et al.*, *J. Chem. Phys.* **136**, 184705 ('12)

Ring Breathing Modes

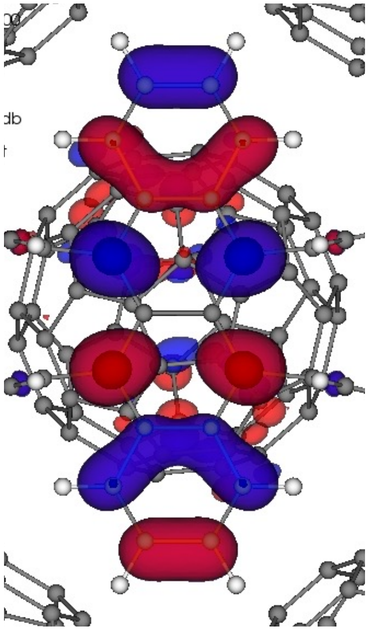

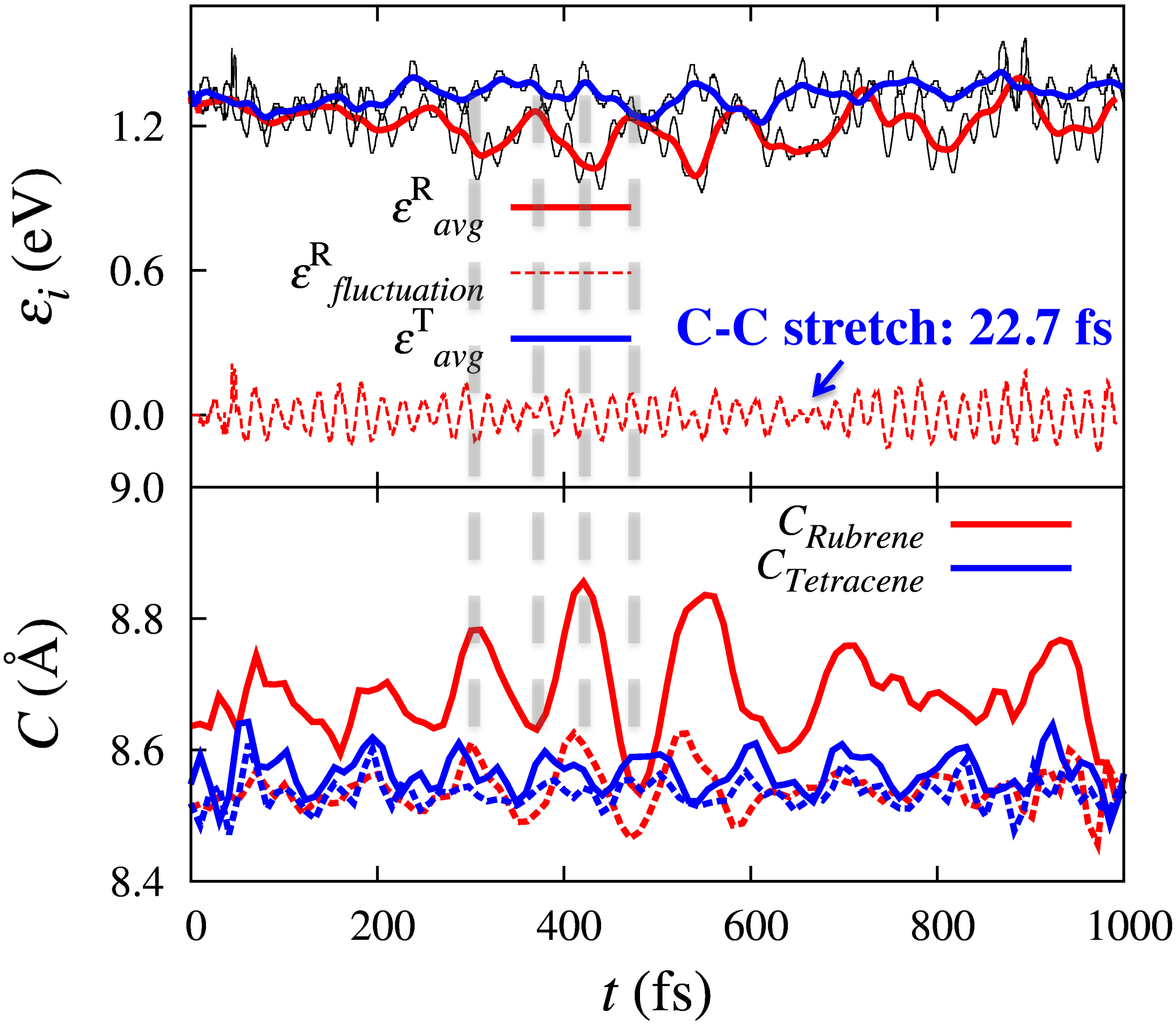

- **The phenyl rings expand the inner rings of the backbone & enhances their breathing modes → increased charge transfer**

Inorganic Nanowire Photovoltaics (NWPV)

GaAs nanowires under electronic microscopy

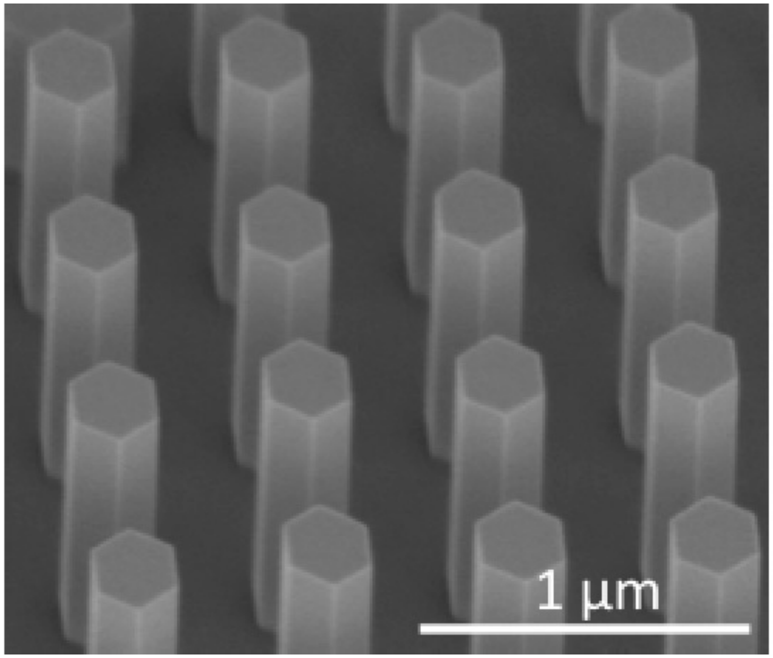

Yao *et al.*, *ACS Nano* **10**, 2424 ('16)

GaAs nanowire with perfect {110} surfaces

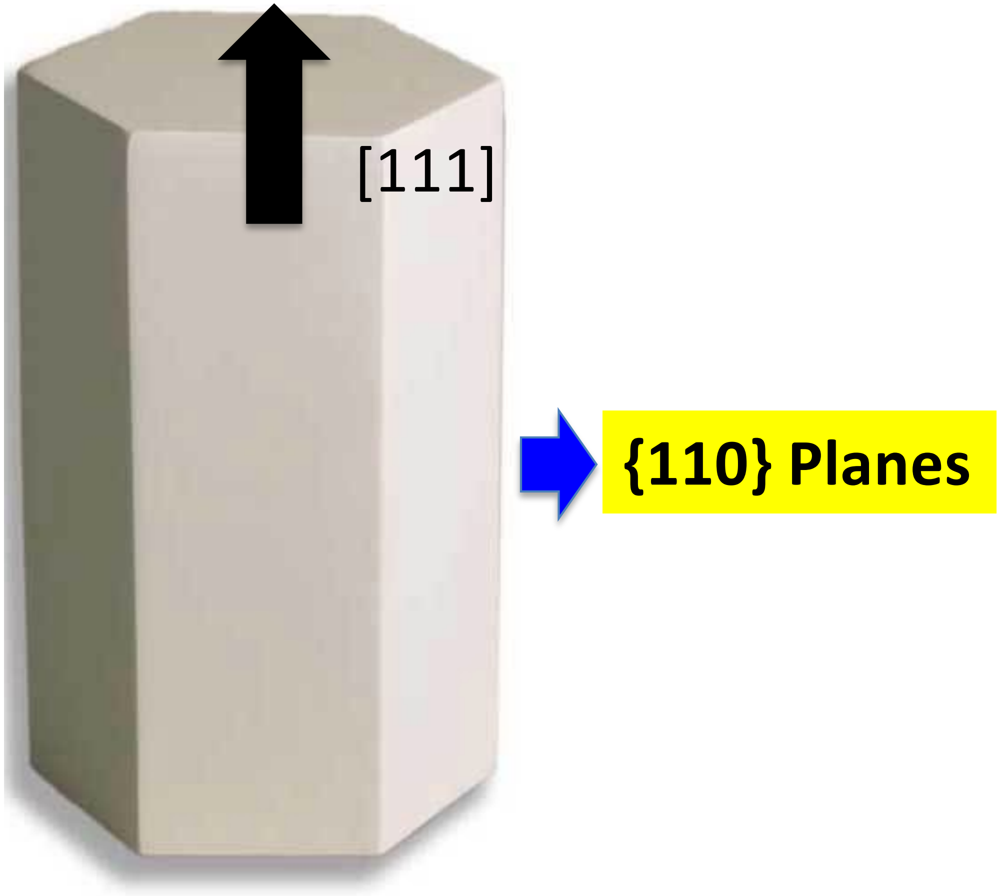

NAQMD Simulation of GaAs (110) Surface

Simulation Setup for GaAs (110)

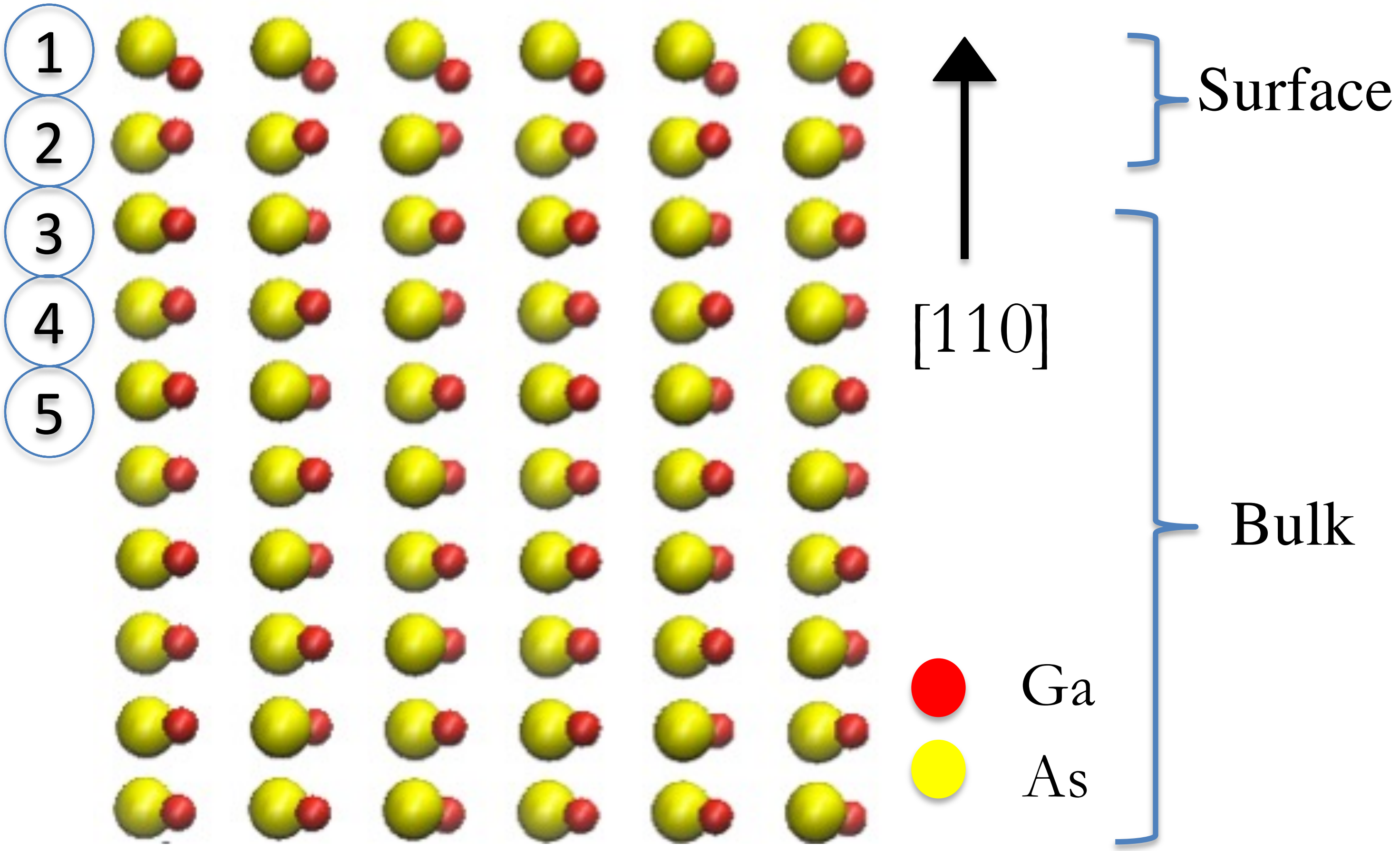

- **Definition of surface and bulk**
- **Atomic bilayers are numbered sequentially**

Brown *et al.*, *J. Appl. Phys.* **117**, 054307 ('15)

Electronic Structure at (110) Surface

- **Electronic partial density of states projected onto the wave functions of atomic bilayers**

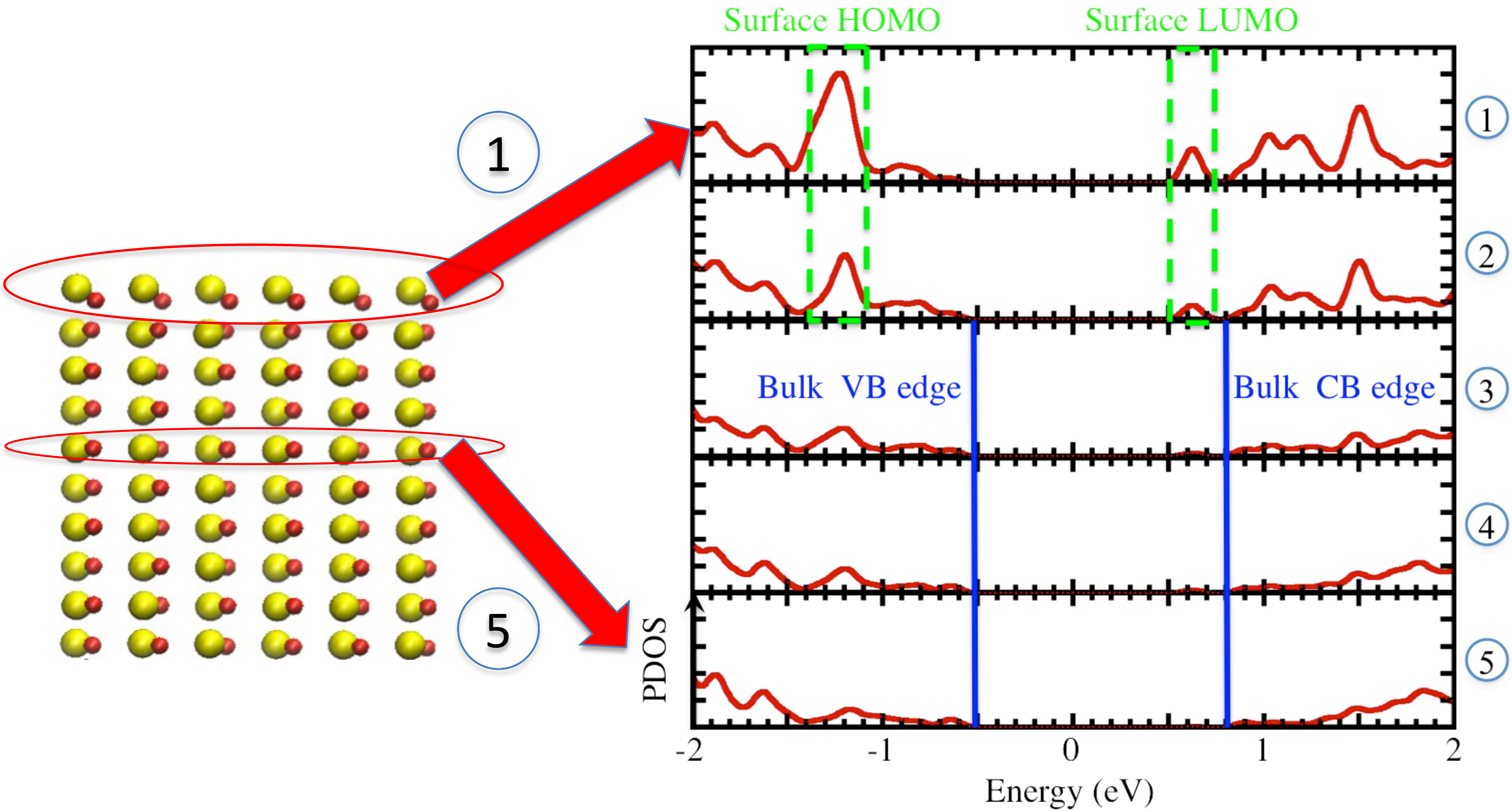

- **Surface relaxation causes spontaneous formation of a type-II (staggered) heterostructure**

Staggered Band Alignment Driven Charge Transfer

Photo excitation & charge recombination in type II heterojunction

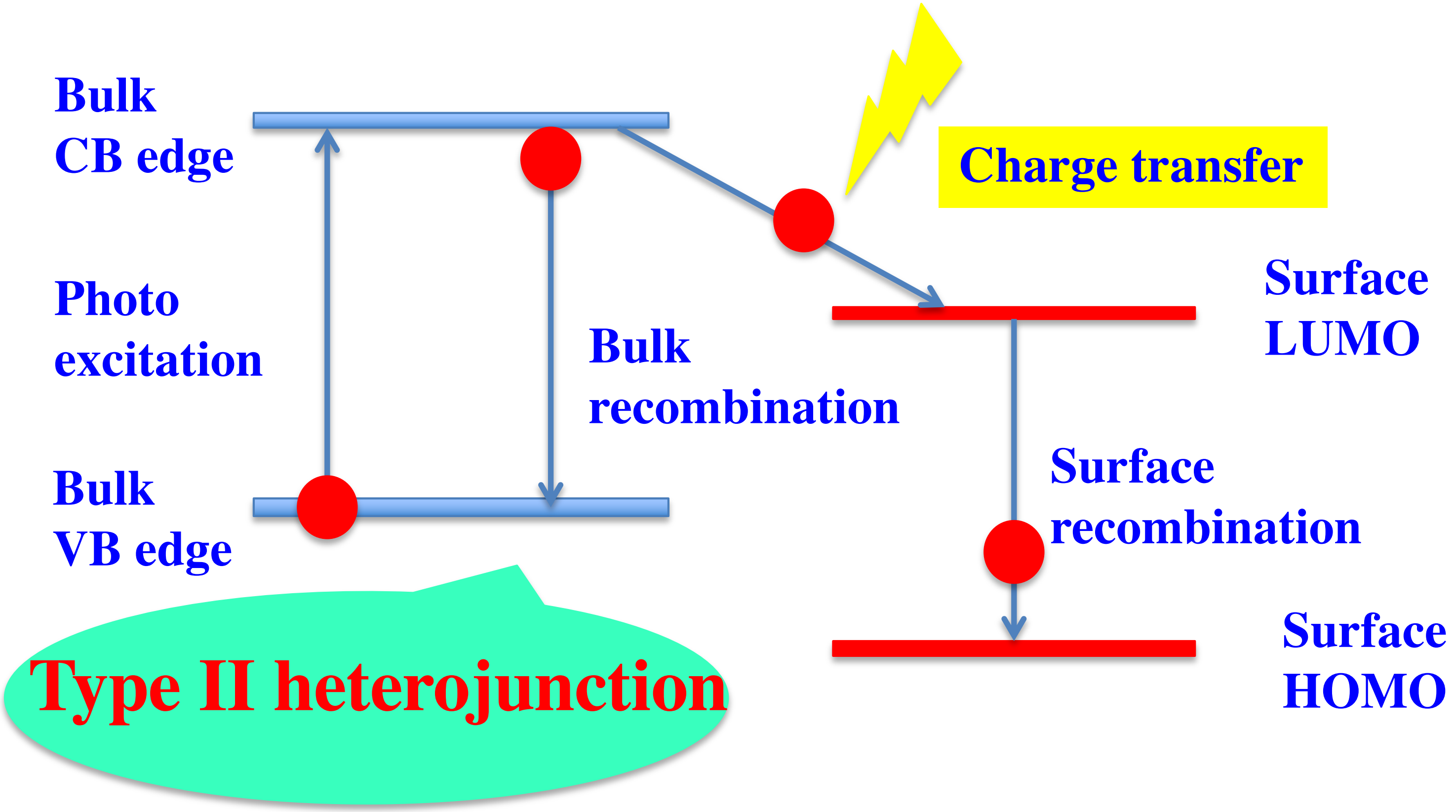

Bulk
CB edge

Charge transfer

Surface
LUMO

Photo
excitation

Bulk
recombination

Surface
recombination

Bulk
VB edge

Surface
HOMO

Type II heterojunction

- Staggered band alignment drives a photoexcited electron in the bulk to lower energy surface states, whereas holes remain near the valence-band (VB) edge (which is a bulk state)

Bulk *vs.* Surface Excitations

- **Existence probability of KS wave functions at the surface as a function of the KS energy.**
- **Two types of excitations by exciting one electron from an occupied orbital to an unoccupied orbital**

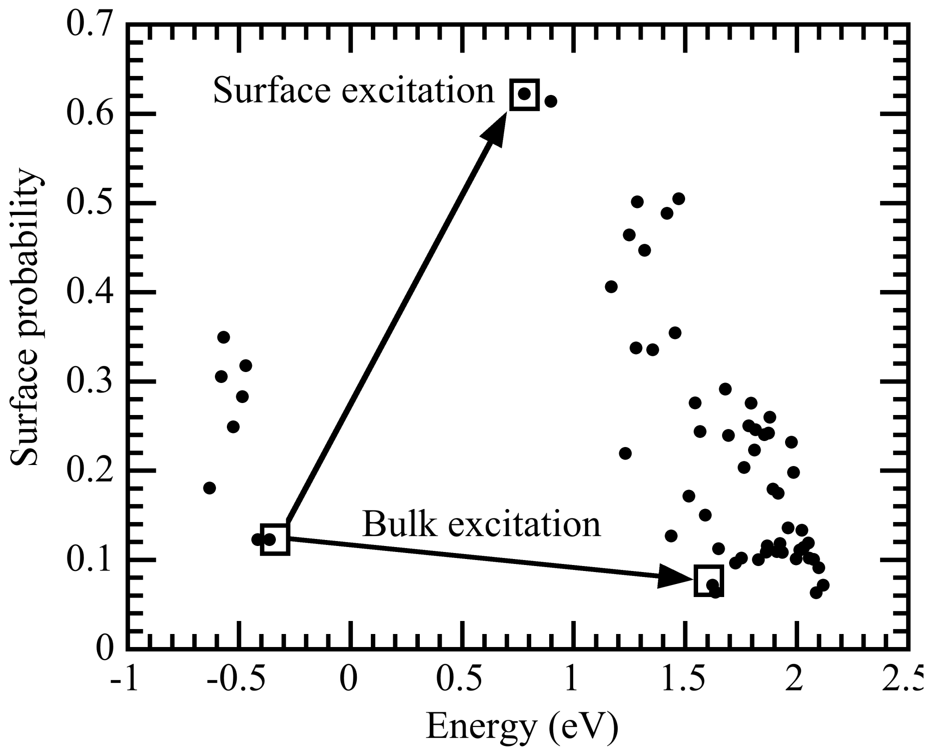

Existence probability at surface

$$P_i^{\text{surface}} = \int_{\mathbf{r}\in\text{surface}}^{\text{electron}} |\Psi_i(\mathbf{r})|^2 d\mathbf{r}$$

Existence probability at bulk

$$P_i^{\text{bulk}} = \int_{\mathbf{r}\in\text{bulk}}^{\text{electron}} |\Psi_i(\mathbf{r})|^2 d\mathbf{r}$$

Bulk- & surface-excitations are initiated by the transitions denoted by arrows

Carrier Wave Functions & Charge Transfer Rate

Electron (orange) & hole (green) wave functions of the bulk-excitation simulation from time 0 and 169 fs, exhibits homogeneous distribution to surface localization

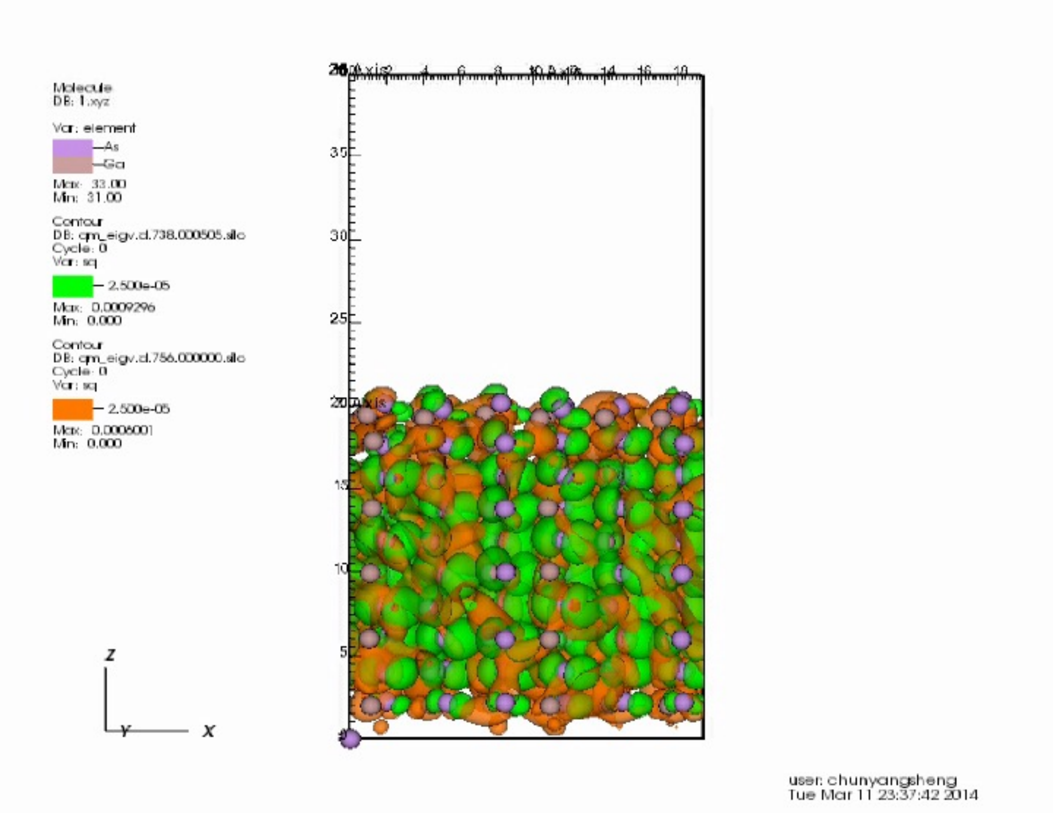

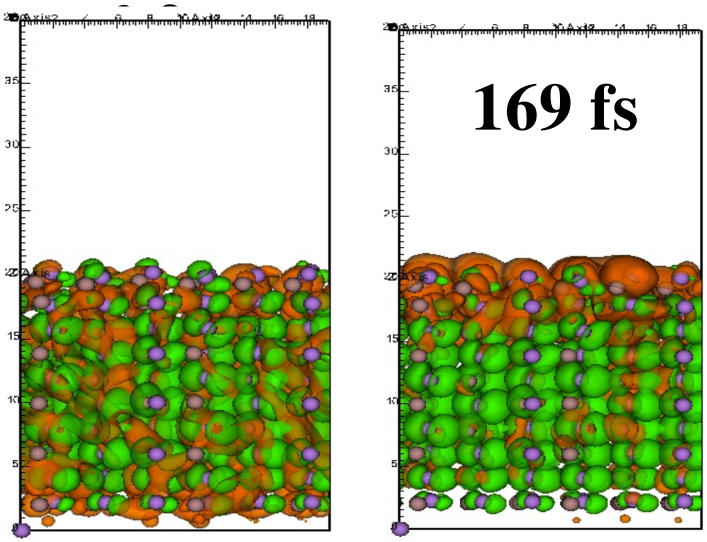

In the NAQMD simulation for bulk excitation, the excited electron quickly transfers to surface

From the time evolution of the surface probability of the excited electron, charge-transfer (CT) rate is estimated to be $k_{\mathrm{CT}} = 6.25\times10^{12}$ s^{-1}

Phonon-Assisted Charge Recombination in Bulk

Transition probability $\gamma_{ij}(t)$ from the current excited state i to another state j as a function of time t

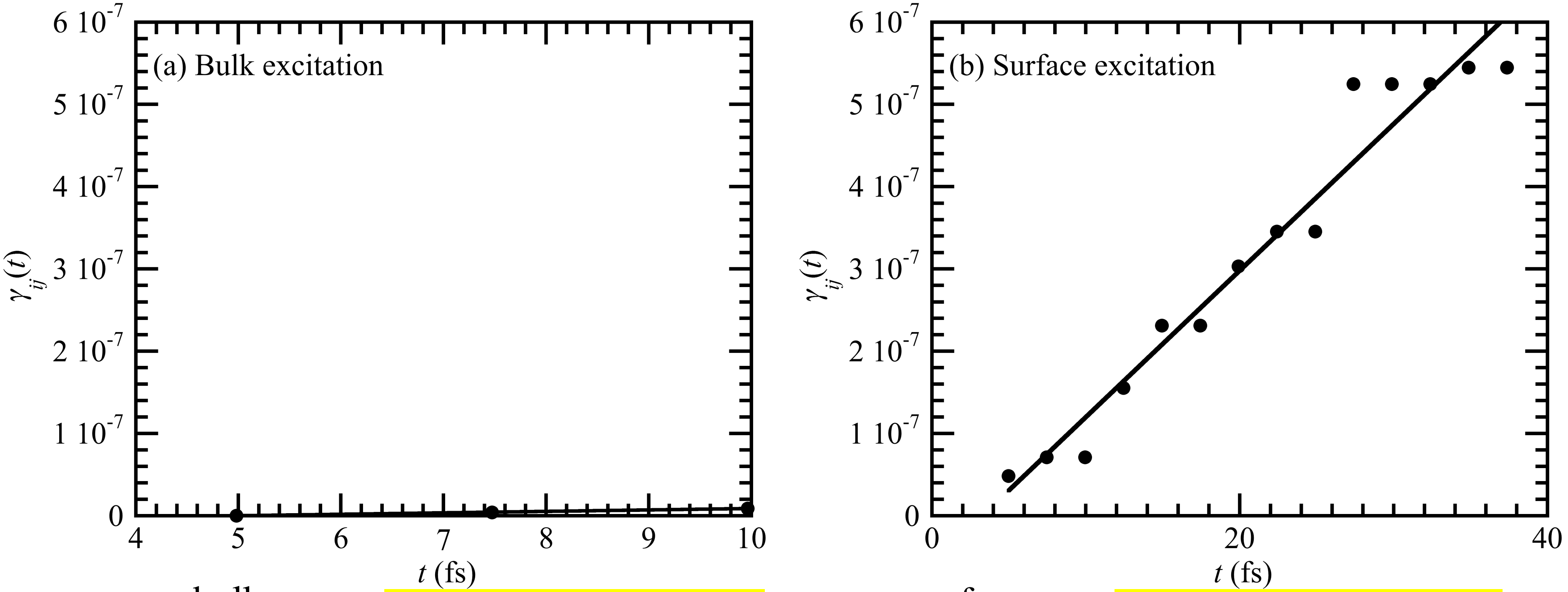

$$k^{\text{bulk}}_{\text{CR-phonon}} = (1.7\pm0.1)\times10^{6}\ \text{s}^{-1}$$

$$k^{\text{surface}}_{\text{CR-phonon}} = (1.8\pm0.1)\times10^{7}\ \text{s}^{-1}$$

Charge-recombination (CR) rate is enhanced by an order-of-magnitude near surface

Spontaneous-Emission CR Rate

$$\gamma_{I,J}^{\text{Dipole}} = \frac{4n(\omega_I - \omega_J)^3 \left|\langle \Phi_I | \hat{\mathbf{r}} | \Phi_J \rangle\right|^2}{3c^3}$$

X. Zhang *et al.*,
PRB **84**, 235208 (‘11)

- Bulk

  $R_{CR\_SE} = 2.8\times10^2$ (s^{-1})

- Surface

  $R_{CR\text{-}SE} = 9.3\times10^3$ (s^{-1})

Comparison with phonon assisted CR rates

	Bulk	Surface
Phonon assisted R_{CR}	$1.7\text{x}10^6$ (s^{-1})	$1.8\text{x}10^7$ (s^{-1})
SE R_{CR}	$2.8\text{x}10^2$ (s^{-1})	$9.3\text{x}10^3$ (s^{-1})

Phonon assisted charge recombination is the dominant CR channel

Modelling Carrier-Population Kinetics

- Core-shell structure GaAs nanowire with diameter *D*
- Carrier populations at the core & shell

- CR at surface: 1.8×10^{7} (s^{-1})
- CR in bulk : 1.7×10^{6} (s^{-1})
- CT rate : 6.25×10^{12} (s-1)

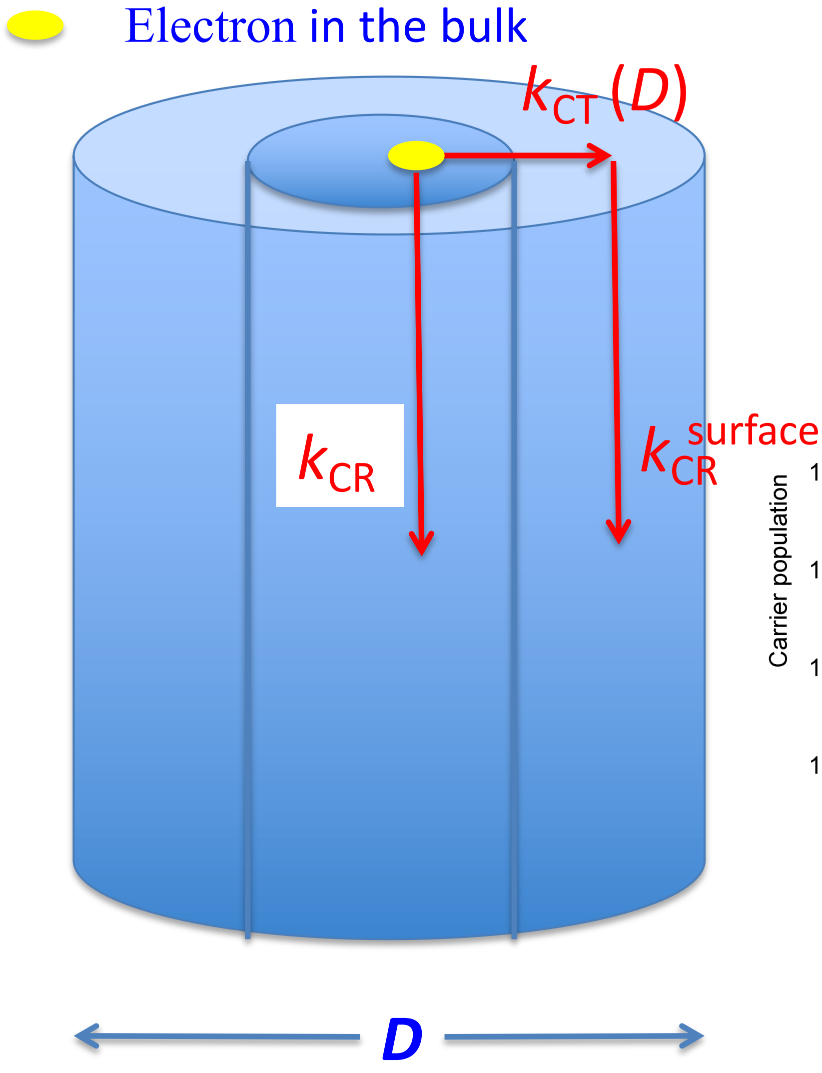

kinetic equation for carrier populations:

$$\frac{d}{dt}\begin{bmatrix} P_{\text{core}} \\ P_{\text{shell}} \end{bmatrix} = -\begin{bmatrix} k_{\text{CT}}(D)+k_{\text{CR}}^{\text{bulk}} & 0 \\ -k_{\text{CT}}(D) & k_{\text{CR}}^{\text{surface}} \end{bmatrix}\begin{bmatrix} P_{\text{core}} \\ P_{\text{shell}} \end{bmatrix}$$

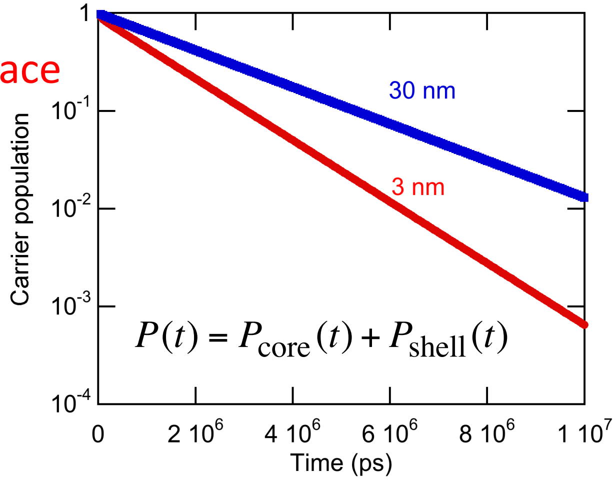

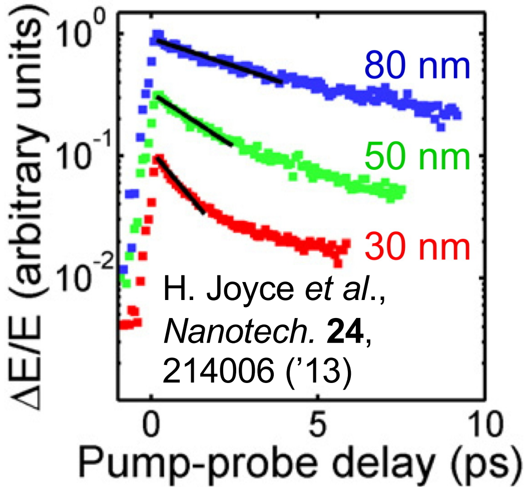

H. Joyce *et al.*, *Nanotech.* **24**, 214006 ('13)

1. Faster decay with decreasing diameter in agreement with experiments
2. Decay time with ideal (110) sidewalls too large → more realistic sidewalls?

Charge Recombination in Twinned NW

SEM image of twinned nanowire **TEM image of twinned nanowire**

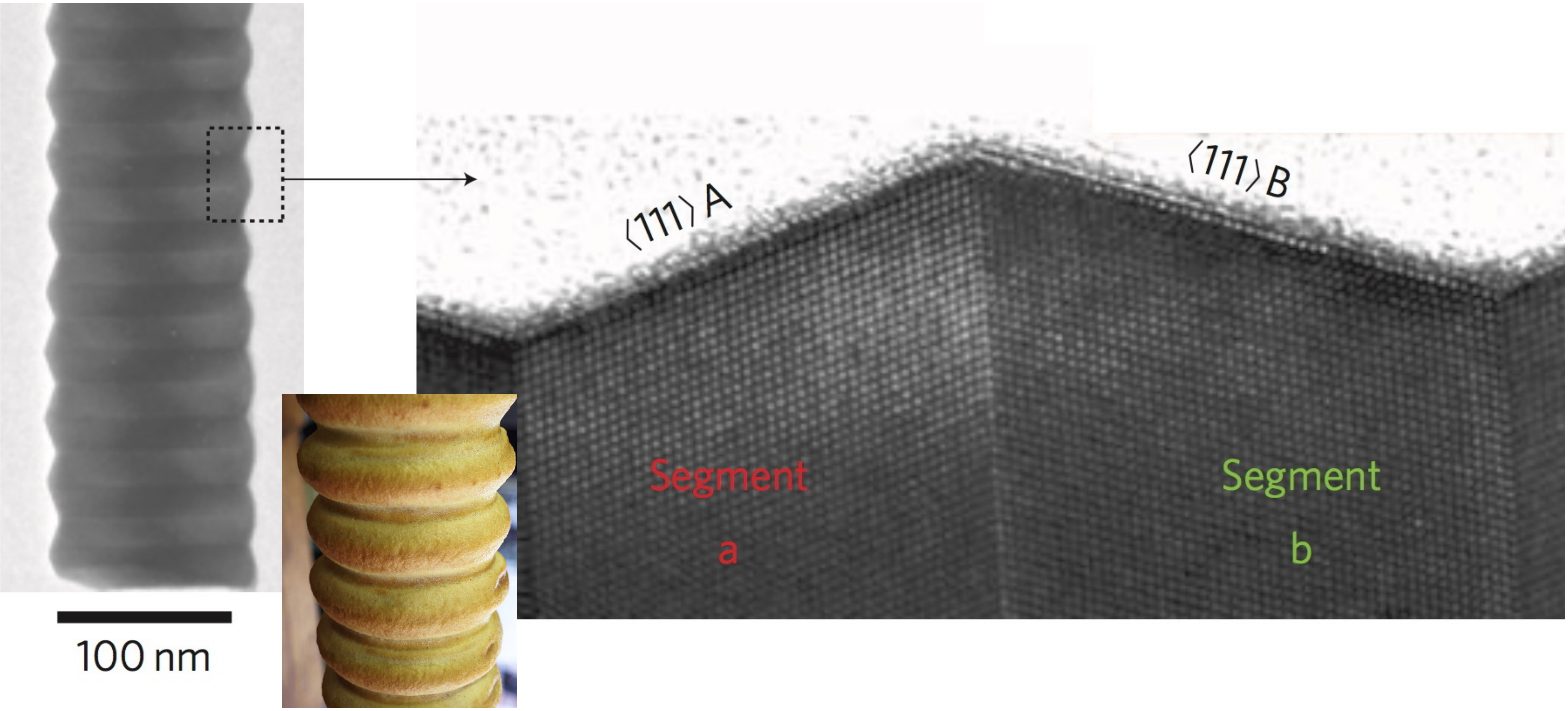

Real GaAs {110} facets contain high density of twin defects

Caroff *et al*., *Nat. Nanotechnol.* **4**, 50 ('09)

Twin-Twin Attraction

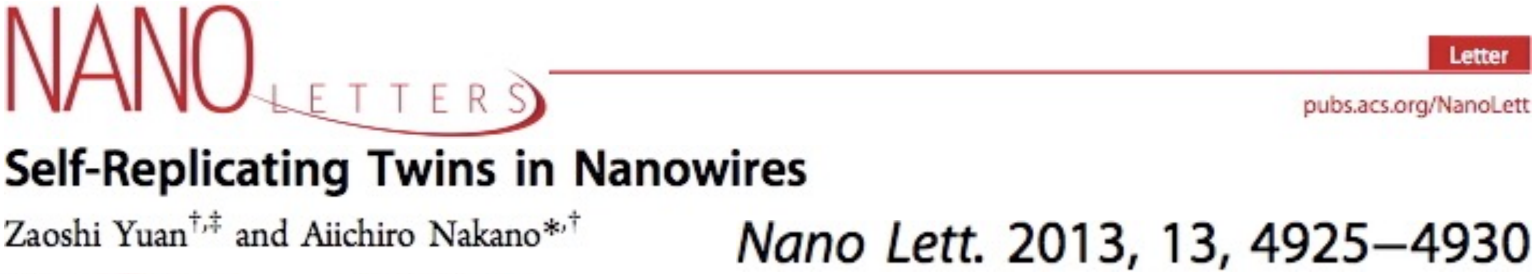

NANO LETTERS
Letter
pubs.acs.org/NanoLett

Self-Replicating Twins in Nanowires

Zaoshi Yuan[†,‡] and Aiichiro Nakano*[,†]

Nano Lett. 2013, 13, 4925–4930

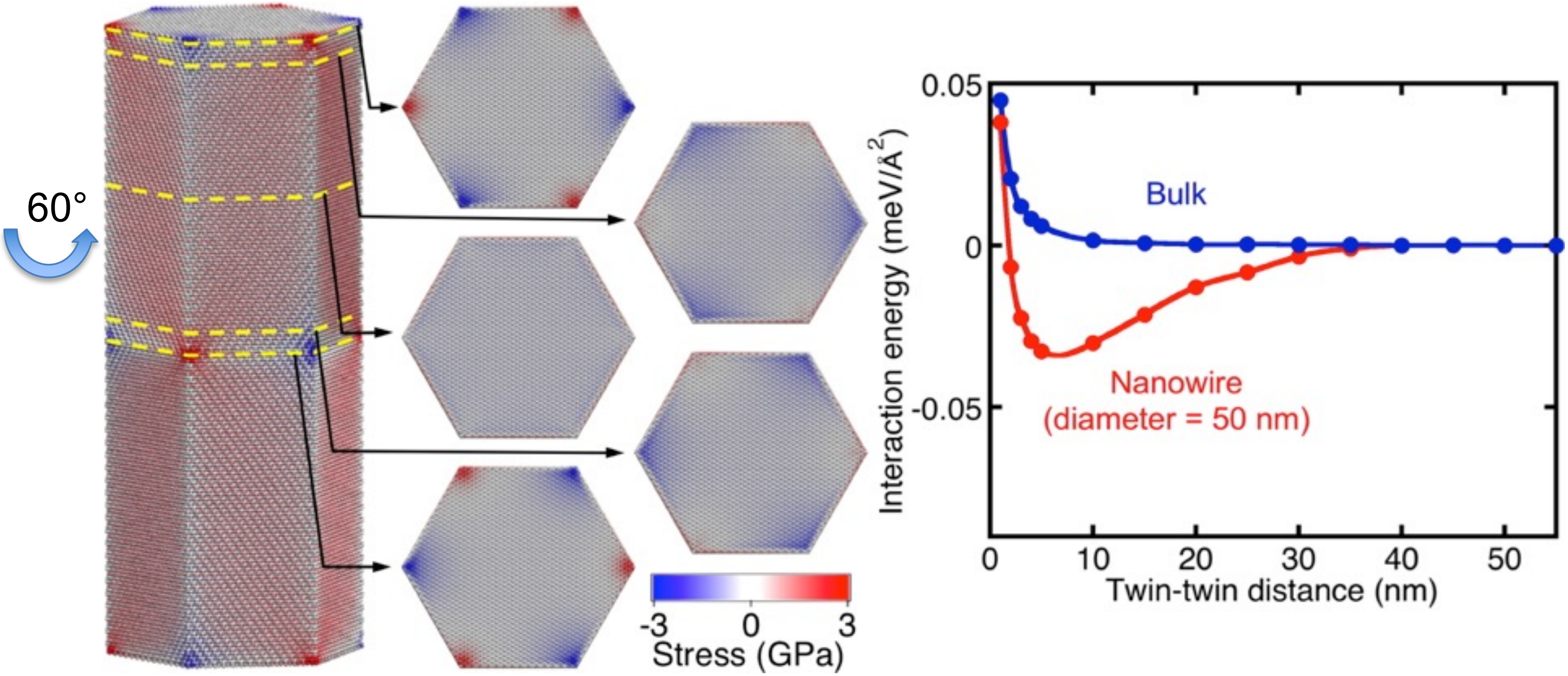

- **Twin planes in a [111] GaAs nanowire attain attractive interaction mediated by surface strain → self-replicating generation of a twin superlattice**

Twinned GaAs Nanosheet (NS)

Relaxed GaAs crystal viewed from the [112] direction

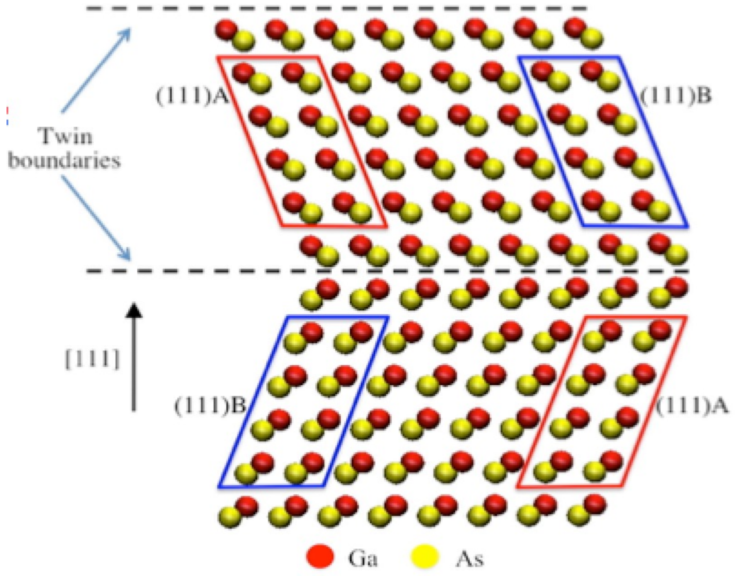

Top view of the Ga-adatom reconstruction of GaAs (111)B surface

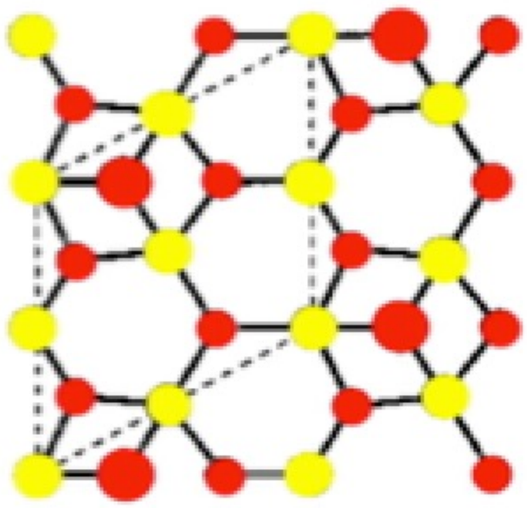

Top view of the Ga-vacancy reconstruction of (111)A surface

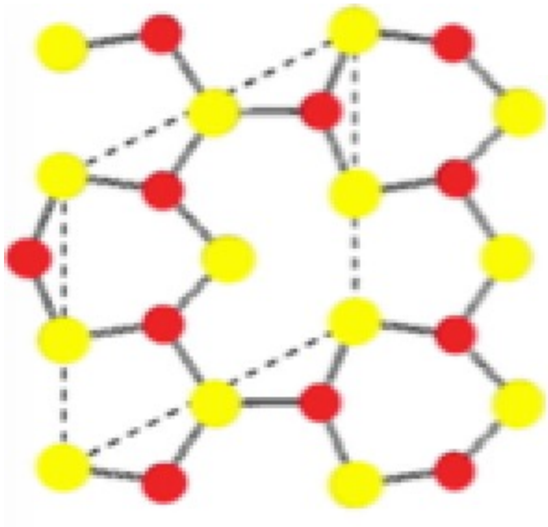

- **These energetically lower reconstructed surfaces are charge-neutral**
- **NS with these reconstructed sidewall surfaces remains stable during quasi-Newton energy minimization**

Sheng *et al.*, *Appl. Phys. Lett*. **105**, 231602 ('14)

KS Energy Projection: Band Alignment

Electronic partial densities-of-states (PDOS) projected onto the (111)A and (111)B sidewall

Schematic of the bulk CB (orange) and VB (green) along with (111)A (red) and (111)B (blue) surface-state energies

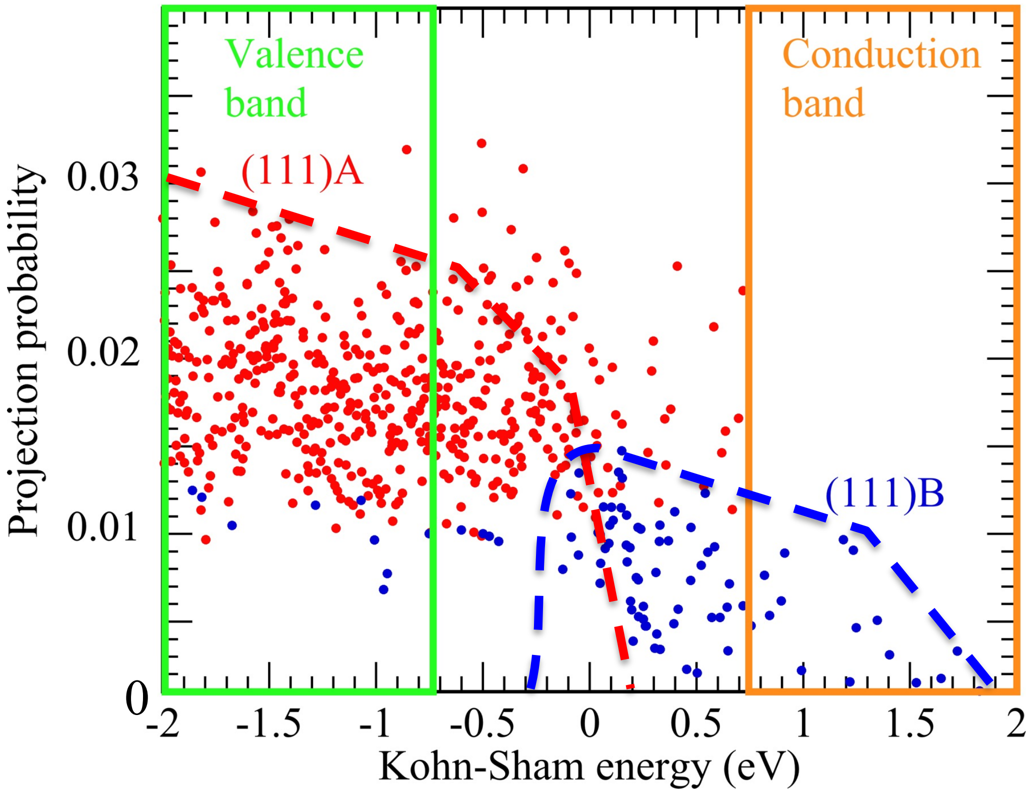

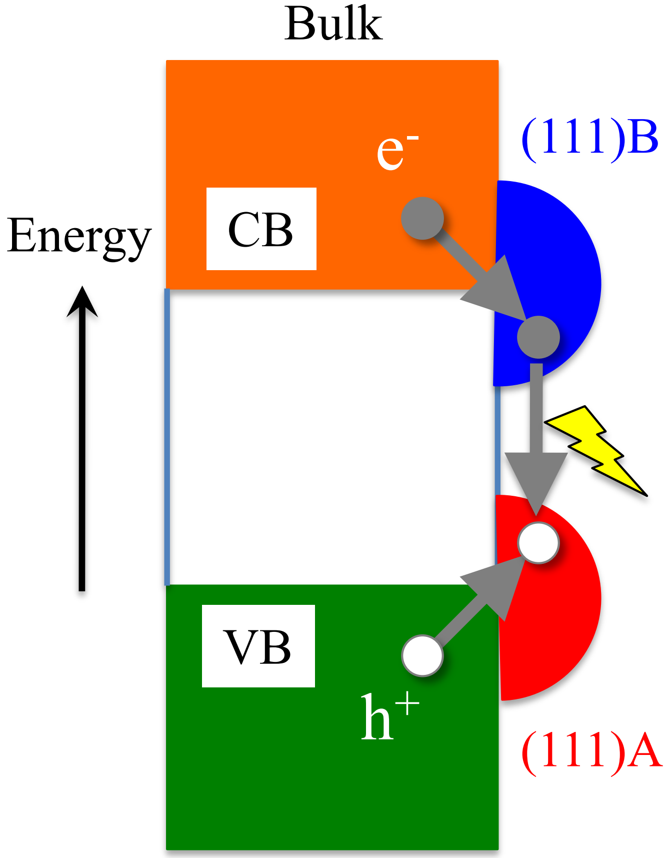

- **Gap states derived from (111)A surfaces are located just above bulk valence band (VB) top**
- **Gap states derived from (111)B surfaces are located just below bulk conduction band (CB) bottom**

Bulk-State Photoexcitation

- NAQMD simulation for electron excitation: bulk VB top → bulk CB bottom
- Energy relaxation of photoexcited electron-hole pairs

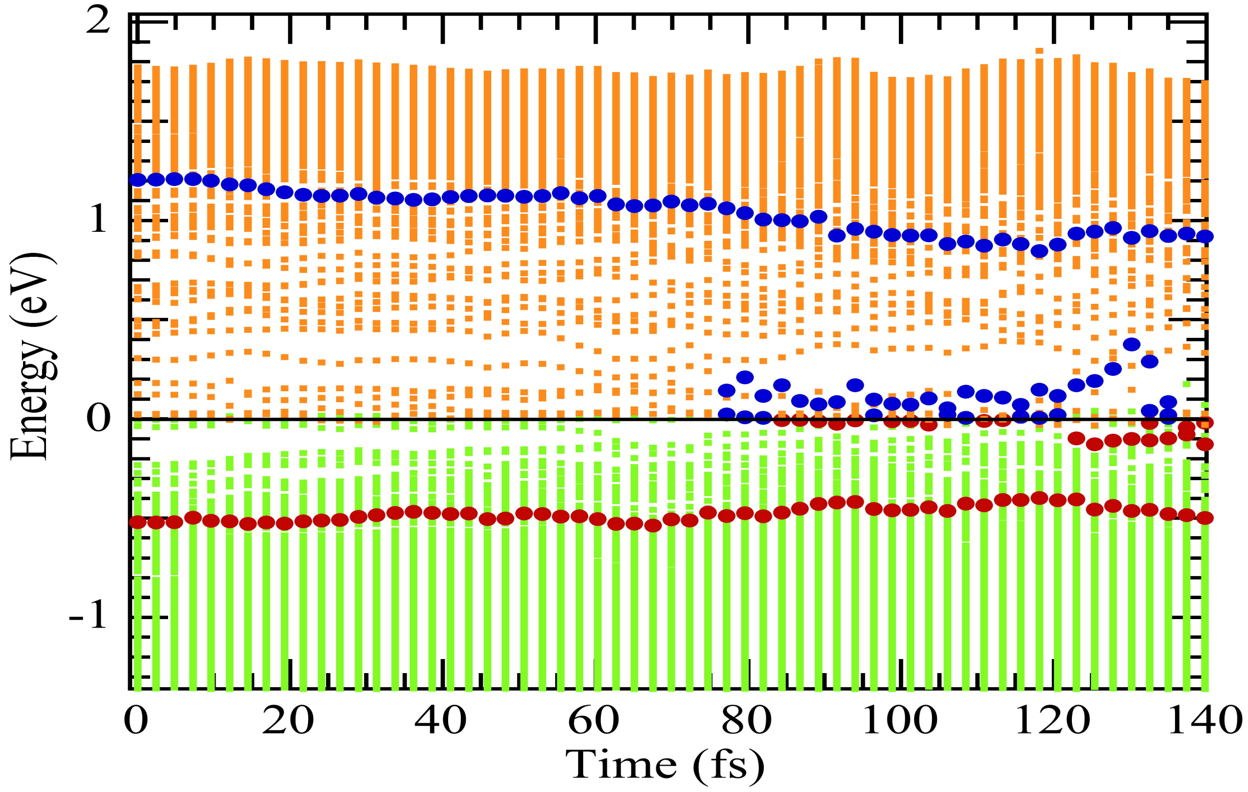

- Initially, only one electron-hole pair exists
- More electron-hole pairs are created starting at ~80 fs near the Fermi energy

Energy Relaxation on Surface

Logarithm of average excitation energy as a function of time

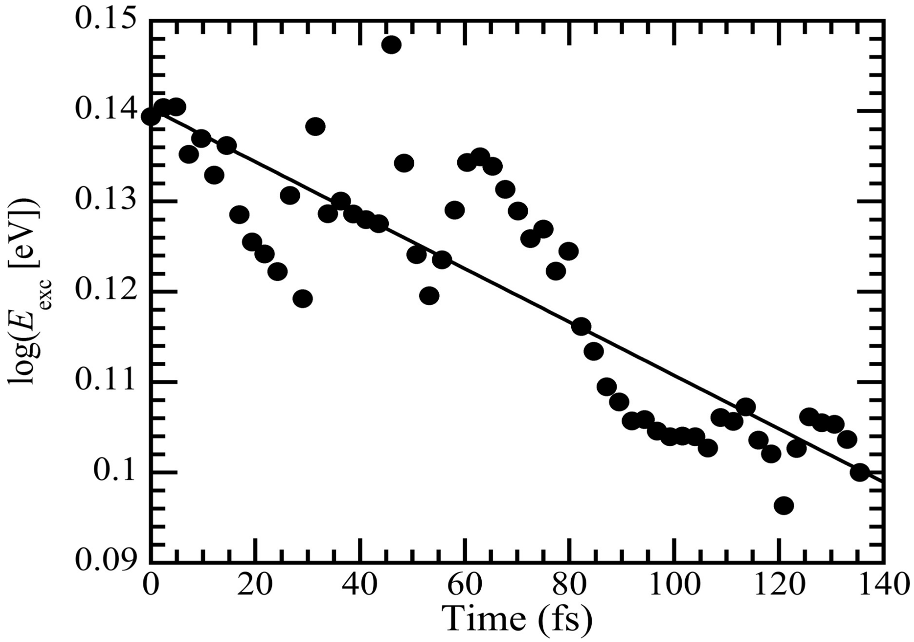

Average electronic excitation energy as a function of time

k_{CR} **= (3.0 ± 0.2)×10^{11} (s^{-1})**

Average electronic excitation energy

$$\bar{E}(t)=\frac{\sum_{i=1}^{iF}(2-n_i(t))(\varepsilon_F(t)-\varepsilon_i(t))+\sum_{i=iF+1}^{\infty}n_i(t)(\varepsilon_i(t)-\varepsilon_F(t))}{\dfrac{\sum_{i=1}^{iF}(2-n_i(t))+\sum_{i=iF+1}^{\infty}n_i(t)}{2}}$$

$\varepsilon_i(t)$ is the *ith* KS energy

Charge recombination rates

k_{CR} **= (3.0 ± 0.2)×10^{11} (s^{-1}) (111)**

k_{CR}**= (1.8 ± 0.1)x10^{7} (s^{-1}) (110)**

- **Calculated CR rate at (110) surface is orders-of-magnitude smaller**
- **Much larger CR rate (~10^{11} s^{-1}) is likely due to the twin superlattice-related surface geometry**

Modelling Carrier-Population Kinetics

- Core-shell structure GaAs nanowire with diameter *D*
- Aiming at estimating the surface recombination velocity

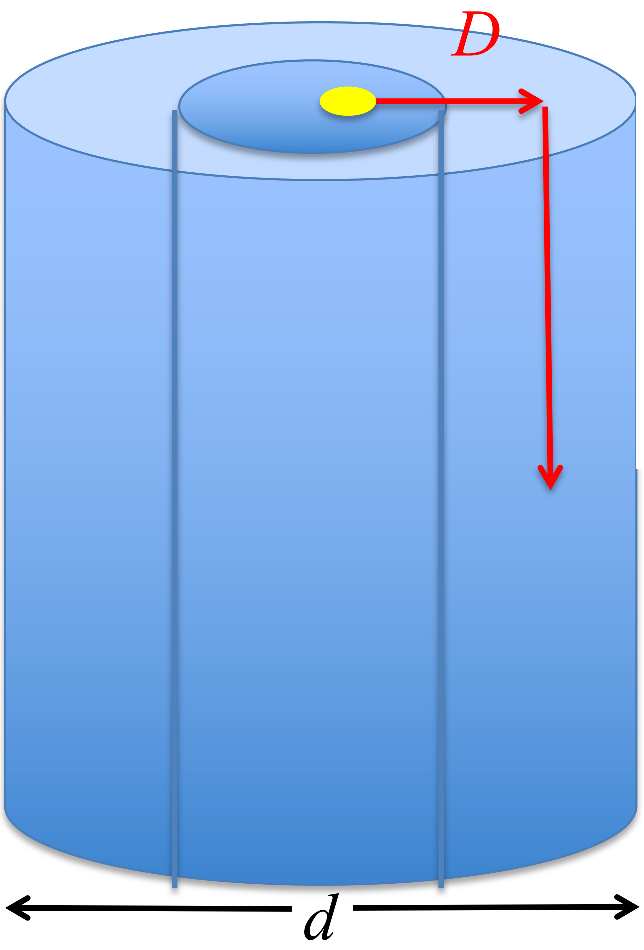

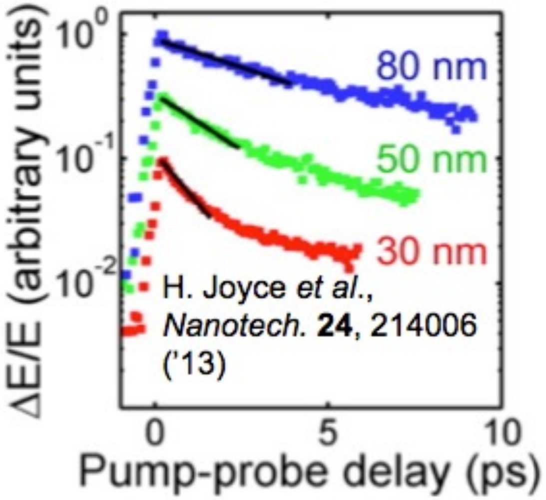

H. Joyce *et al.*, *Nanotech.* **24**, 214006 ('13)

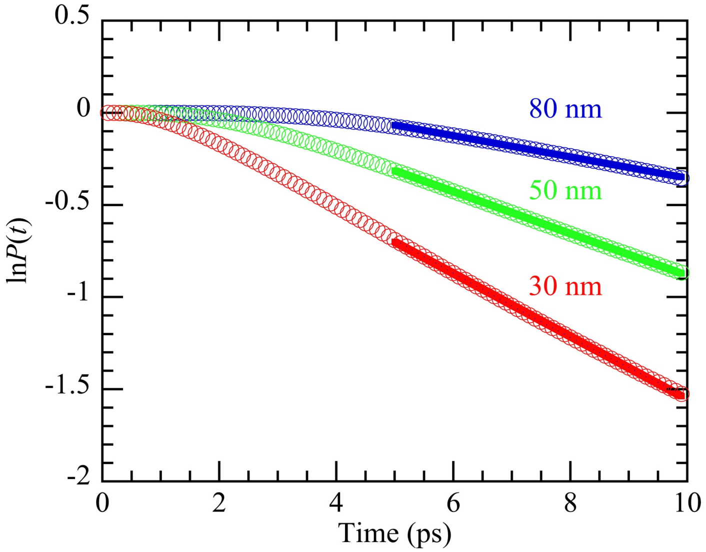

1. Faster decay with decreasing diameter in agreement with experiments;
2. Decay time with realistic [111] sidewalls is consistent with experimental data

Surface Recombination Velocity

CR rate as a function of the NW diameter

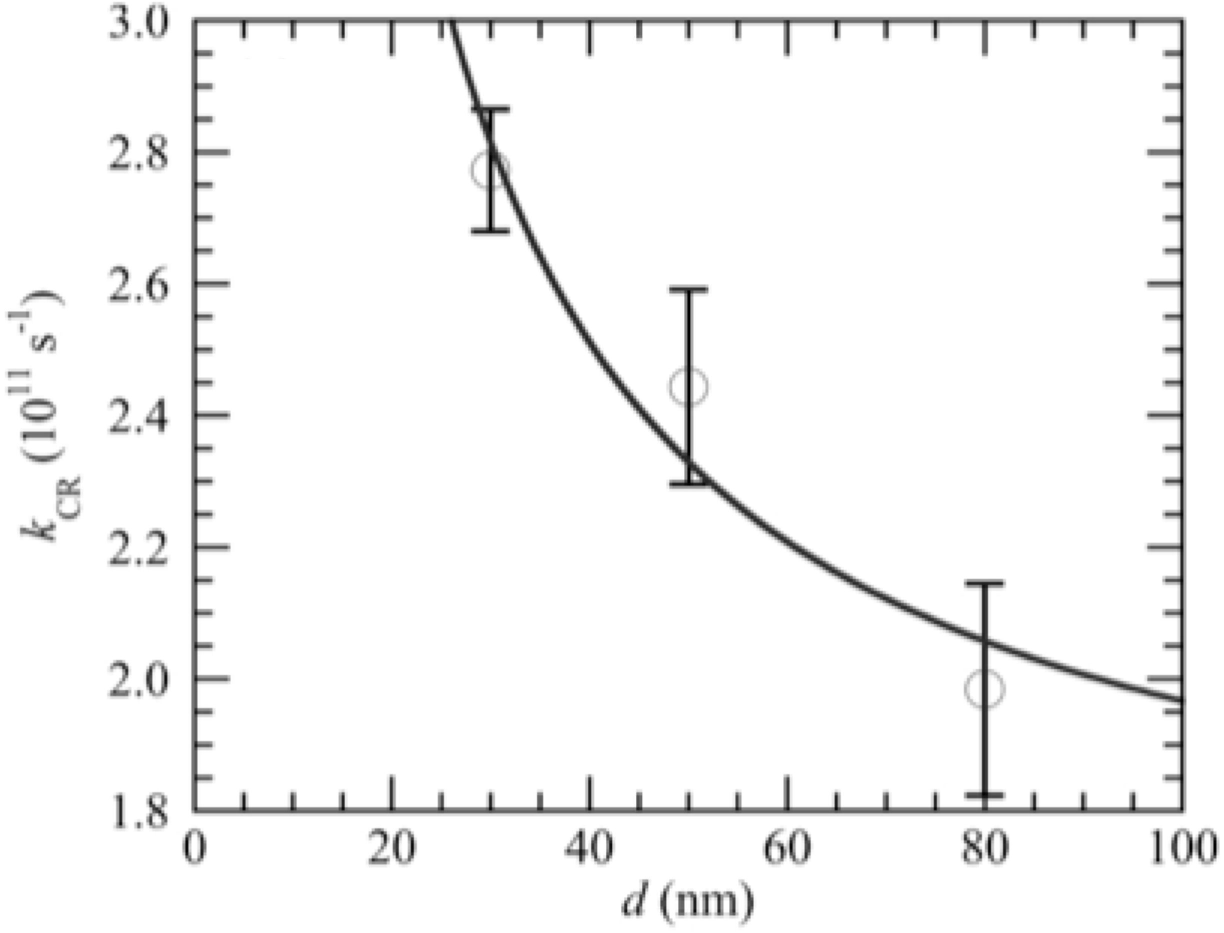

Surface recombination velocity (SRV) in NW

$$k_{CR}(D) = k_{CR}^{\infty} + \frac{4S}{D}$$

- **Calculated SRV = (3.6 ± 0.9)×10³ m/s** [Sheng *et al.*, *Appl. Phys. Lett*. **105**, 231602 ('14)]
- **Good agreement with the experimental value (5.4×10³ m/s)** [Joyce *et al.*, *Nanotechnol* **24**, 214006 ('13)]

Hybrid Organic/Inorganic Photovoltaics

- **Hybrid P3HT (poly[3-hexylthiophene])/ZnO-nanowire photovoltaics for scalable manufacturing**

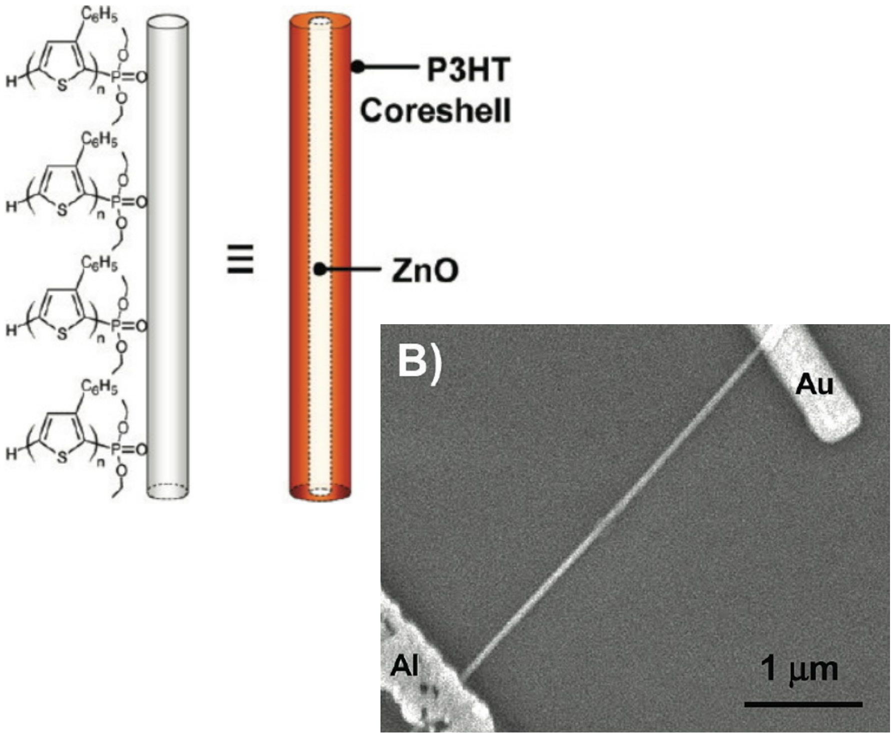

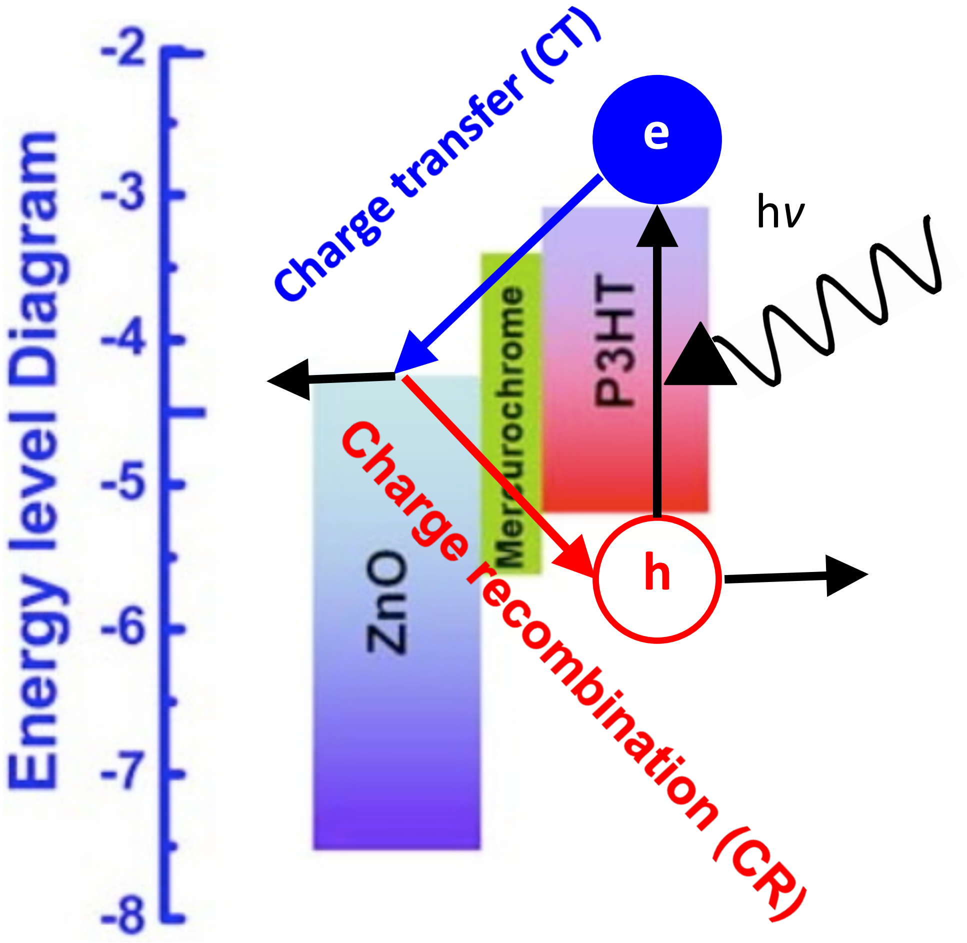

Briseno *et al.*, *Nano Lett.* **10**, 334 ('10)

Lin *et al.*, *Appl. Phys. Lett.* **94**, 064308 ('09)

- **Problem: Interfacial molecular design principles for enhancing charge transfer (CT) & suppressing charge recombination (CR)?**

Effects of Molecular Disorder on CT/CR

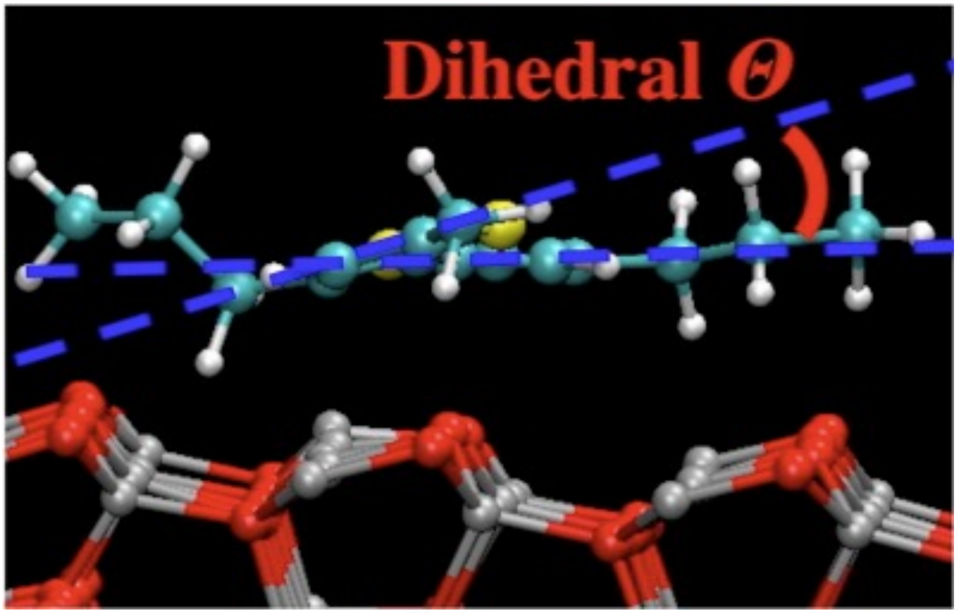

- **552-atom nonadiabatic quantum molecular dynamics simulation of P3HT on ZnO $(10\bar{1}0)$**
- **Twisting of P3HT (static disorder) increases charge-recombination (CR) rate, but not affects charge-transfer (CT) rate**

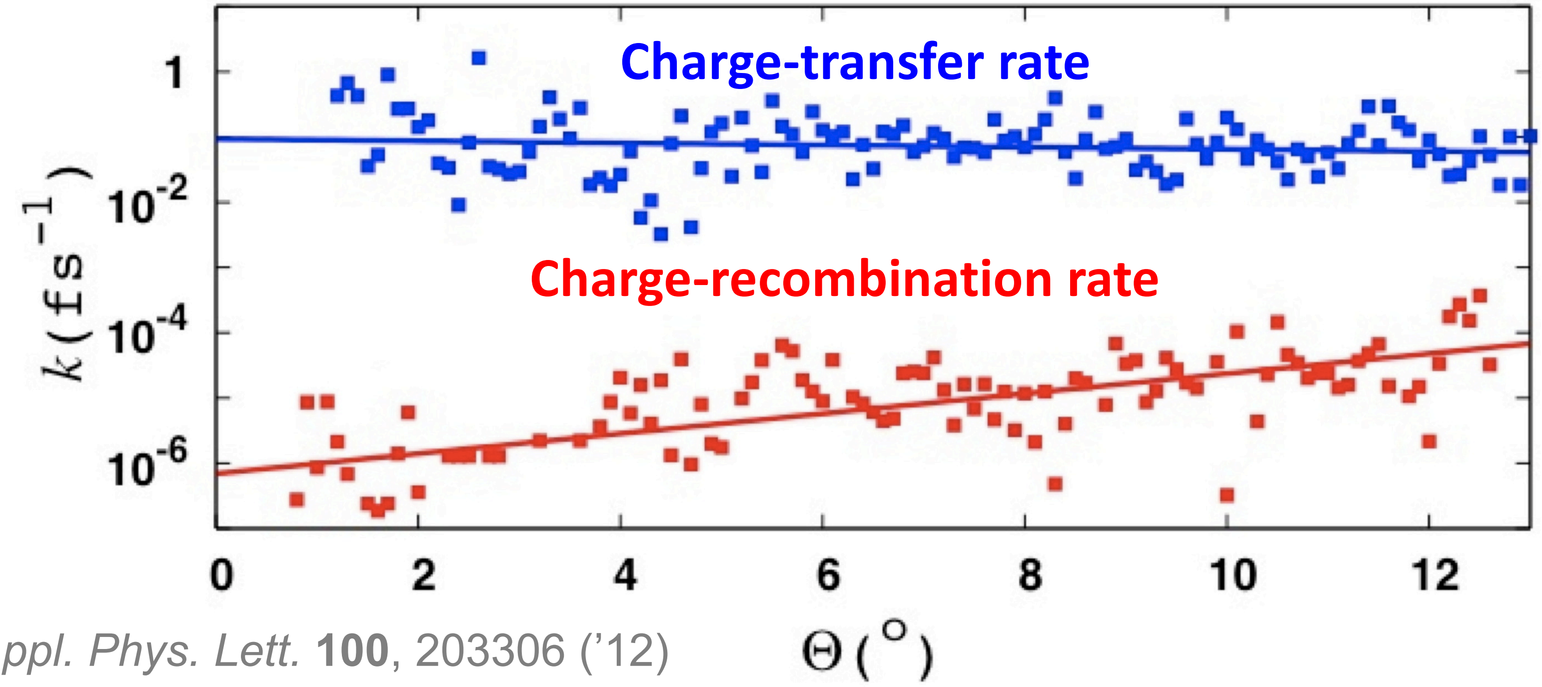

Mou *et al.*, *Appl. Phys. Lett.* **100**, 203306 ('12)

Molecular Mechanism

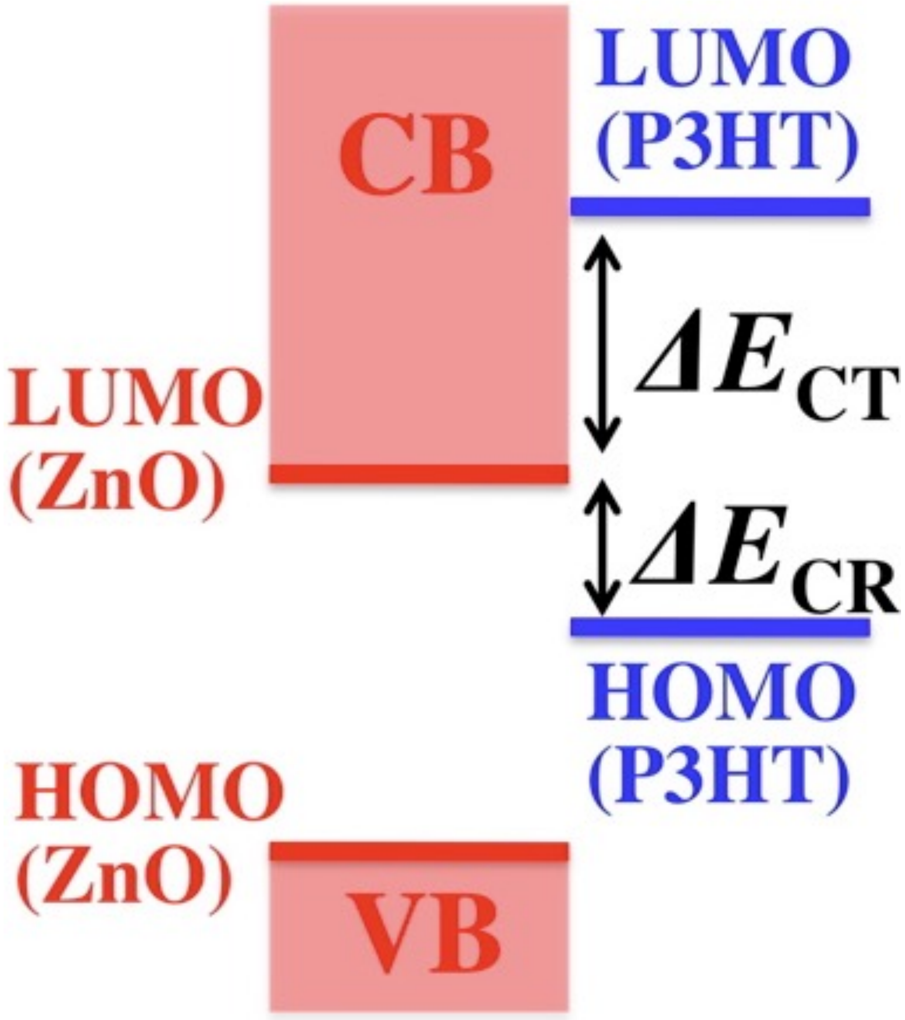

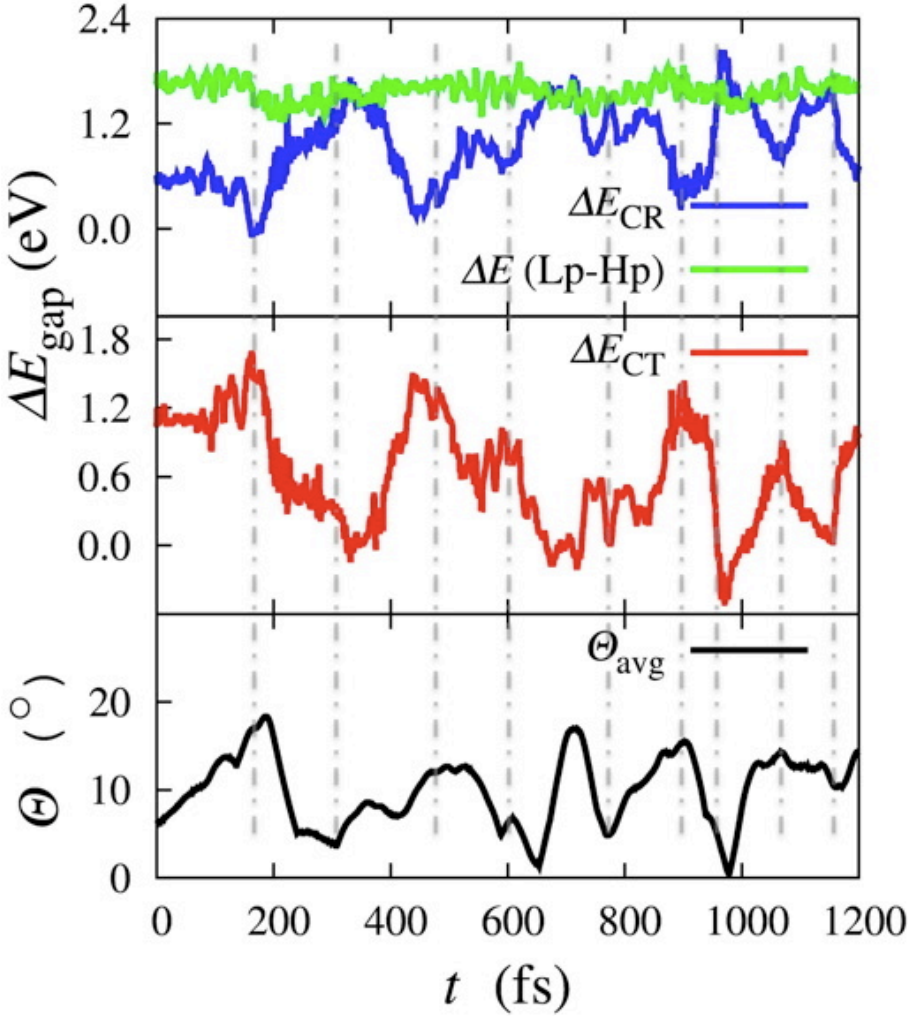

Effect of Dynamic Disorder

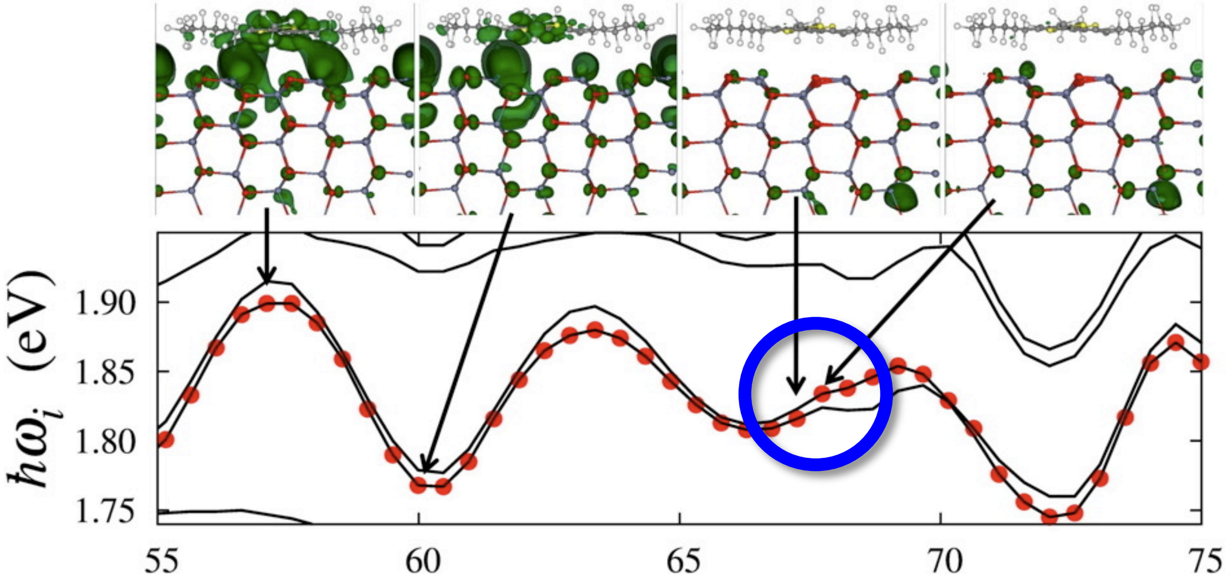

- **Energy-level fluctuation of period ~6 fs assists electronic transition**

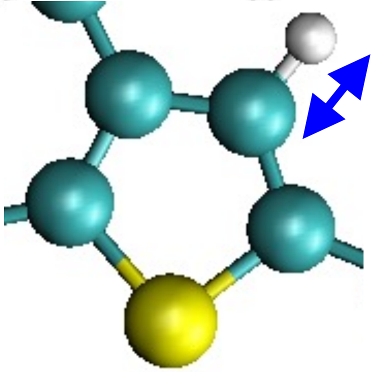

- **Thermal vibration of C-H bonds on the backbone chain around their equilibrium length assists charge transfer**

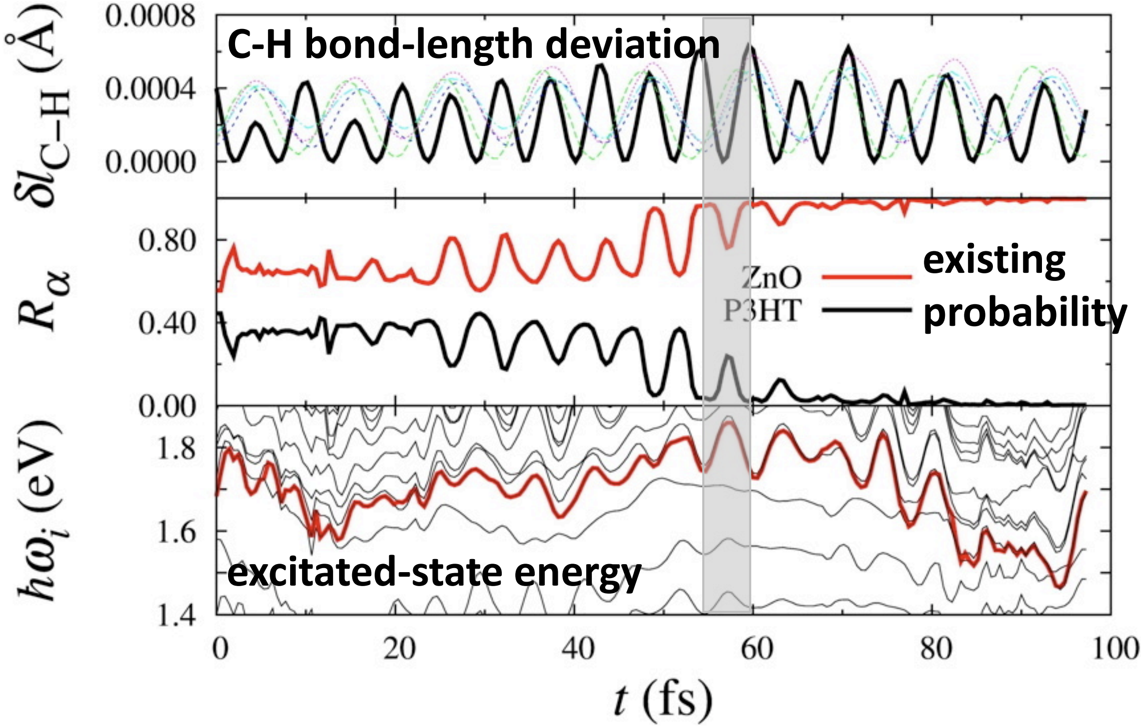

Interfacial Molecular-Design Principle

- *Static disorder* of P3HT conformation is *detrimental* to the efficiency of hybrid P3HT/ZnO photovoltaics by increasing the charge-recombination rate
- *Dynamic disorder* (*i.e.*, thermal fluctuation of C-H bonds in P3HT) is *essential* for high efficiency by assisting charge transfer
- A design principle for efficient photovoltaics—weak interfacial bonding: (1) avoid *static disorder*; (2) promote *dynamic disorder*
- **Example:** Grazing incidence x-ray diffraction & photocurrent measurements show increase of photocurrent with improved P3HT crystallinity near P3HT/ZnO interfaces due to the insertion of an alkane-thiol self-assembled monolayer

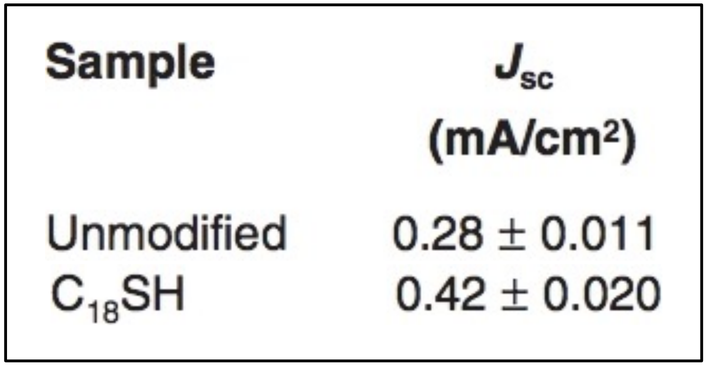

Sample	J_{sc} (mA/cm²)
Unmodified	0.28 ± 0.011
$C_{18}SH$	0.42 ± 0.020

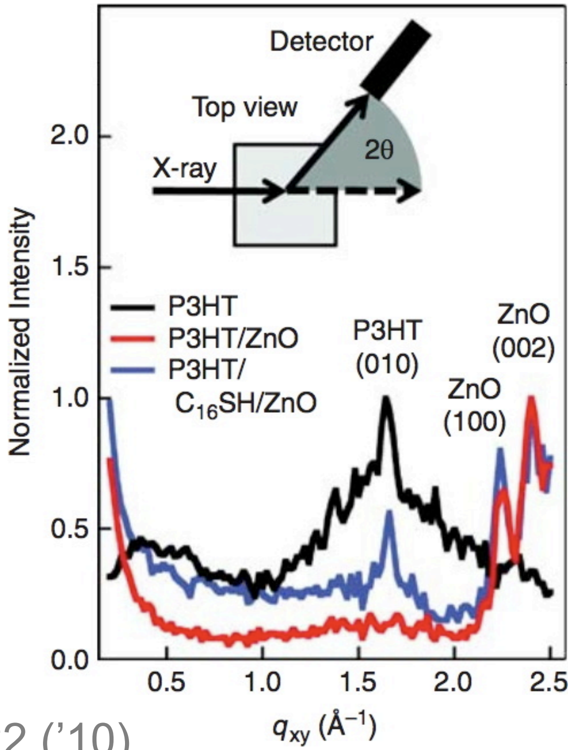

Hsu & Lloyd, *MRS Bulletin* **35**, 422 ('10)

Photoexcited Carriers in MAPbI$_3$

- **Organometal halide perovskites (*e.g.* methylammonium lead iodide, $CH_3NH_3PbI_3$ or $MAPbI_3$) for solar cells with high power conversion efficiency > 20%**
  Stranks & Snaith, *Nat. Nanotechnol.* **10**, 391 ('15)

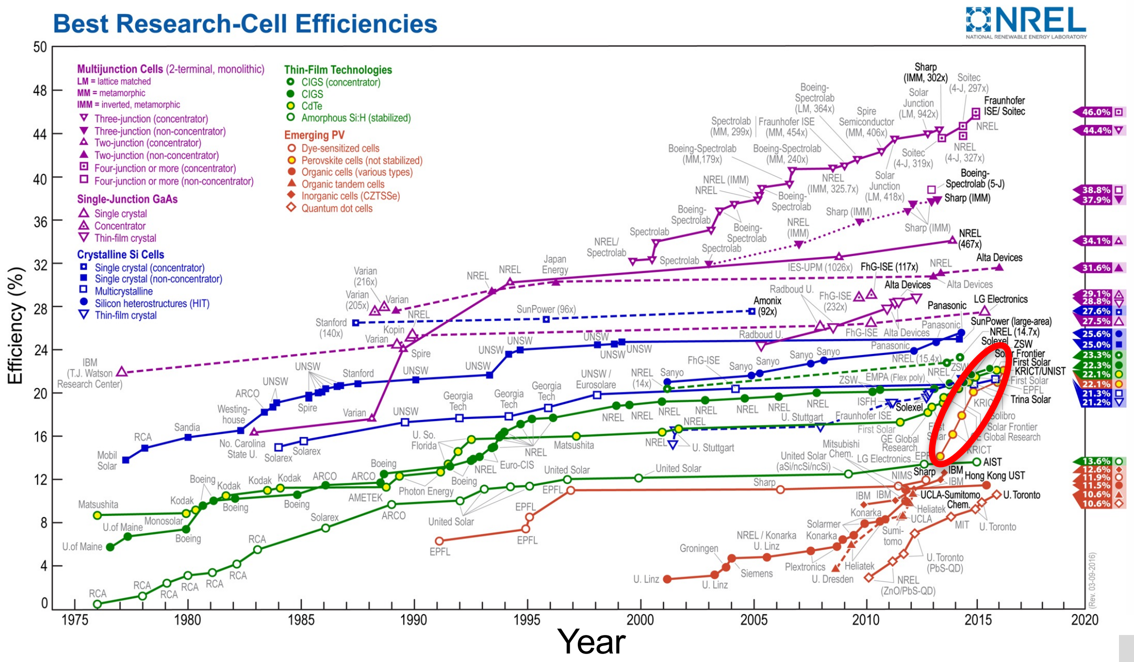

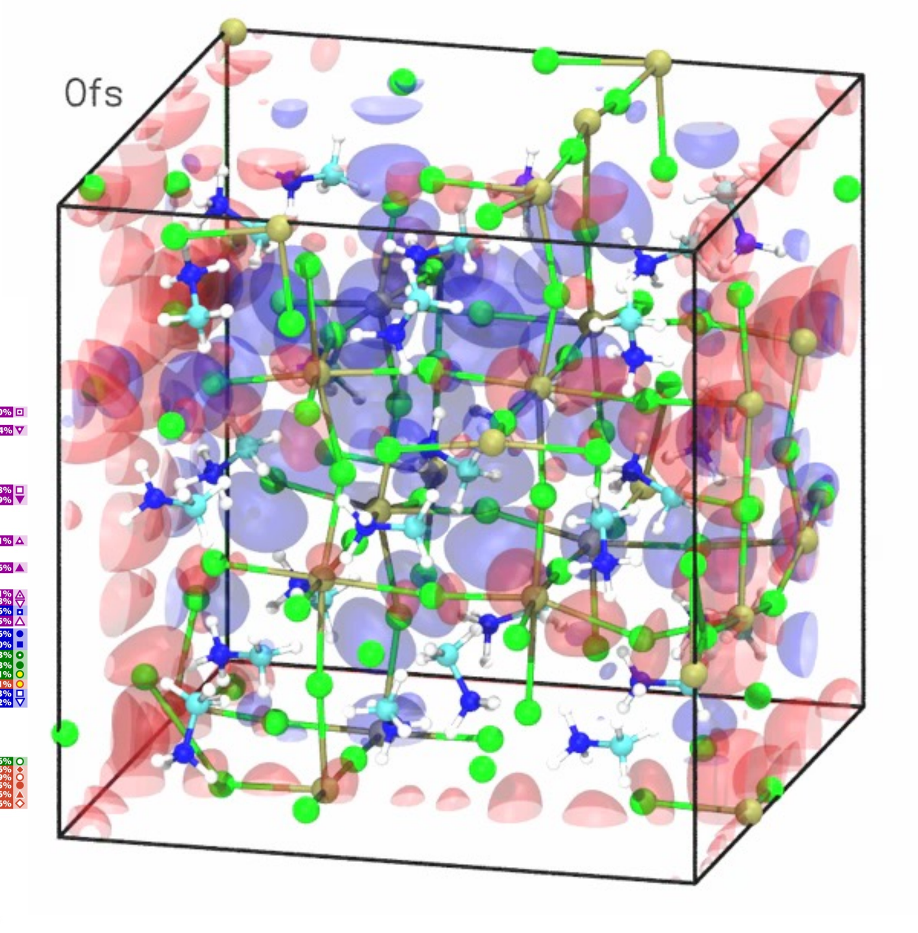

Quasi-electron Quasi-hole H, C, N, I, Pb

- **Nonabiabatic QMD simulation**
  Pb & I sublattices act as disjunct pathways for rapid & balanced transport of free electrons & holes—electron (63% Pb-6p) & hole (90% I-5p); diffusion coefficients $D_e = (1.16\pm0.31)\times10^{-2}$ cm^2/s & $D_h = (1.01\pm0.42)\times10^{-2}$ cm^2/s
  Expt: $D_e = (1.7\pm1.1)\times10^{-2}$ cm^2/s & $D_h = (1.1\pm0.7)\times10^{-2}$ cm^2/s [Stranks *et al.*, *Science* **342**, 341 ('13)]

Rapid & Balanced Carrier Transport

- **Separate electron & hole express lanes are the key nanostructural feature for rapid & balanced carrier transport: $D_e = (1.16 \pm 0.31) \times 10^{-2}$ cm²/s & $D_h = (1.01 \pm 0.42) \times 10^{-2}$ cm²/s**

Expt: $D_e = (1.7 \pm 1.1) \times 10^{-2}$ cm²/s & $D_h = (1.1 \pm 0.7) \times 10^{-2}$ cm²/s [Stranks *et al*., *Science* ’13]

Mean-square displacements

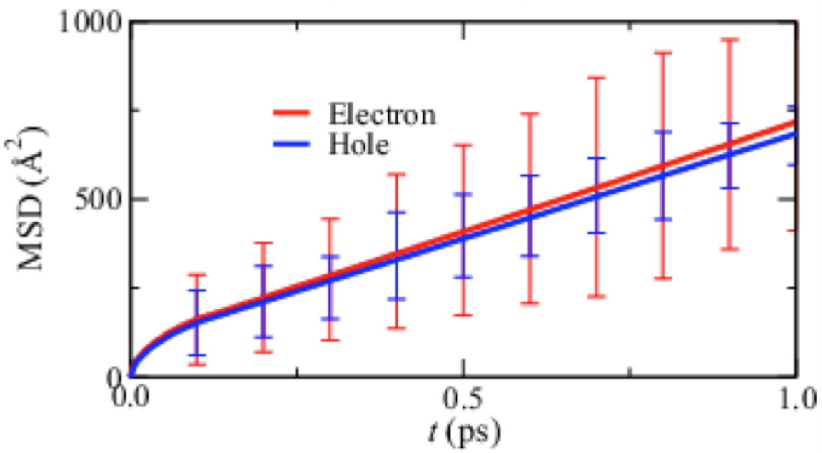

$$x_{\text{COM-PBC}} = \frac{L}{2\pi} \mathrm{Im} \ln \int d\mathbf{r} \, |\psi(\mathbf{r})|^2 \exp(i \frac{2\pi}{L} x)$$

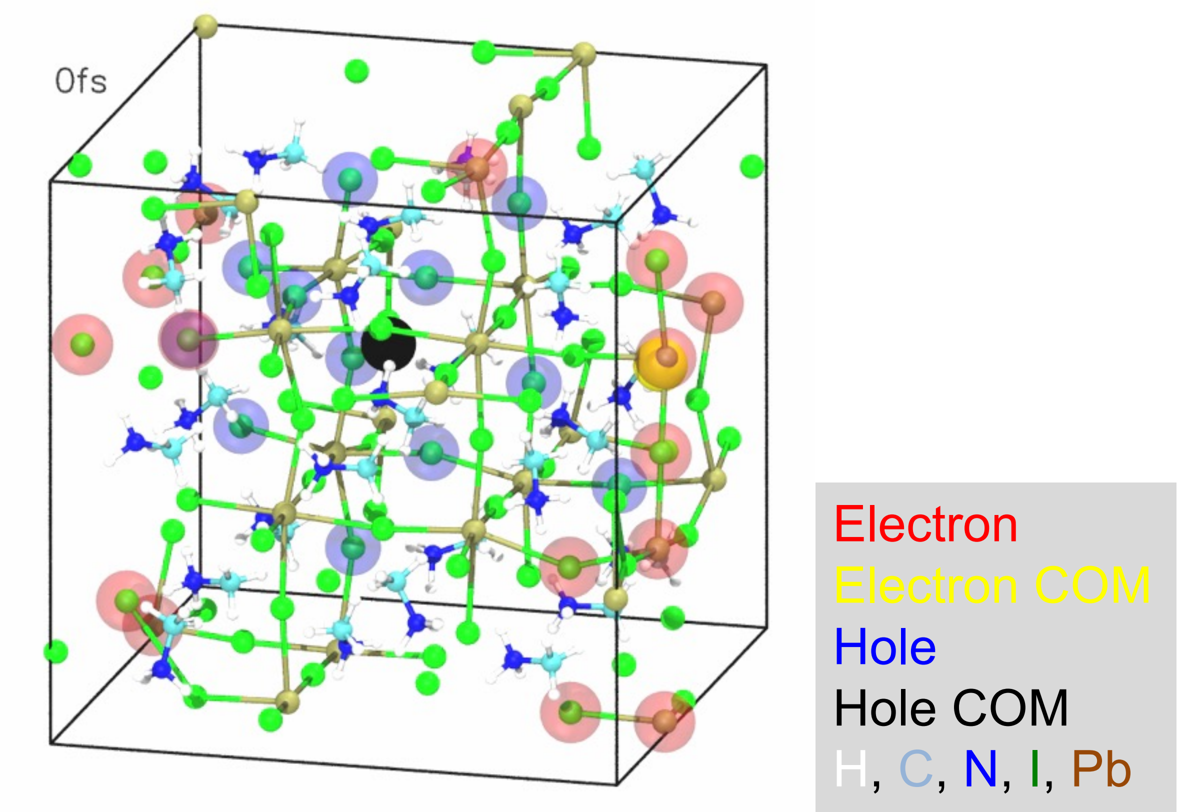

- **Small radiative recombination rate: $\tau^{-1}/\rho = (1.99 \pm 0.43) \times 10^{-12}$ cm³/s**

Hakamata *et al*., *Sci. Rep.* **5**, 19599 (’16)

Screening Role of Methylammonium Sublattice

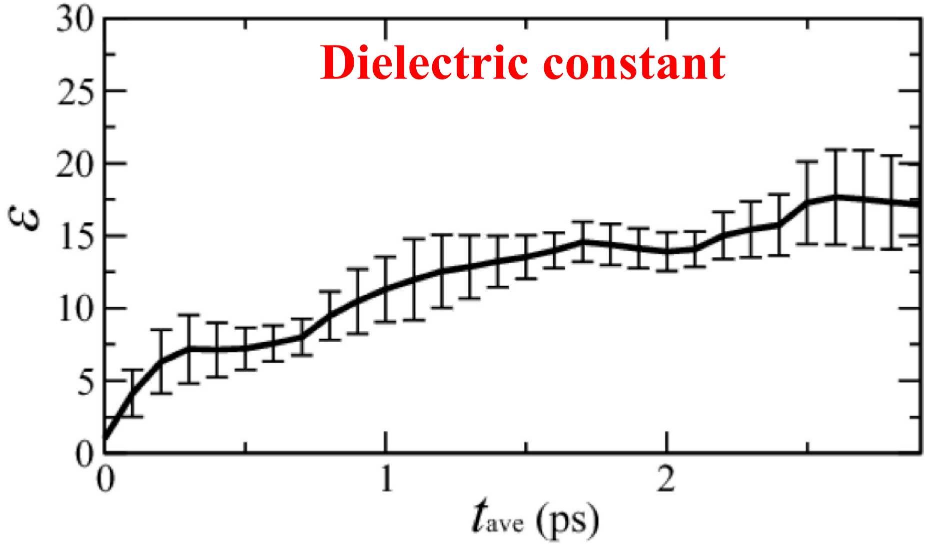

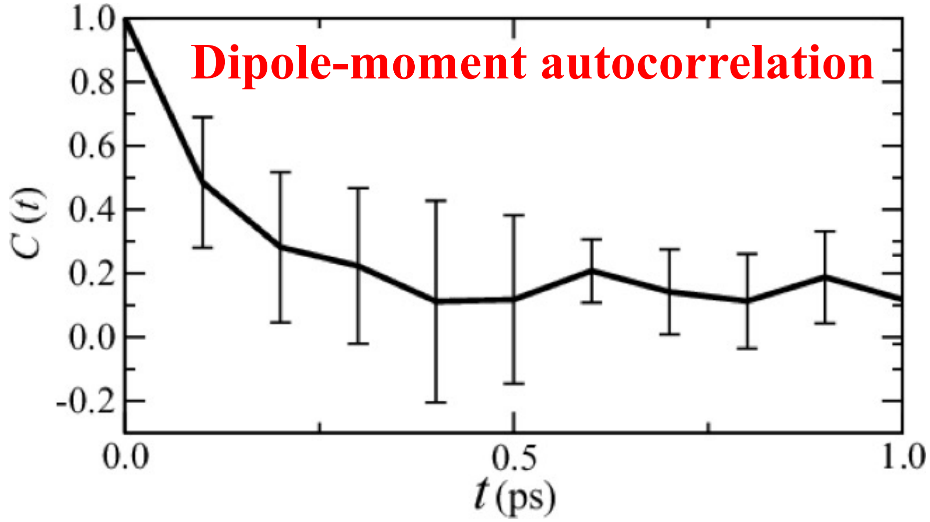

$$\varepsilon = 1 + \frac{4\pi}{3k_B TV}\left(\langle \mathbf{M}^2 \rangle - \langle \mathbf{M} \rangle^2\right)$$

time average

dipole moment

cf. $\varepsilon_{\text{expt}}$ (10^{12} Hz) = 7-10

Lin *et al.*, *Nat. Photonics* **9**, 106 ('15)

$$C(t) = \frac{\langle \mathbf{M}(t+t_0) \cdot \mathbf{M}(t_0) \rangle}{\langle \mathbf{M}(t_0) \cdot \mathbf{M}(t_0) \rangle}$$

Rapid response time ~ 1 ps

cf. $\tau_{\text{expt}} = 2$ ps

Deschler *et al.*, *JPCL* **5**, 1421 ('15)

- **Large dielectric constant of MA sublattice causes small exciton binding energy, 0.012 ± 0.009 eV (experimental upper bound = 0.05 eV** [D'Innocenzo *et al.*, *Nat. Commun*. **5**, 3586 ('14)]**)**
- **MA sublattice quickly screens out electrostatic electron-hole attraction to unbind an exciton & generate free carriers within 1 ps** [*cf*. Zhu *et al.*, *Science* **353**, 1409 ('16)]

Hakamata *et al.*, *Sci. Rep.* **5**, 19599 ('16)

Dielectric Breakdown of Polyethylene

- **NAQMD simulation of hot electrons & holes in polyethylene (PE) slab under electric filed (600 MV/m)**
- **Projected electronic density-of-states (DOE) shows band bending & voltage drop**

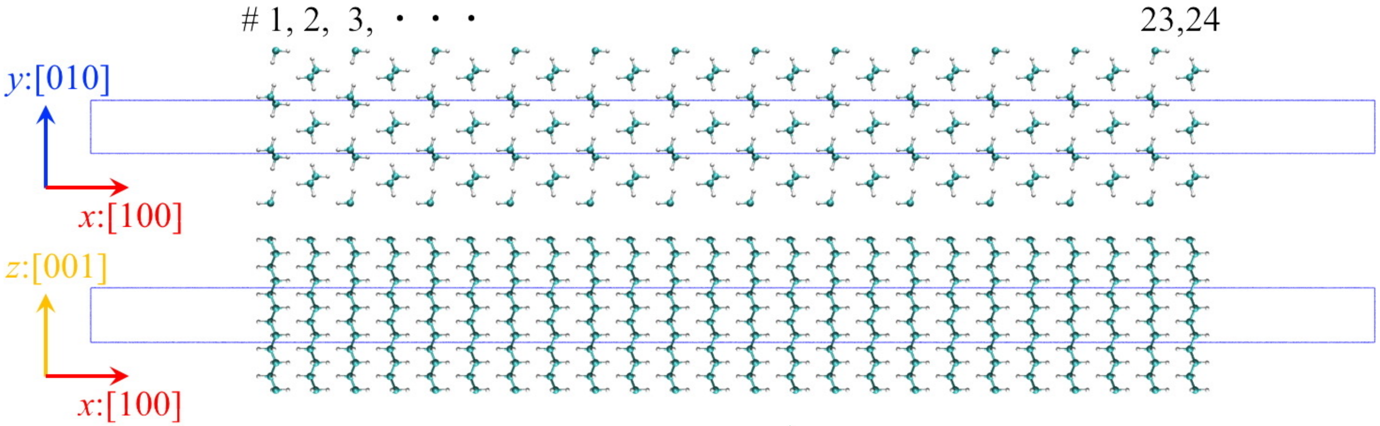

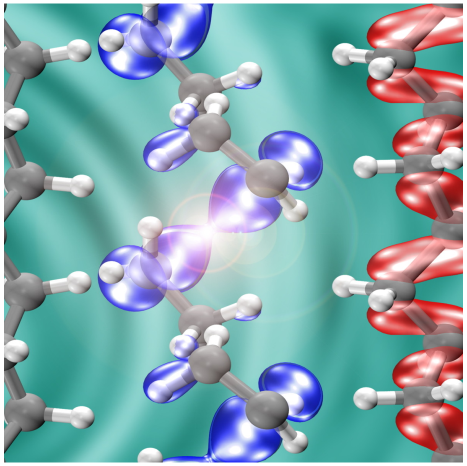

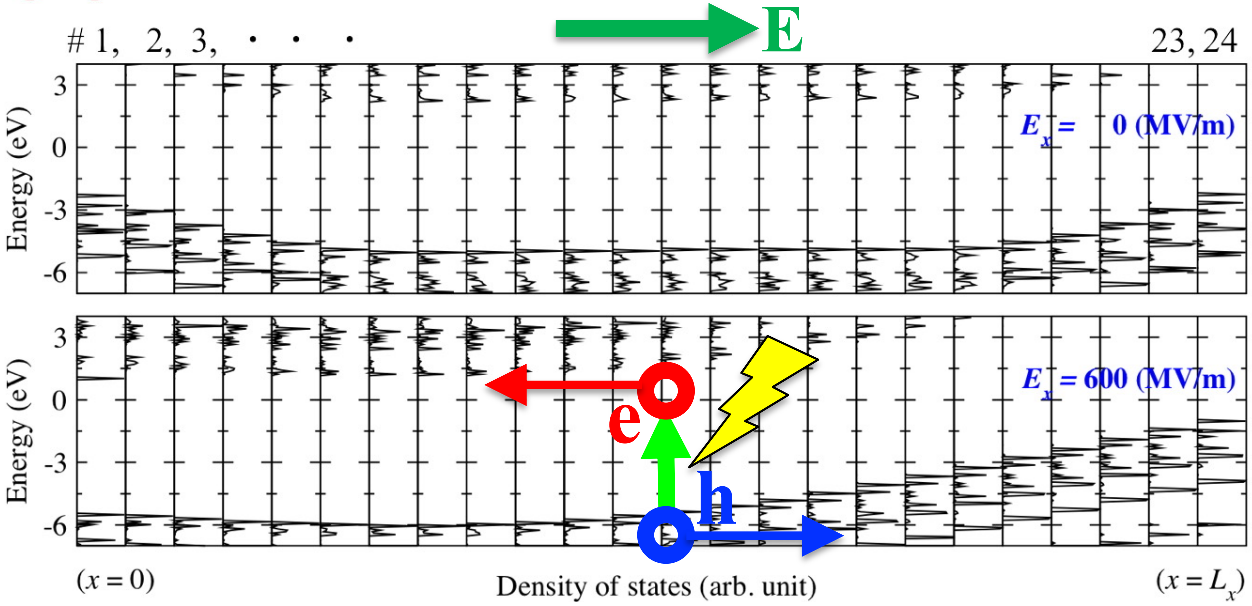

Kumazoe *et al.*, *J. Phys. Chem. Lett*. **10**, 3937 ('19); *ibid*. **11**, 352 ('20)

Rapid Energy Dissipation of Hot Carriers

- **Time evolution of Kohn-Sham energies & average excitation energy**

$$E_{\mathrm{exc}}(t) = \frac{\sum_i f_i(t)\varepsilon_i(t)\Theta\big(\varepsilon_i(t)\big) - \sum_i\big(1 - f_i(t)\big)\varepsilon_i(t)\Theta\big(-\varepsilon_i(t)\big)}{\sum_i f_i(t)\Theta\big(\varepsilon_i(t)\big) + \sum_i\big(1 - f_i(t)\big)\Theta\big(-\varepsilon_i(t)\big)}$$

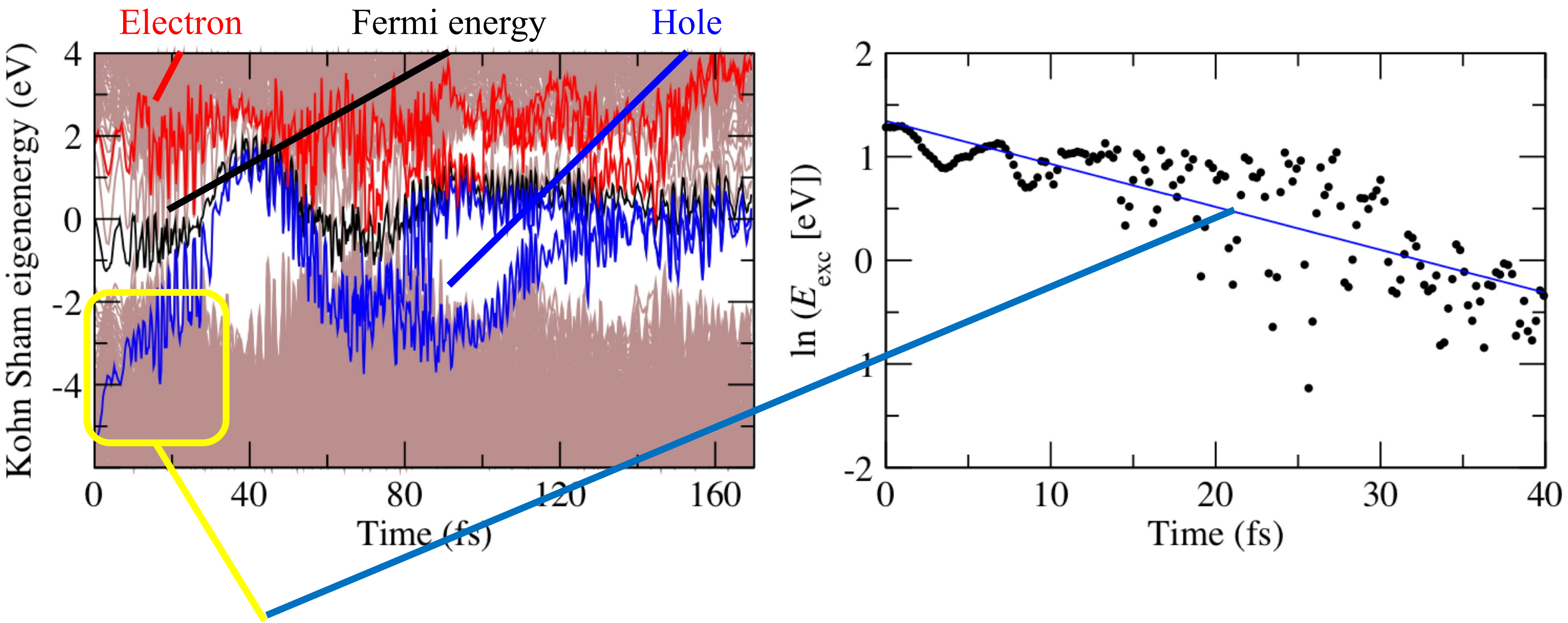

- **Hot carrier relaxes to the band edge within 20 fs at a rate of $k = 4.1\times10^{13}$ s^{-1} due to strong electron-phonon scattering**

Kumazoe *et al.*, *J. Phys. Chem. Lett.* **10**, 3937 ('19); *ibid*. **11**, 352 ('20)

Field-Induced Electron & Hole Dynamics

- **Time evolution of Kohn-Sham energies shows carrier multiplication**

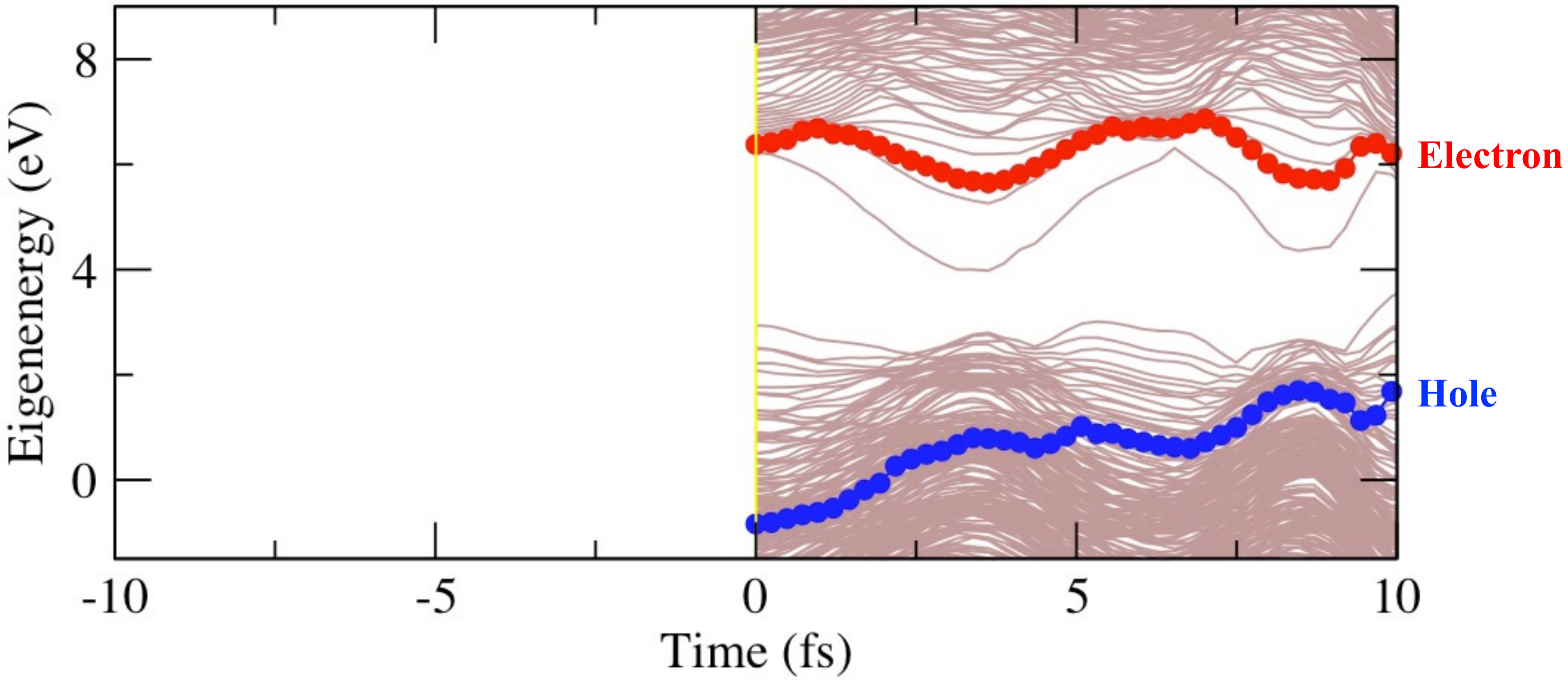

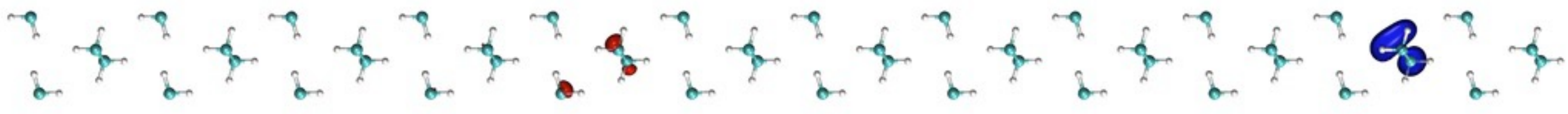

- **Electron (red) & hole (blue) wave functions; holes travel to a slab surface & localize on C-H bonds**

Hot-Carrier Chemistry

- **Highly-localized holes are driven to the low-voltage surface by electric field, causing the elongation & cleavage of C-C bonds**

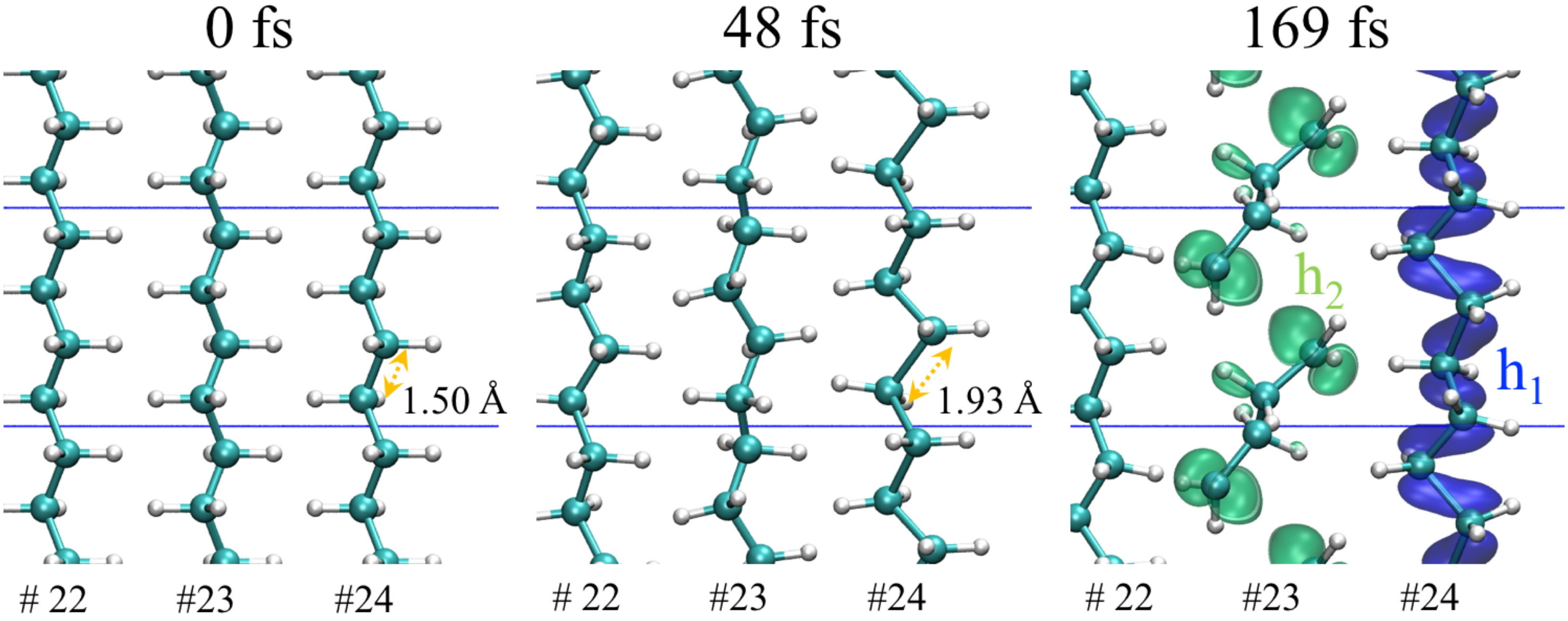

Kumazoe *et al*., *J. Phys. Chem. Lett*. **10**, 3937 ('19); *ibid*. **11**, 352 ('20)

Breakdown-Resistant Coating

- NAQMD shows that coating polyethene (PE) with hexagonal boron nitride (hBN) traps hot carriers injected from metal electrode, thereby mitigating detrimental dielectric breakdown

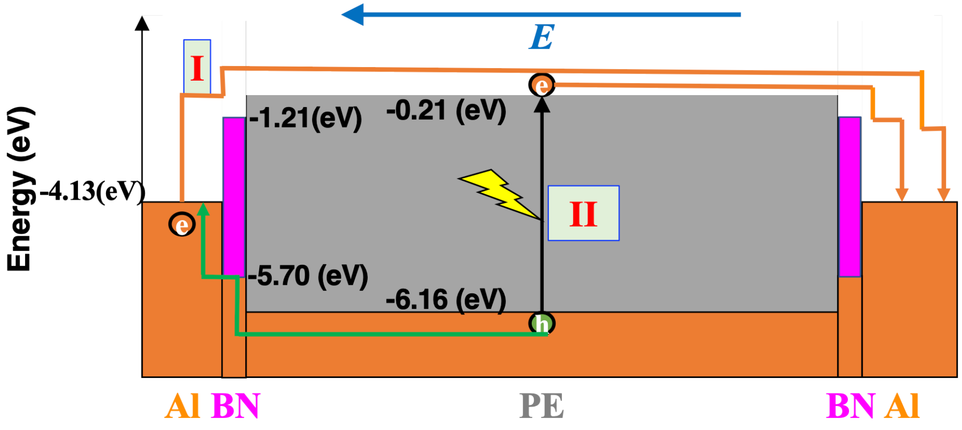

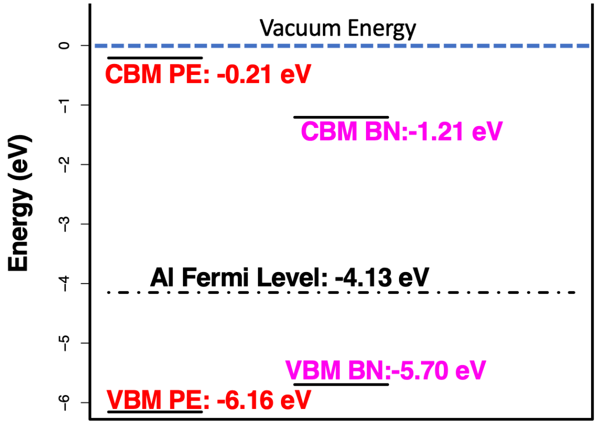

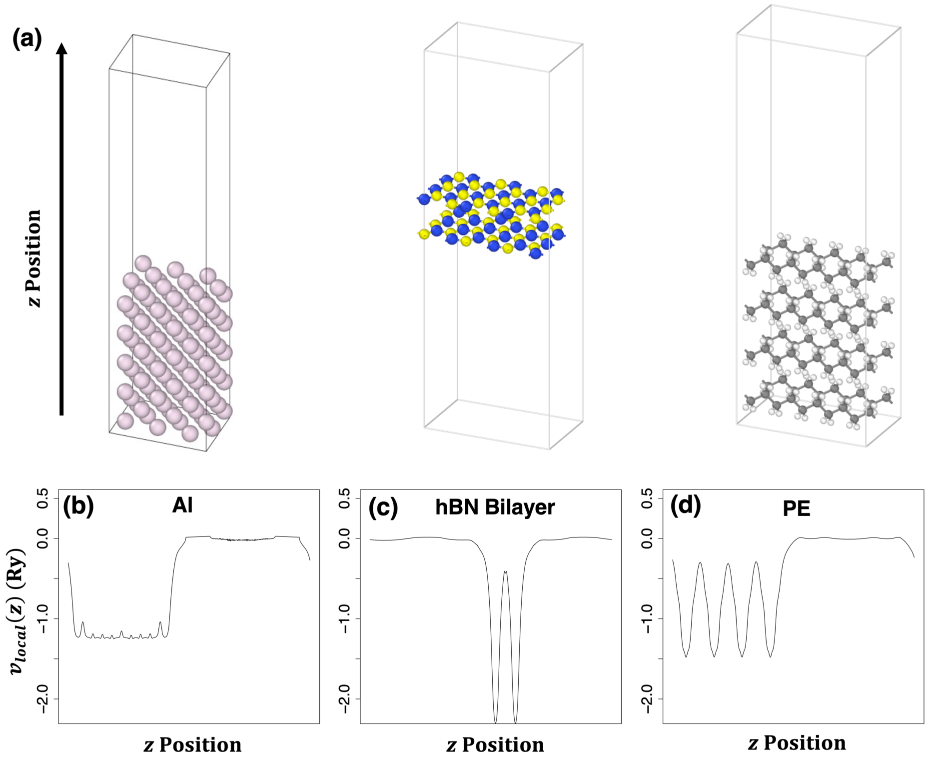

Linker *et al*., *ACS Appl. Mater. Interf*. **13**, 60393 ('21)

Ultrafast Control of Quantum Materials

Goal: Use ultrafast laser pulses to transform material structures & properties (*e.g.*, semiconductor-to-metal) on demand

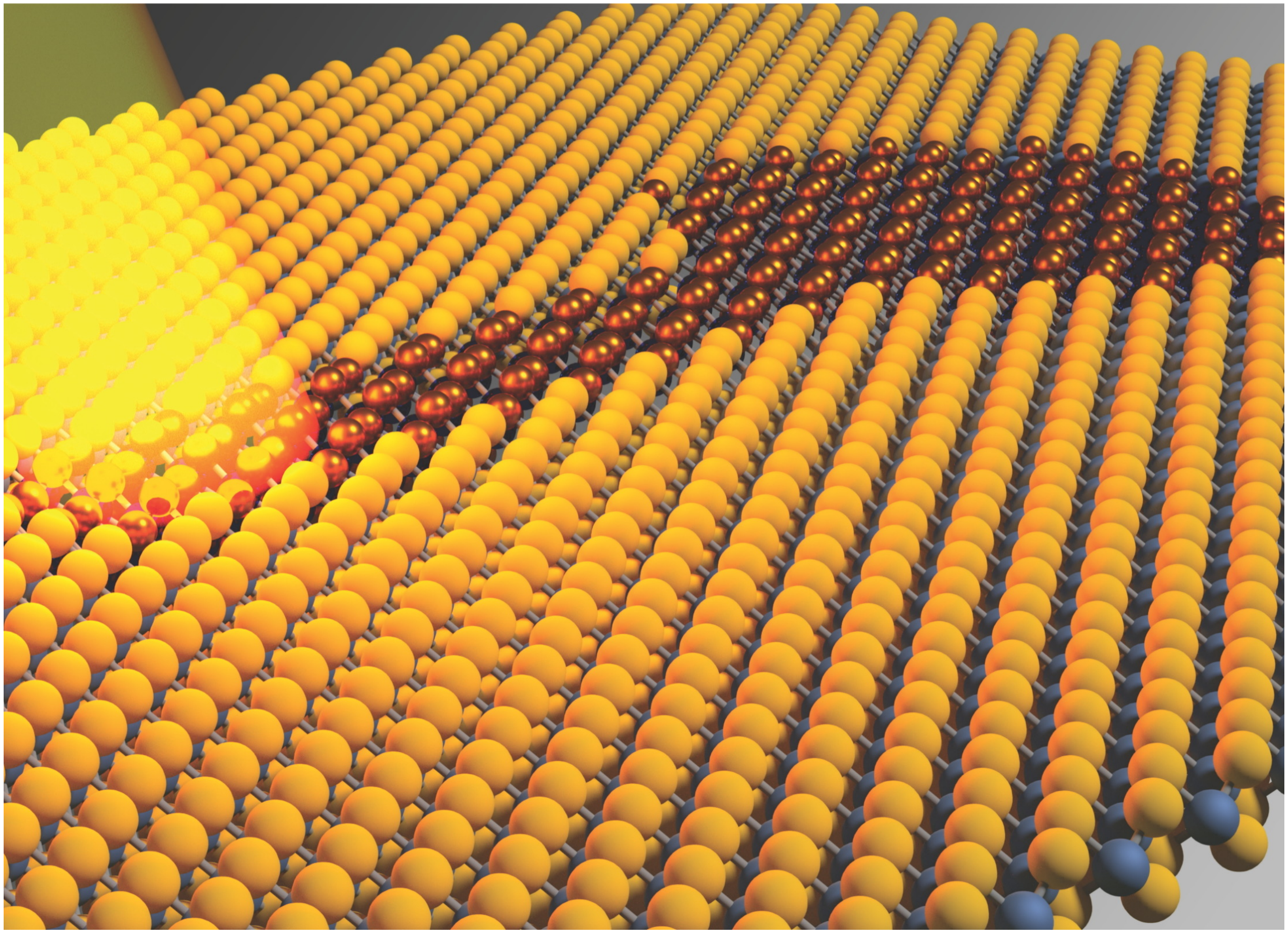

A. Krishnamoorthy *et al.*, *Nanoscale* **10**, 2742 ('18); journal cover

Simulation-Experiment Synergy

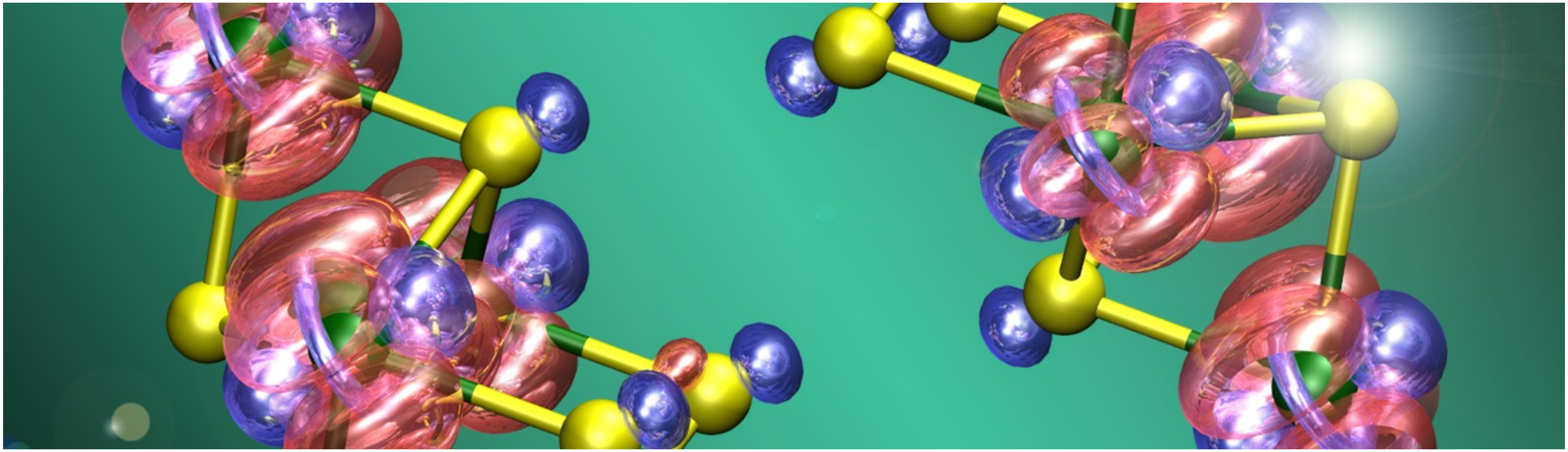

- **In ultrafast 'electron & X-ray cameras,' laser light hitting a material is almost completely converted into nuclear motions — key to switching material properties on & off at will for future electronics applications.**
- **High-end nonadiabatic quantum molecular dynamics simulations reproduce the ultrafast energy conversion at exactly the same space & time scales, and explain it as a consequence of photo-induced phonon softening.**

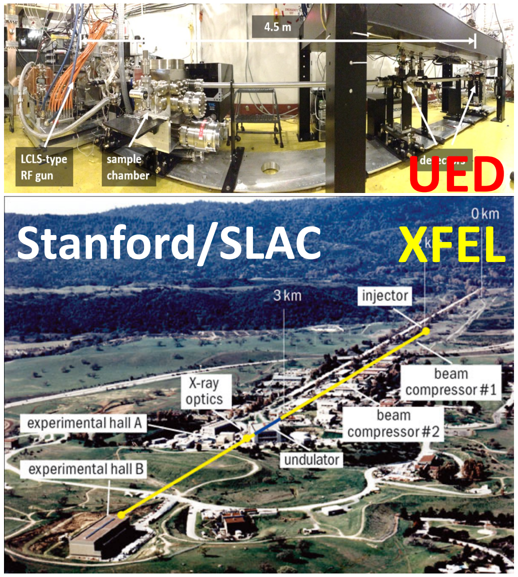

Ultrafast electron diffraction: M. F. Lin *et al*., *Nature Commun*. **8**, 1745 ('17)
X-ray free-electron laser: I. Tung *et al*., *Nature Photon*. **13**, 425 ('19)

Ultrafast Coupled Electron-Lattice Dynamics

- **Ultrafast electron diffraction experiment shows nearly perfect energy conversion from electronic excitation to lattice motions within ps**

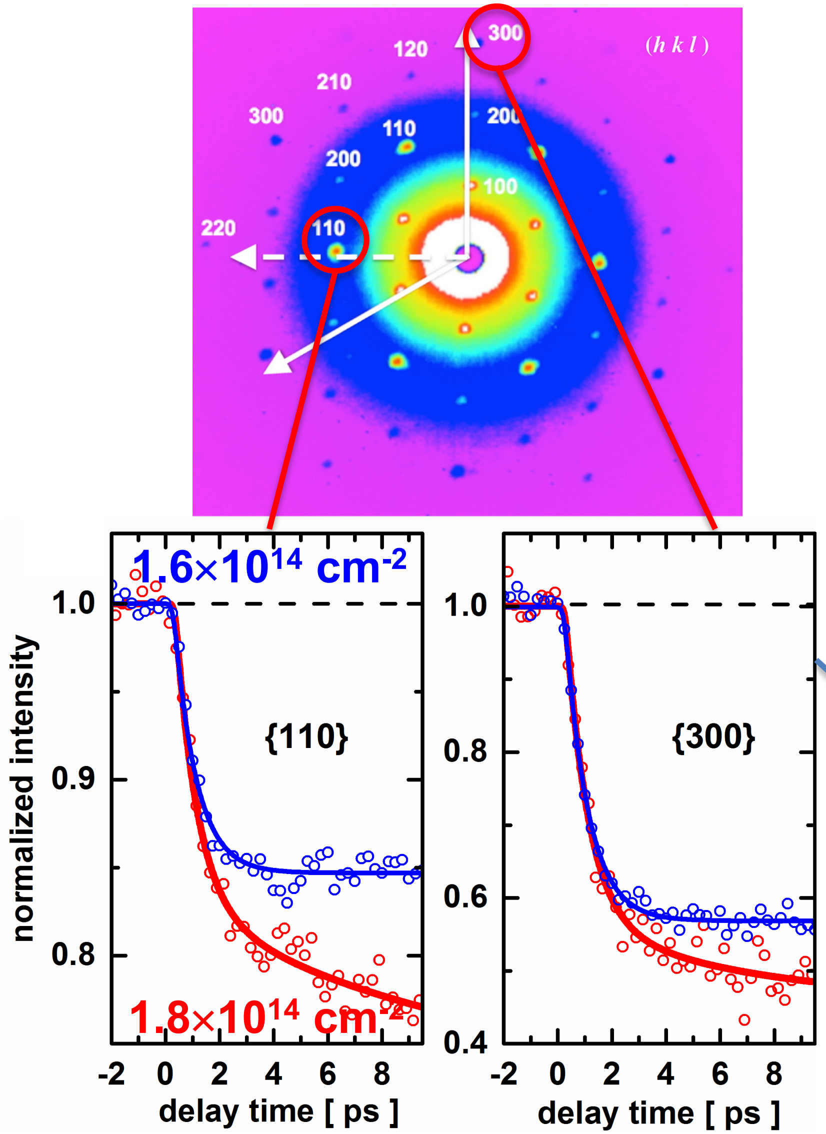

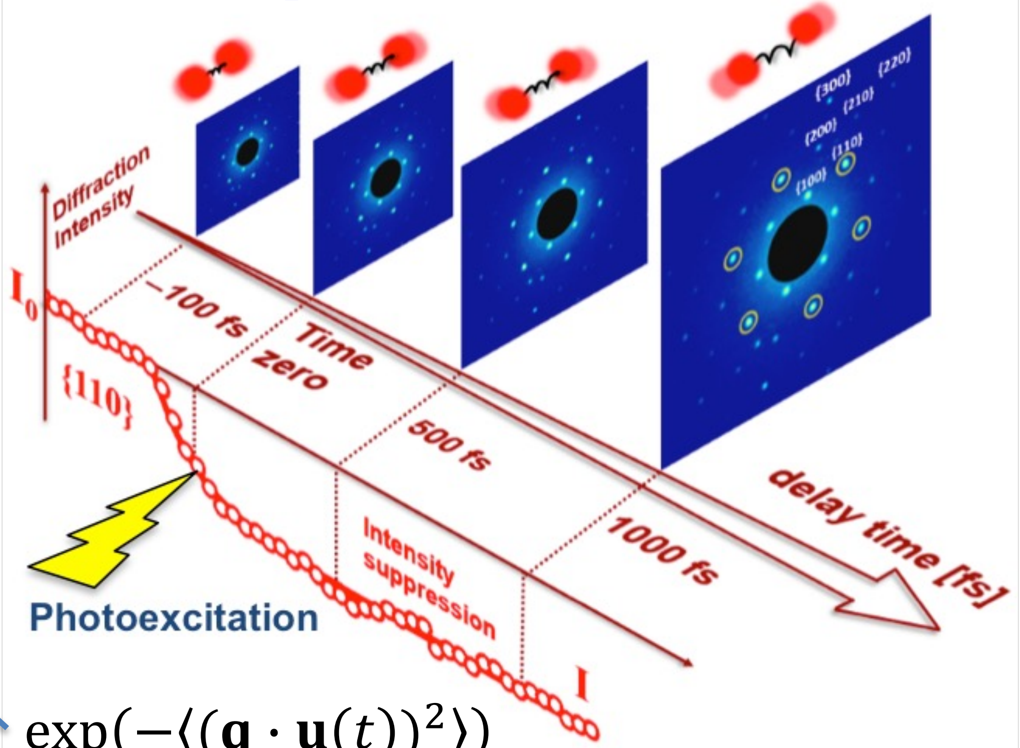

$$\exp(-\langle(\mathbf{q}\cdot\mathbf{u}(t))^2\rangle)$$

atomic displacement

- **Dynamics of Debye-Waller factor reveals rapid disordering for both {300} & {110} peaks**
- **Transition from mono- to bi-exponential decay at higher electron-hole density**

M.F. Lin *et al.*, *Nature Commun*. **8**, 1745 ('17)

Strong Electron-Lattice Coupling in $MoSe_2$

- **NAQMD simulations reproduce (1) rapid photo-induced lattice dynamics & (2) mono- to bi-exponential transition at higher electron-hole density**

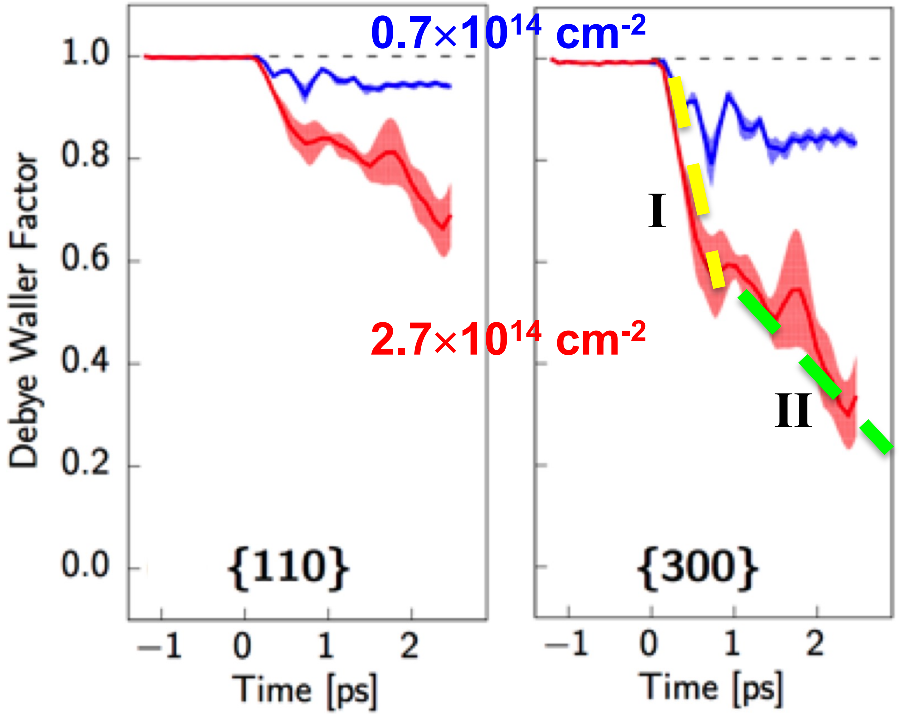

- **Rapid lattice dynamics is explained by the softening of M-point (1/2 0 0) phonon**
- **Bi-exponential transition is explained by the softening of additional phonon modes at higher electron-hole densities**

Lin *et al*., *Nature Commun*. **8**, 1745 ('17)
Bassman *et al*., *Nano Lett*. **18**, 4653 ('18)

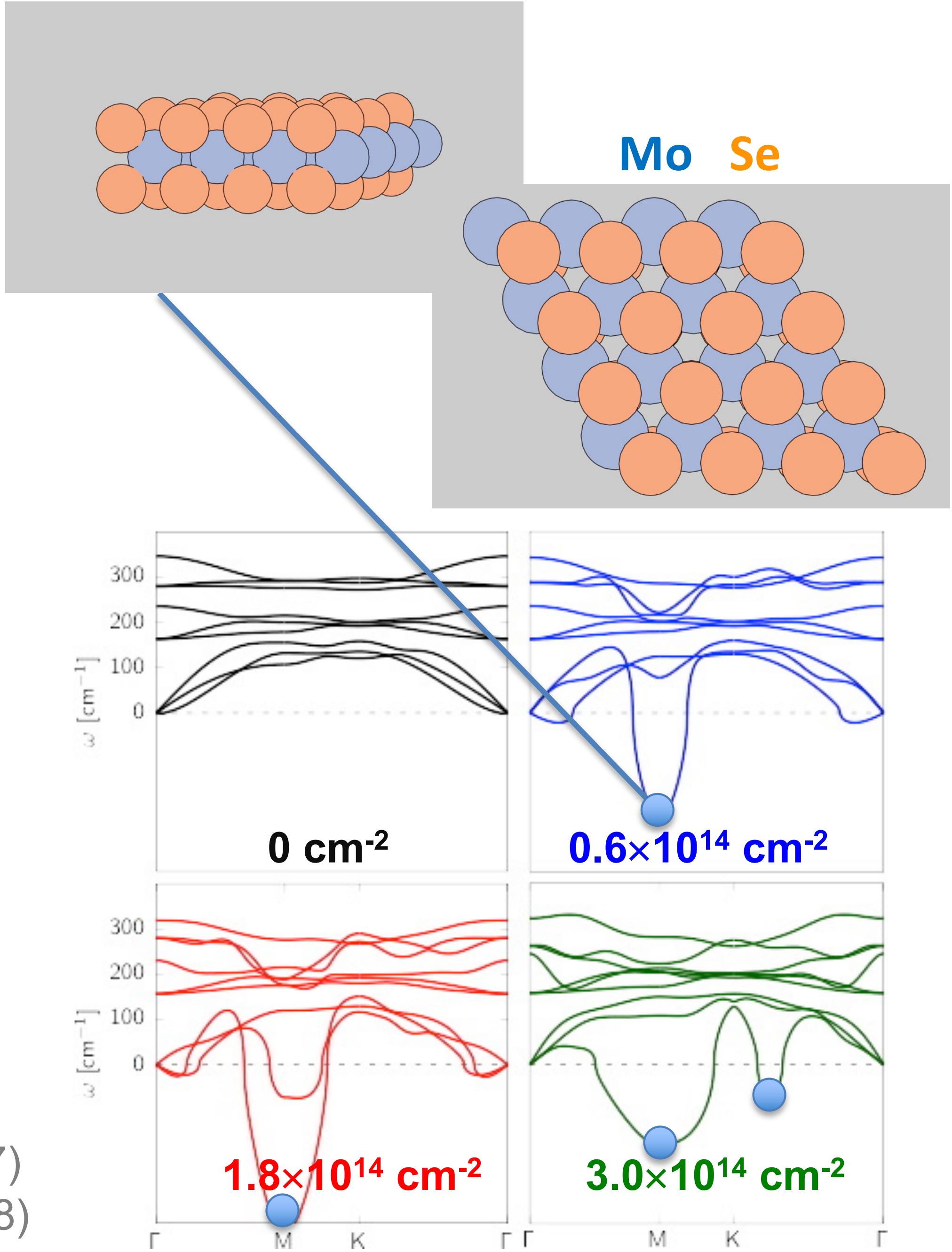

Electronic Origin of Phonon Softening

- Electronic Fermi surface for the electron-hole density *n*(e-h) ranging from 0.2 to 2×10^{14} cm^{-2}

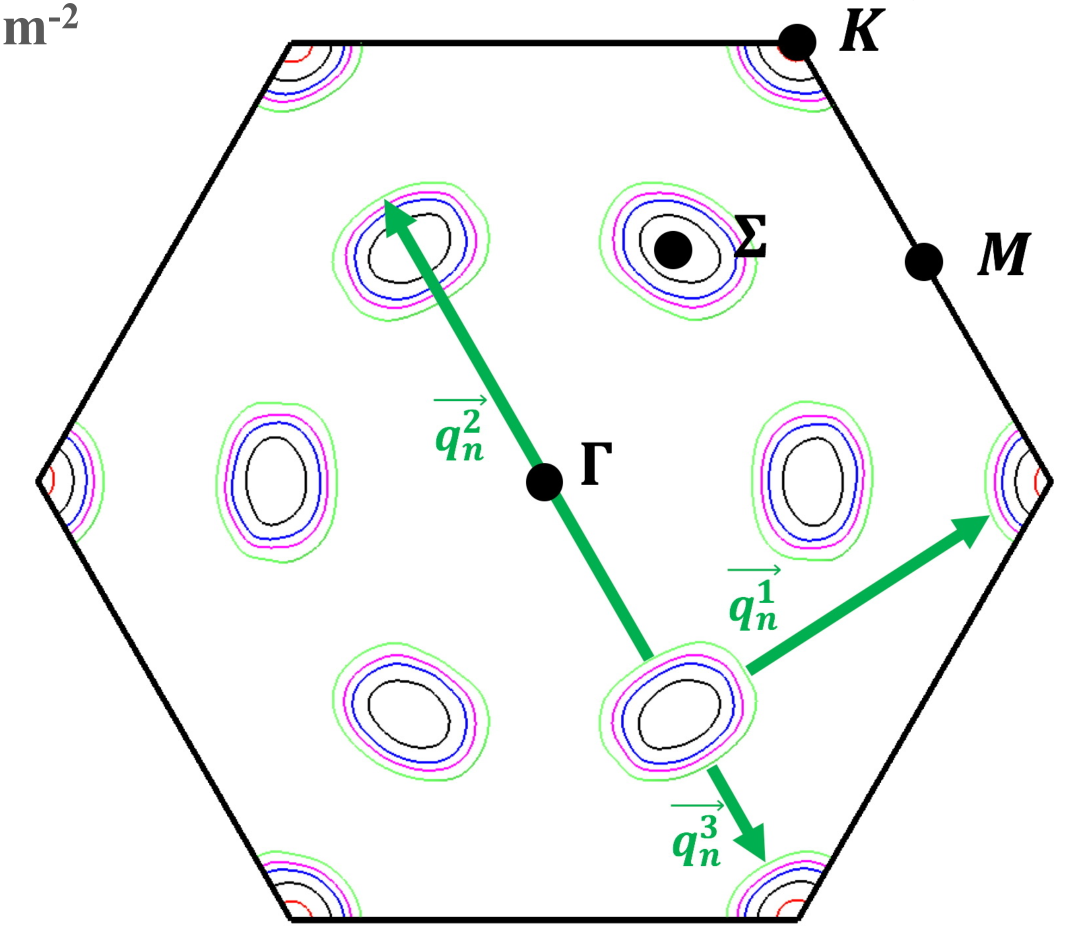

n(e-h) = 0.22, 1, 2, 3, 4 ×10^{14} cm^{-2}

- While the Fermi surface is localized at K-points at minimal excitation (red), it occupies Σ-pockets at larger *n*(e-h) (**black** & blue), enabling electron scattering by emitting $\vec{q}_n^1$ (**M**), $\vec{q}_n^2$ (**Σ**) and $\vec{q}_n^3$ (**K**) phonons

WSe$_2$ Monolayer on Al$_2$O$_3$ Substrate

- NAQMD simulation to study photoexcitation dynamics of WSe$_2$ monolayer on Al$_2$O$_3$ substrate

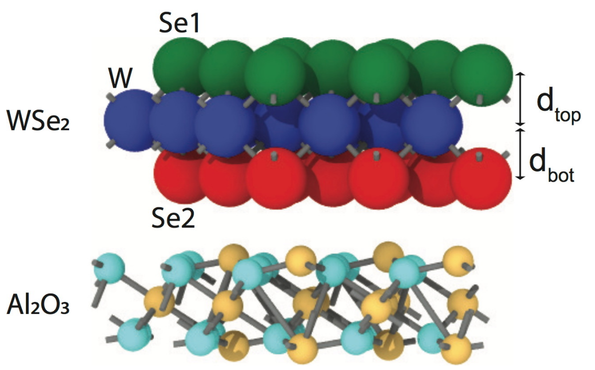

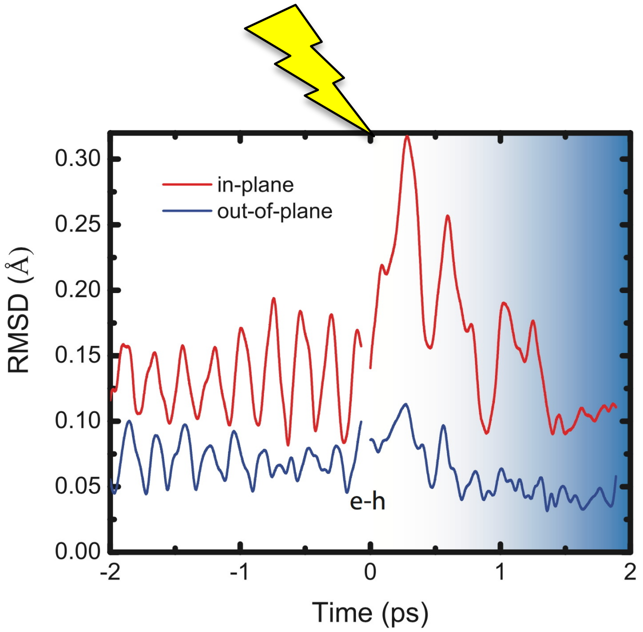

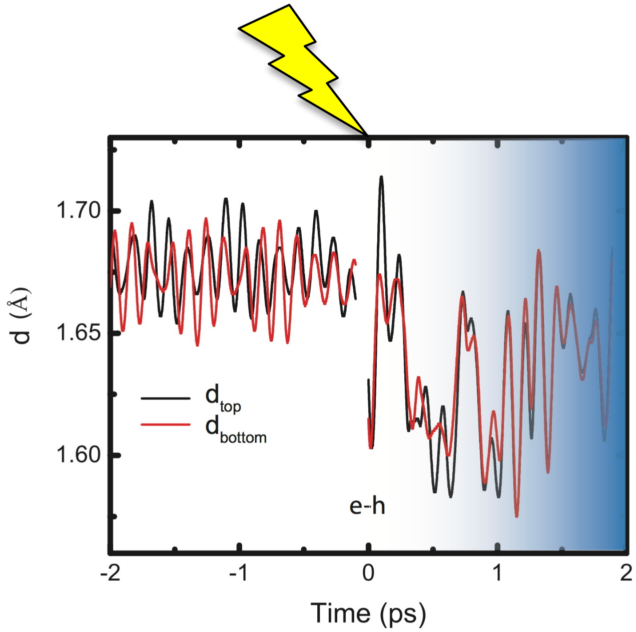

- Enhanced in-plane atomic displacements upon photoexcitation
- Photo-induced intralayer contraction of W-Se distances
- Good agreement with femtosecond surface X-ray scattering experiments at Stanford SLAC/LCLS

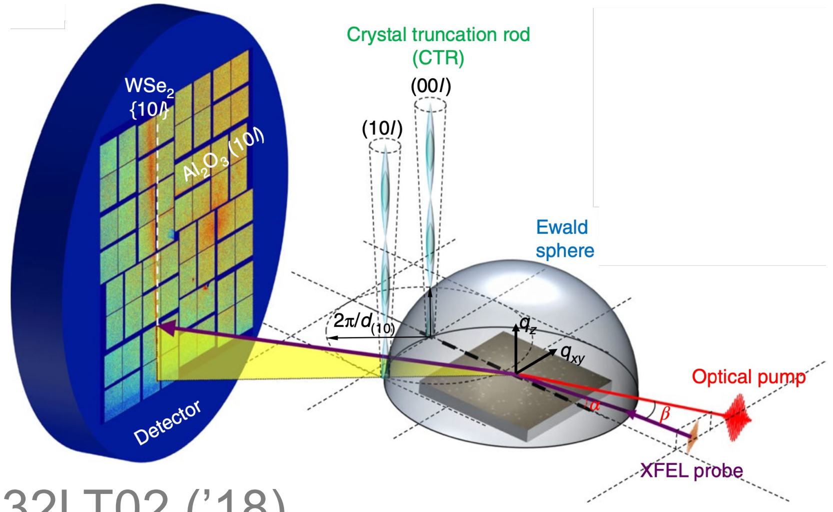

Tung *et al*., *Nature Photonics* **13**, 425 ('19);
Kumazoe *et al*., *J. Phys.: Condens. Matter* **30**, 32LT02 ('18)

Ferroelectric Opto-Topotronics

- **Quantized ferroelectric topology is protected against thermal noise → ultralow-power opto-electronics**

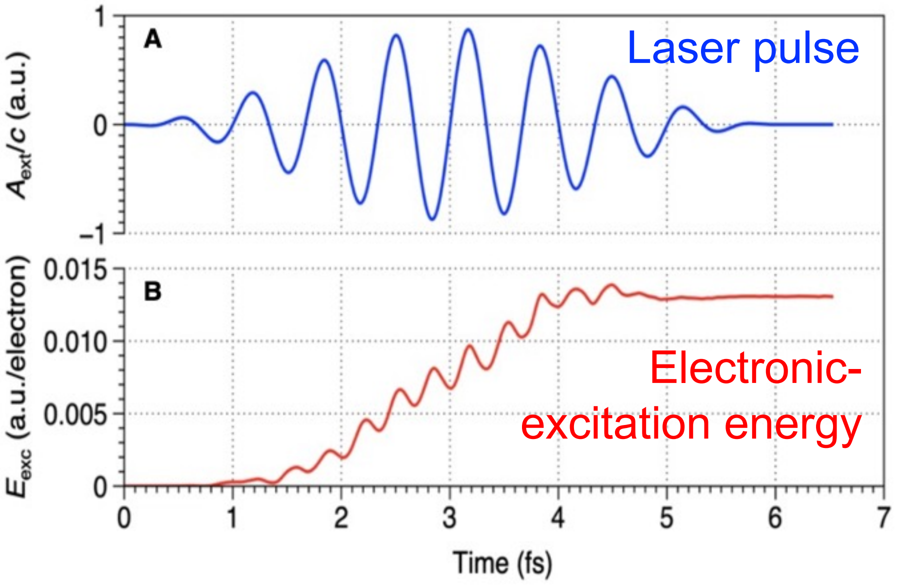

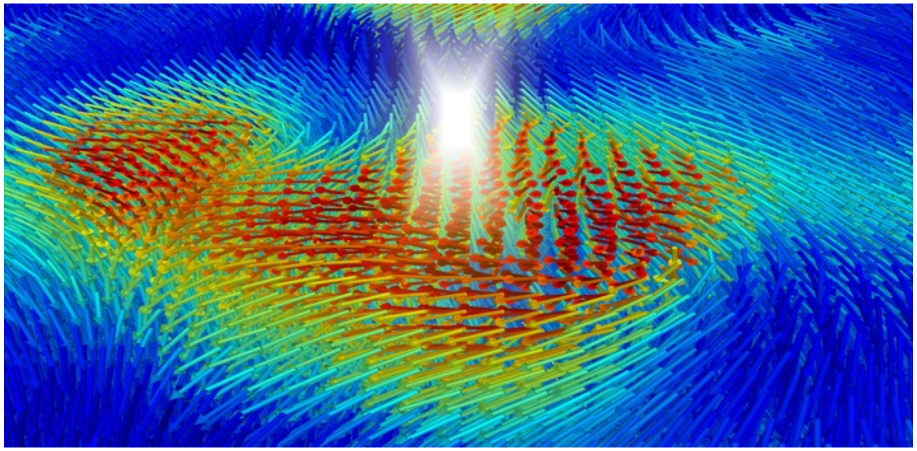

- **Ehrenfest NAQMD simulation of photoexcited $PbTiO_3$ shows rapid thermalization of electron excitation energy into Fermi distribution within a few femtoseconds**

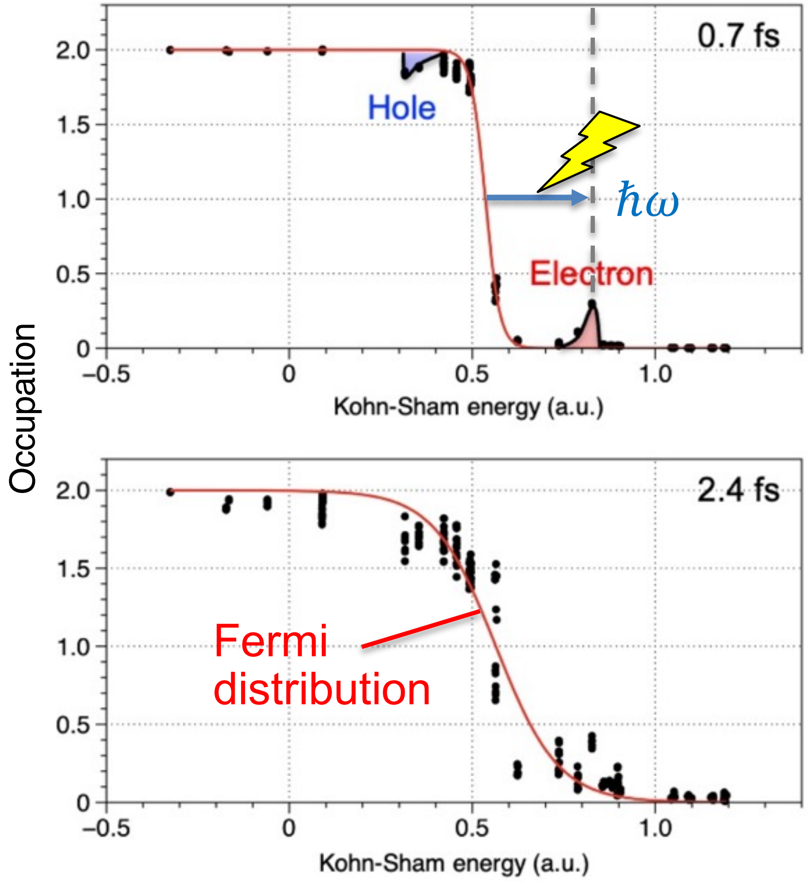

Linker *et al.*, *Science Adv.* **8**, eabk2625 ('22)

Photo-induced Matter

- **Surface-hopping & Fermi-temperature NAQMD simulations show the disappearance of a ferroelectric order parameter & emergence of a new rotational order parameter due to the excited-state energy landscape**

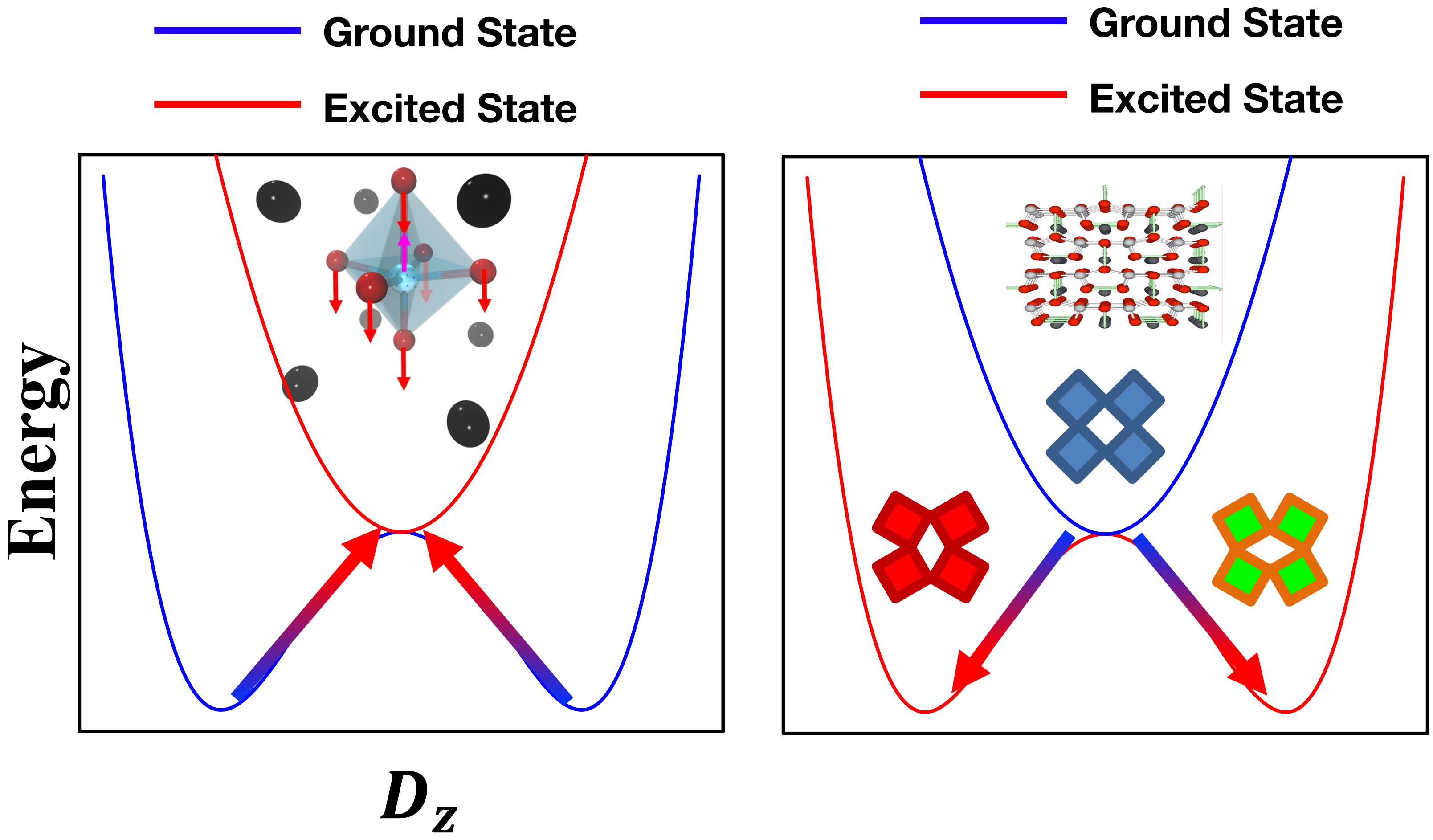

Linker *et al.*, *Science Adv.* **8**, eabk2625 ('22)

Multiscale Ferroelectric Opto-Topotronics

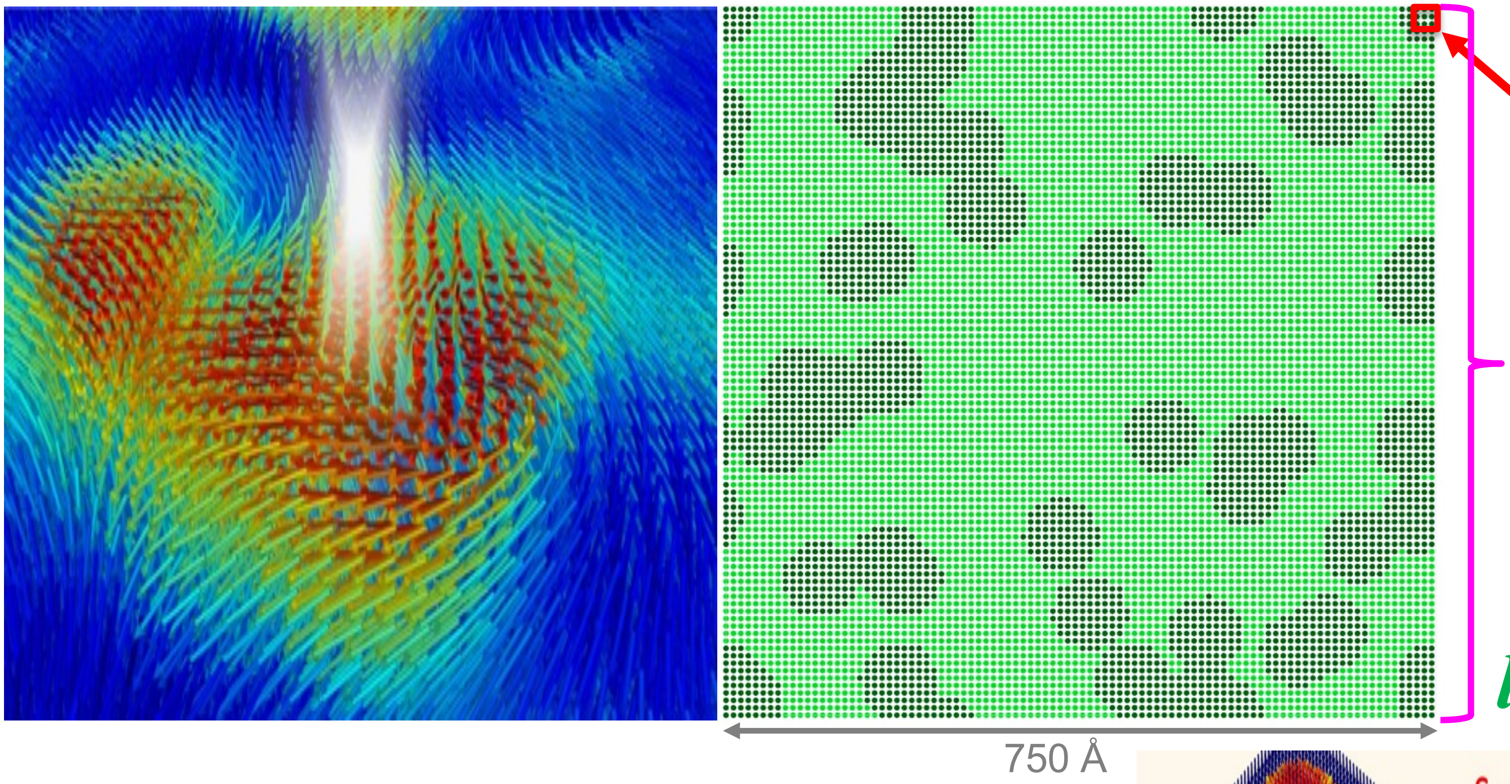

System size simulated with NAQMD

Large-scale structure simulated with NNQMD

ML for large scale!

- **Billion-atom neural-network quantum molecular dynamics (NNQMD) trained by NAQMD revealed photo-induced topological phase-transition dynamics (*cf*. Kibble-Zurek mechanism in cosmology)**
- **Symmetry-controlled skyrmion-to-skyrmionium* switching**

*Composite of skyrmions with opposite topological charges

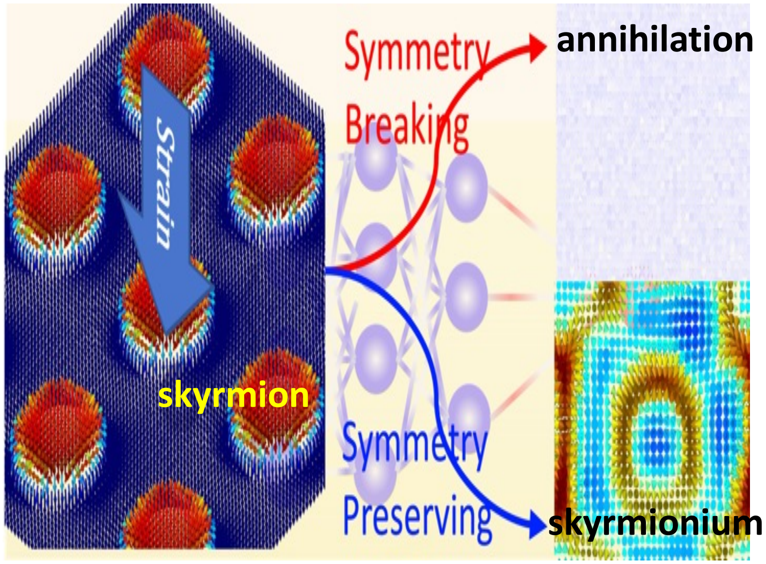

Linker *et al., Science Adv.* **8**, eabk2625 ('22);
JPCL **13**, 11335 ('22); *Nano Lett*. **23**, 7456 ('23)

Optical Retinal Neuron

- **Interplay between electronic band alignment & charge transfer rates of photoexcited carriers gives rise to intrinsic negative differential resistance (NDR) at a graphene/silicon interface under illumination, thus enabling oscillatory retinal neurons (ORN) to perform in-sensor image computing without external power in the era of ubiquitous AI in sustainable society**

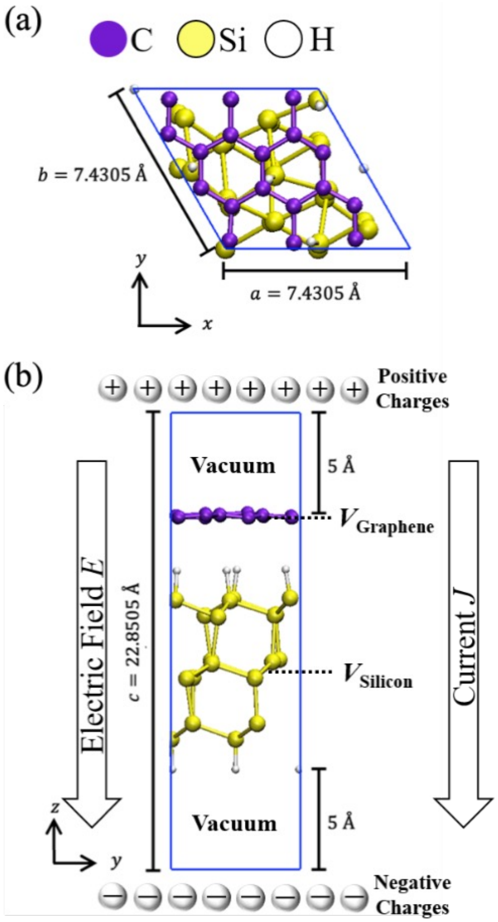

Hokyo *et al.*, *J. Phys. Chem. Lett*. **15**, 9226 ('24)

Photo-Induced NDR

- **NAQMD simulation of an electron-hole pair photoexcited in Si substrate exhibits nonlinear voltage dependence of electron & hole charge-transfer (CT) rates to graphene, which explains photoinduced NDR in experiments**

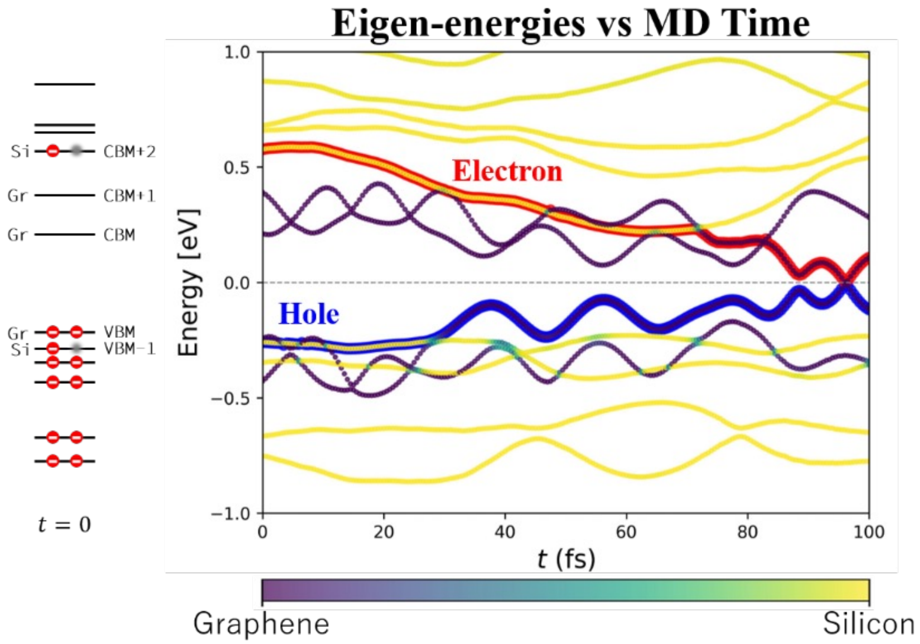
Eigen-energies vs MD Time

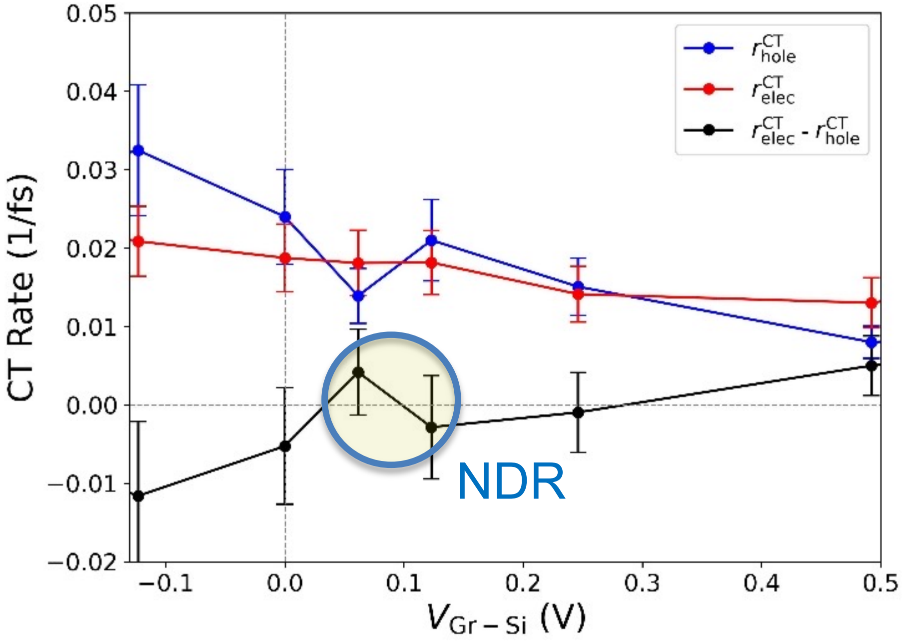

Hokyo *et al.*, *J. Phys. Chem. Lett*. **15**, 9226 ('24)

Laser-Driven Surface Chemistry

- **NAQMD simulation shows enhanced O-H breakage on a hydrogenated surface of a laser-ionized SiO_2 nanoparticle**

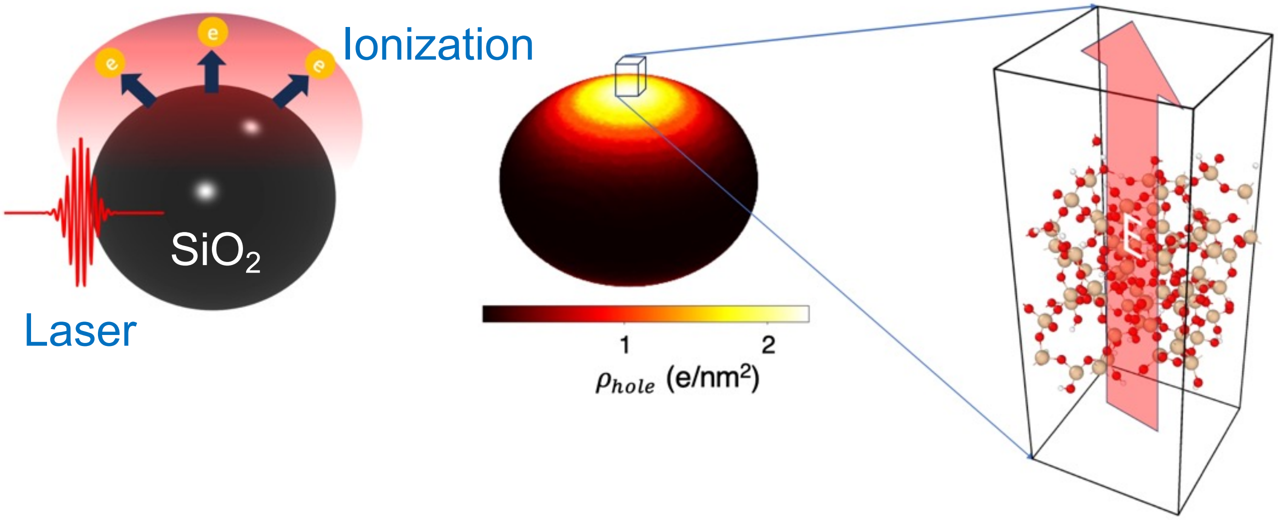

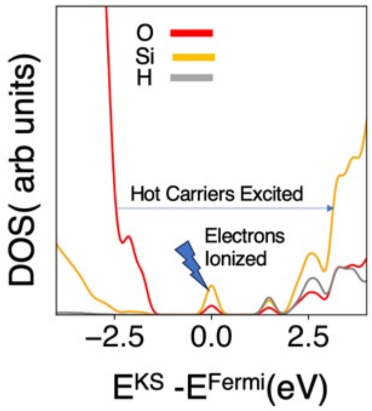

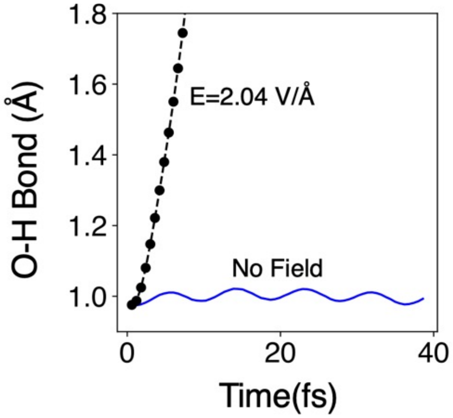

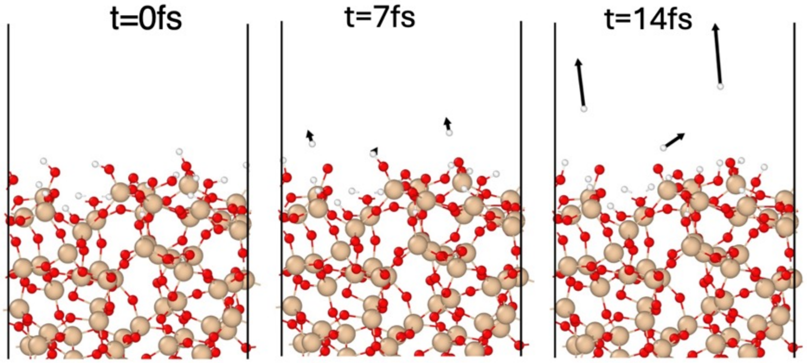

T. Linker *et al.*, *J. Am. Chem. Soc.*, **146**, 27563 ('24)

III. Advanced NAQMD

Many-Body Excited States

- **Surface-hopping NAQMD with adiabatic Kohn-Sham basis does not represent many-body excited states such as an exciton (*i.e.*, electron-hole pair bound by electrostatic attraction)**

- **Linear-response time-dependent density-functional theory (LR-TDDFT) obtains many-body electronic excition energies as poles of the frequency-dependent electron-hole-pair response function** [Casida, '95]

Excitonic Effects: LR-TDDFT

- **Excited electron-hole pairs within the linear-response time-dependent density functional theory (LR-TDDFT)**

$$\delta V(t) = \delta v_{kl\tau}(t)\hat{a}^{+}_{k\tau}\hat{a}_{l\tau} \longrightarrow \delta P_{ij\sigma}(t) = \delta\left\langle\Phi(t)\middle|\hat{a}^{+}_{i\sigma}\hat{a}_{j\sigma}\middle|\Phi(t)\right\rangle$$

$$\chi_{ij\sigma,kl\tau}(t-t') = \delta P_{ij\sigma}(t)/\delta v_{kl\tau}(t')$$

electron hole

- **Excitation energies from the poles of the response function $\chi_{ij\tau,kl\sigma}(\omega)$**

$2N_{\text{unoccupied}}N_{\text{occupied}} \times 2N_{\text{unoccupied}}N_{\text{occupied}}$ matrix eigenequation

$$\begin{pmatrix} \mathbf{A} & \mathbf{B} \\ \mathbf{B}^{*} & \mathbf{A}^{*} \end{pmatrix}\begin{pmatrix} \mathbf{X}_I \\ \mathbf{Y}_I \end{pmatrix} = \hbar\omega_I \begin{pmatrix} \mathbf{1} & \mathbf{0} \\ \mathbf{0} & \mathbf{-1} \end{pmatrix}\begin{pmatrix} \mathbf{X}_I \\ \mathbf{Y}_I \end{pmatrix}$$

I-th excitation energy

Kohn-Sham energy

$$A_{ia\sigma,jb\tau} = \delta_{\sigma,\tau}\delta_{i,j}\delta_{a,b}\left(\varepsilon_{a\sigma} - \varepsilon_{i\sigma}\right) + K_{ia\sigma,jb\tau} \qquad B_{ia\sigma,jb\tau} = K_{ia\sigma,bj\tau}$$

$$K_{ia\sigma,i'a'\sigma'} = \iint \psi^{*}_{i\sigma}(\mathbf{r})\psi_{a\sigma}(\mathbf{r})\left(\frac{e^2}{|\mathbf{r}-\mathbf{r}'|} + \frac{\delta^2 E_{\text{xc}}}{\delta\rho_\sigma(\mathbf{r})\delta\rho_{\sigma'}(\mathbf{r}')}\right)\psi_{i'\sigma'}(\mathbf{r}')\psi^{*}_{a'\sigma'}(\mathbf{r}')\,d\mathbf{r}\,d\mathbf{r}'$$

Coulomb & exchange-correlation interaction matrix elements

Electronic Excited States

- ***I*-th excited state**

$$\left|\Phi_I(\mathbf{r};\mathbf{R})\right\rangle = \sum_{i\in\{\mathrm{occupied}\}} \sum_{a\in\{\mathrm{unoccupied}\}} \sum_{\sigma} \sqrt{\frac{\varepsilon_{a\sigma}-\varepsilon_{i\sigma}}{\hbar\omega_I}} \left(X_{I,ia\sigma}+Y_{I,ia\sigma}\right) \hat{a}^{+}_{a\sigma}\hat{a}_{i\sigma}\left|\Phi_0(\mathbf{r};\mathbf{R})\right\rangle$$

electron-hole pair ground state

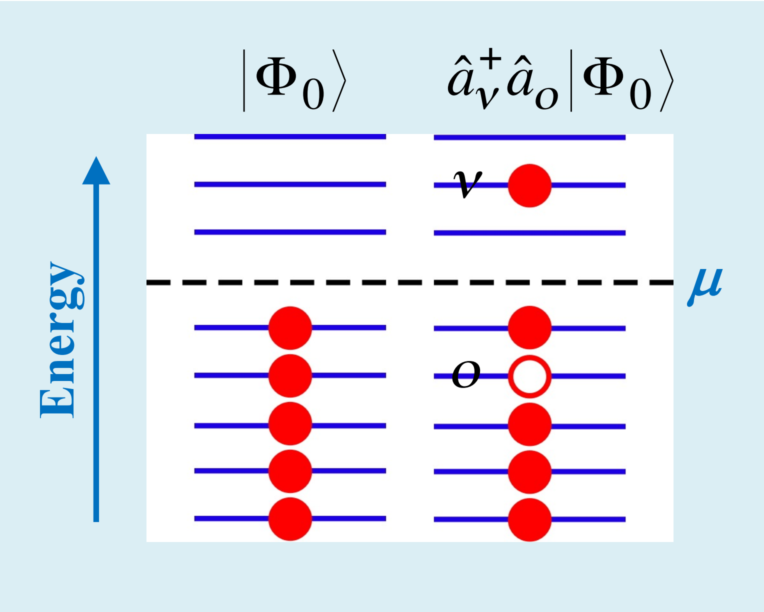

See notes on (1) general time-dependent perturbation, (2) density response with time-dependent Kohn-Sham basis, (3) Fourier transform of step function, (4) excitation energies by LR-TDDFT, (5) many-body wave function

Many-Body Effects: Excitons

- **Incorporating exact-exchange is indispensable for LR-TDDFT to describe $1/R$ binding energy of charge-transfer excitation (where electron moves from a donor to a spatially separated acceptor)**
- **Exchange integral is responsible for the $1/R$ attraction**

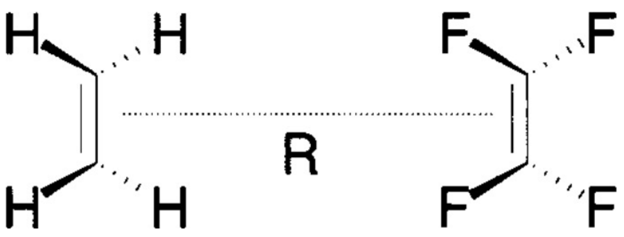

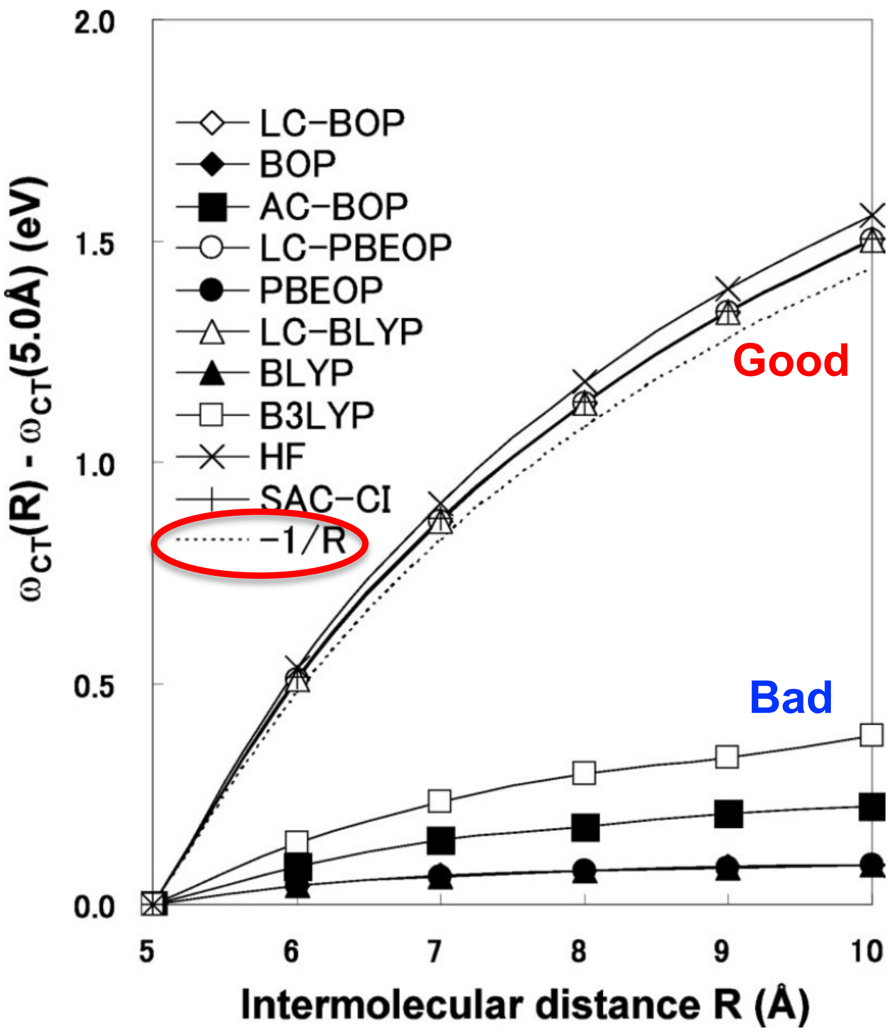

Dreuw *et al.*, *J. Chem. Phys*. **119**, 2943 ('03); Tawada *et al.*, *J. Chem. Phys*. **120**, 8425 ('04)

See notes on (1) range-separated exact-exchange functional,
(2) excited-state forces,* (3) excitation-energy balance sheet

* See Harris, *Phys. Rev. B* **31**, 1770 ('85); Foulkes & Haydock, *Phys. Rev. B* **39**, 12520 ('89)

Accelerating Exact-Exchange Computation

- **Exact-exchange computation is highly compute-intensive: $O(N^5)$**

$$(si|it) = \int d\mathbf{r}_1 \int d\mathbf{r}_2 \phi_s^*(\mathbf{r}_1)\phi_i(\mathbf{r}_1)|\mathbf{r}_1 - \mathbf{r}_2|^{-1}\phi_i^*(\mathbf{r}_2)\phi_t(\mathbf{r}_2)$$

- **Resolution-of-identity (ROI, closure by projection to a small augmenting basis set) or density-fitting approach reduces its computation to $O(N^4)$**

  Weigend, *Phys. Chem. Chem. Phys*. **4**, 4285 ('02)

$$(si|it) \cong \sum_{P,Q}(si|P)(P|Q)^{-1}(Q|it)$$

- **Adaptive compression (or low-rank tensor product) to reduce the complexity to near GGA-type computation?**

  Lin, *J. Chem. Theory Comput*. **12**, 2242 ('16)

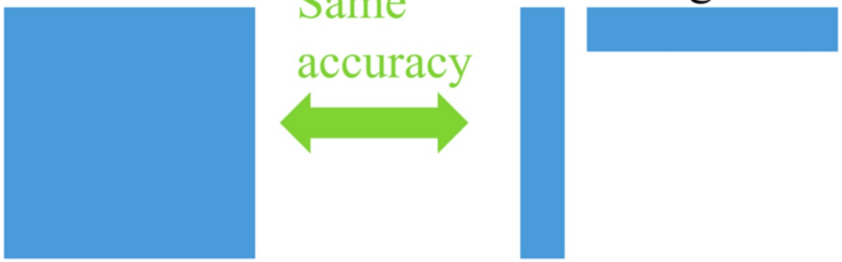

Uncompressed Exchange

Adaptively Compressed Exchange

Same accuracy

Full rank
Cost:
Hybrid ≫ GGA

Low rank
Cost:
Hybrid ≈ GGA

Application: Optical Absorption Spectrum

- **Oscillator strength calculated by the linear-response TDDFT**

I-th excitation energy

Poralizability:

$$\alpha(\omega) = \sum_I \frac{f_I}{\omega - \omega_I}$$

Oscillator strength:

$$f_I = \frac{2\omega_I}{3} \sum_{\alpha=x,y,z} |\langle 0|\hat{\alpha}|I\rangle|^2$$

I-th excited state

See 08Casida-TDDF-LR.pdf
& note on many-body wave function

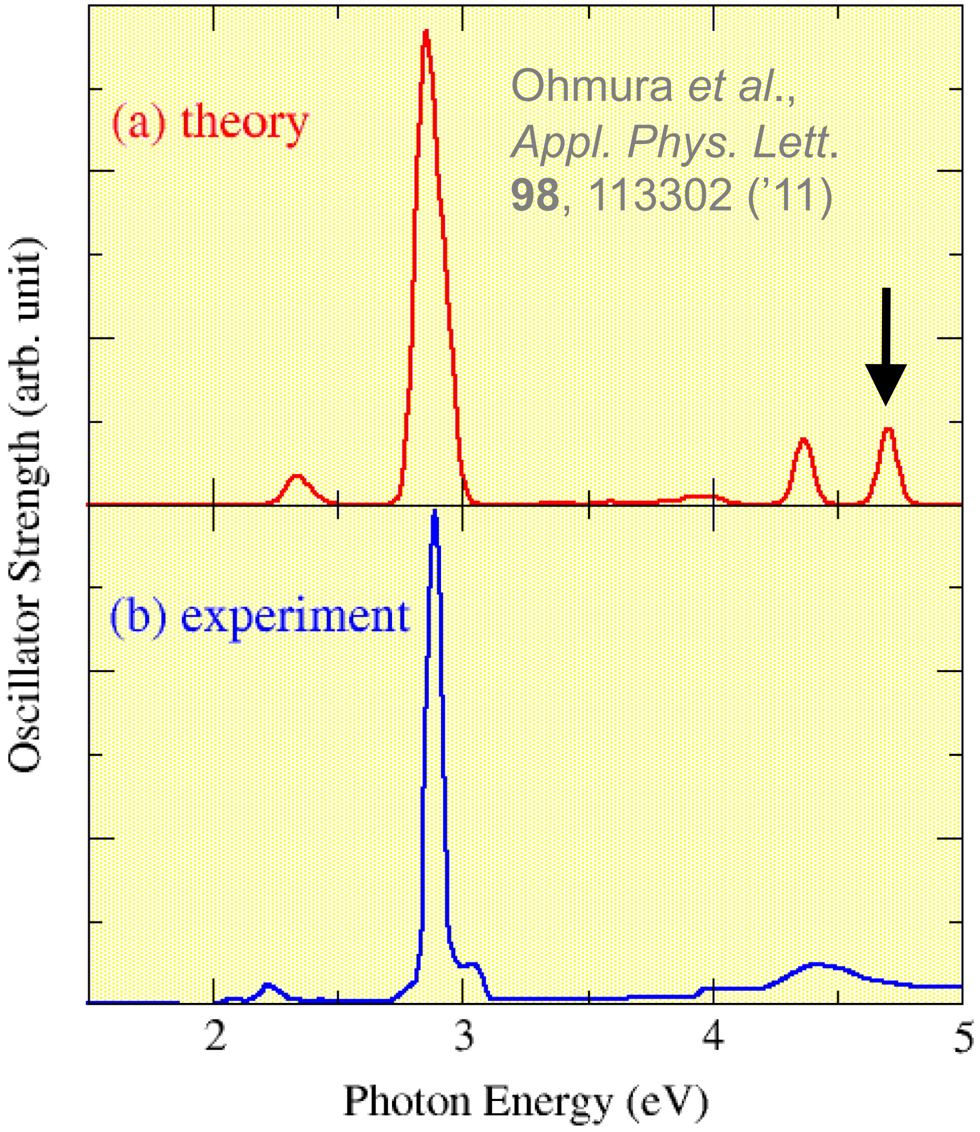

Ohmura *et al.*, *Appl. Phys. Lett.* **98**, 113302 ('11)

- **Excellent agreement with experimental data** [Akai *et al.*, '06]

Singlet Fission in Amorphous DPT

- **Photo-current doubling by splitting a singlet exciton into 2 triplet excitons**
- **Singlet fission (SF) in mass-produced disordered organic solid → efficient low-cost solar cells**
- **Exp'l breakthrough: SF found in amorphous diphenyl tetracene (DPT)**
- **Ultrafast transient absorption measurements identified *two time-scales* (1 & 100 ps) for exciton population dynamics**
- **Hypothesis: Existence of *SF hot spots*** [S. T. Roberts *et al.*, *JACS* **134**, 6388 ('12)]

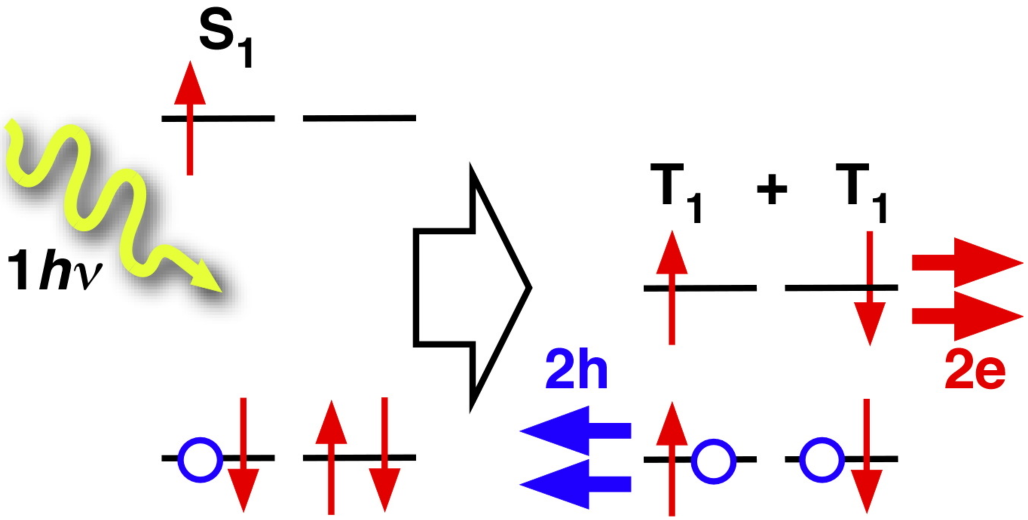

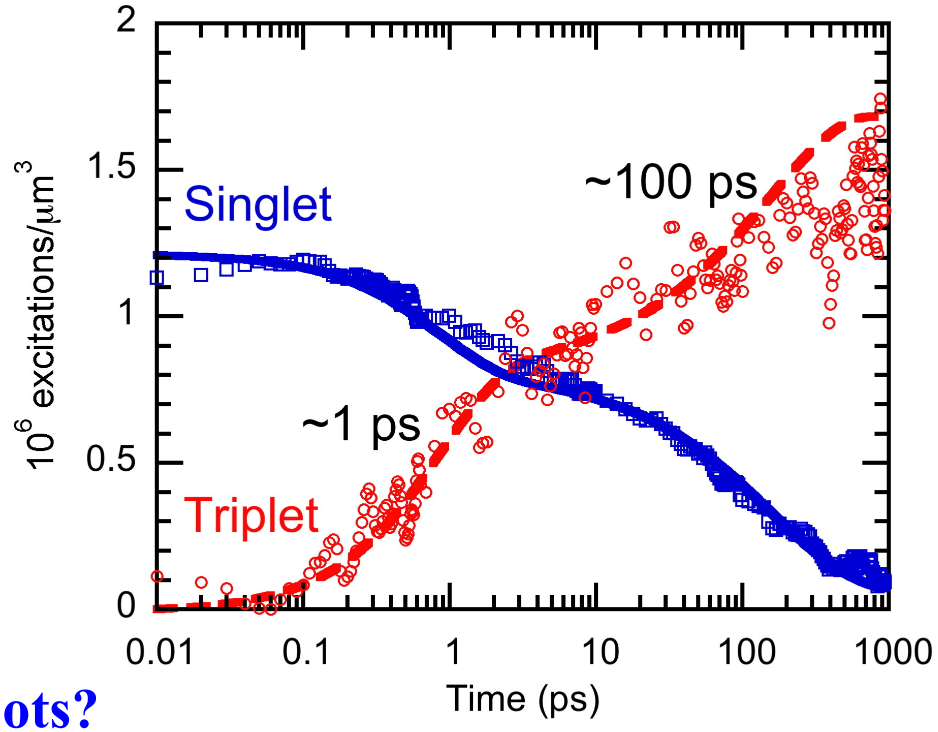

- **Problem: *Molecular origin* of SF hot spots?**

Singlet Fission in Amorphous DPT

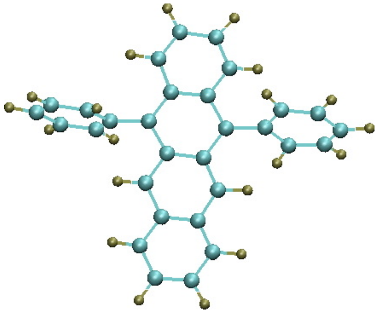

DPT molecule

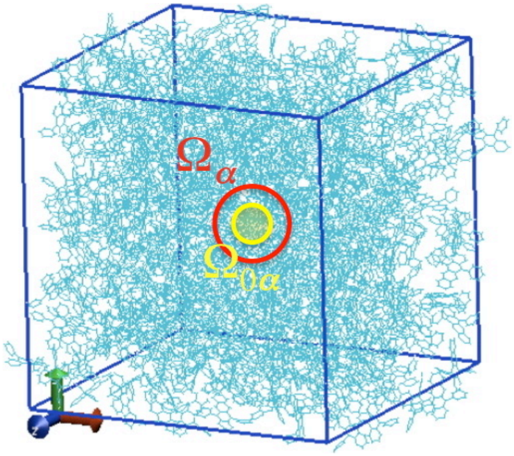

Amorphous DPT

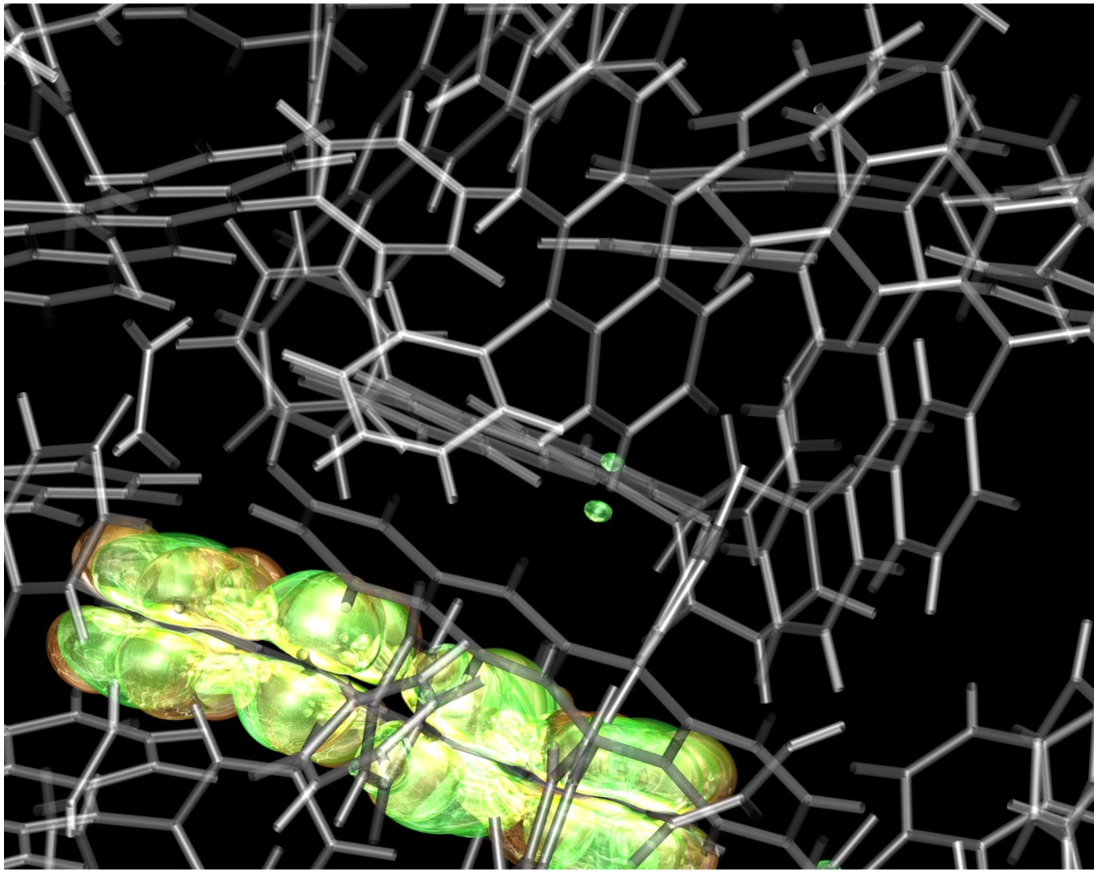

- **Divide-conquer-recombine nonadiabatic QMD (phonon-assisted exciton dynamics) + time-dependent perturbation theory (singlet-fission rate) + kinetic Monte Carlo calculations of exciton population dynamics in 6,400-atom amorphous DPT**

Divide-Conquer-Recombine Electronic Excitation

Divide **Conquer** **Recombine**

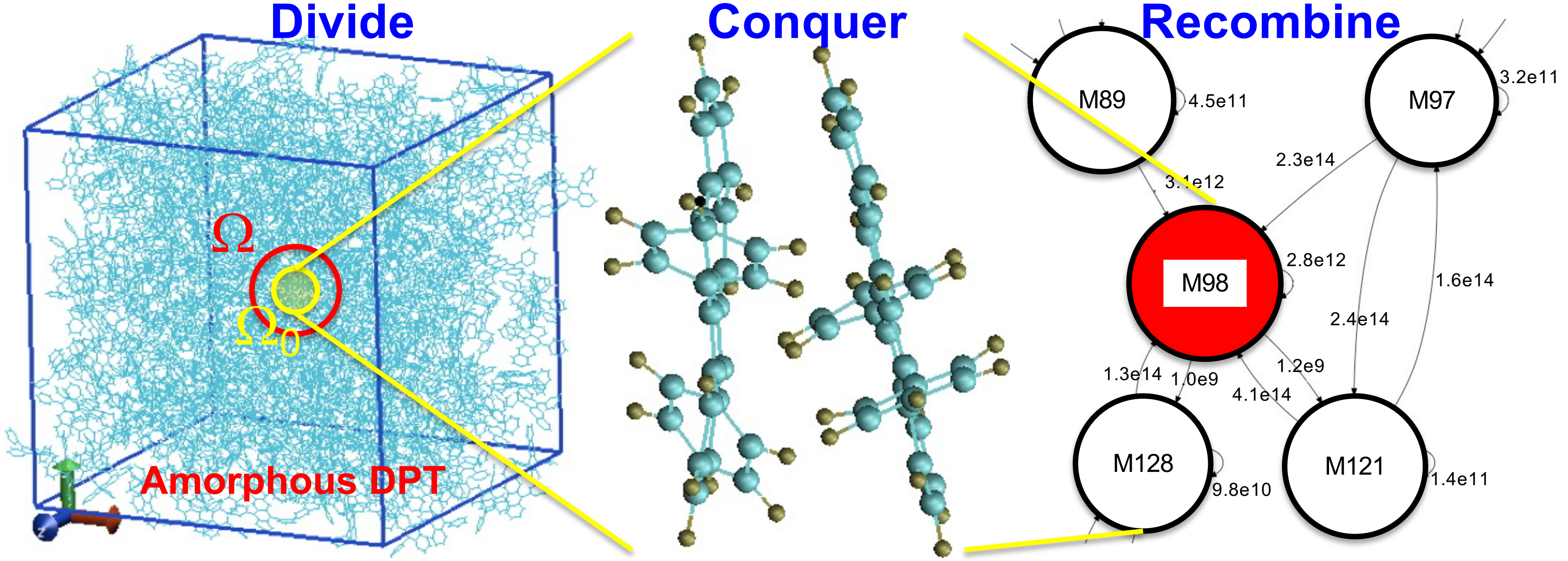

Molecular Dynamics **Quantum Molecular Dynamics** **Kinetic Monte Carlo**

Experimental Length & Time Scales

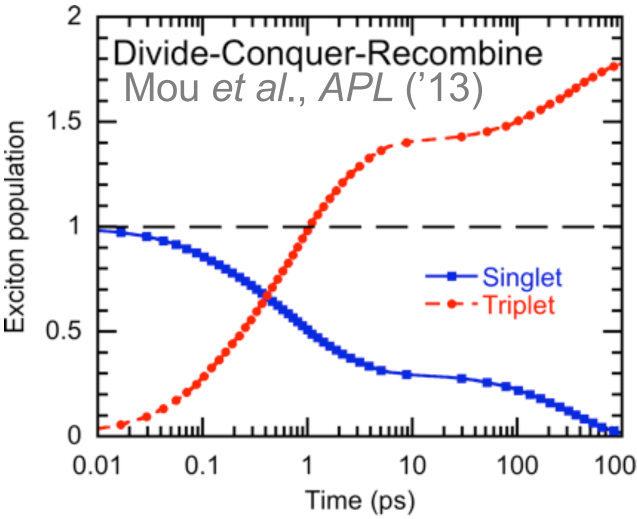

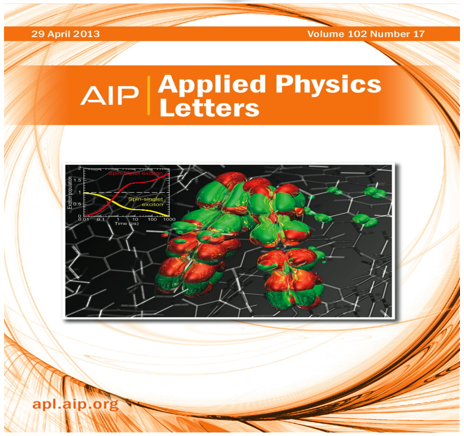
29 April 2013 Volume 102 Number 17

AIP Applied Physics Letters

apl.aip.org

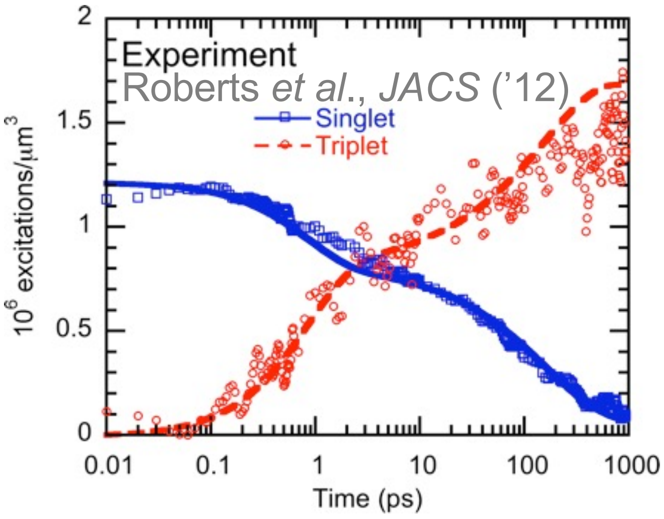

Singlet-Fission Hot Spot

- **Nonadiabatic quantum molecular dynamics simulations not only reproduced experimentally measured exciton population dynamics but also revealed unknown molecular geometry of singlet fission hot spots**

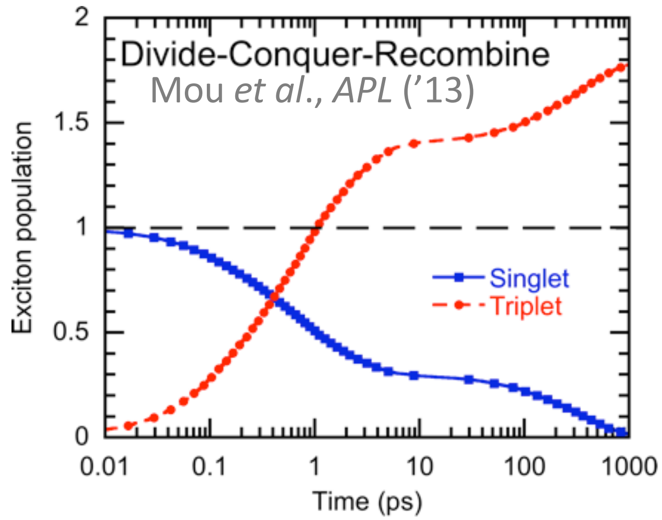

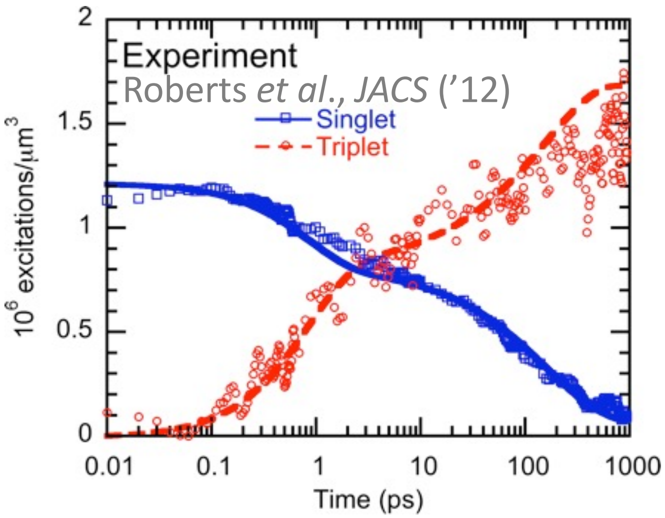

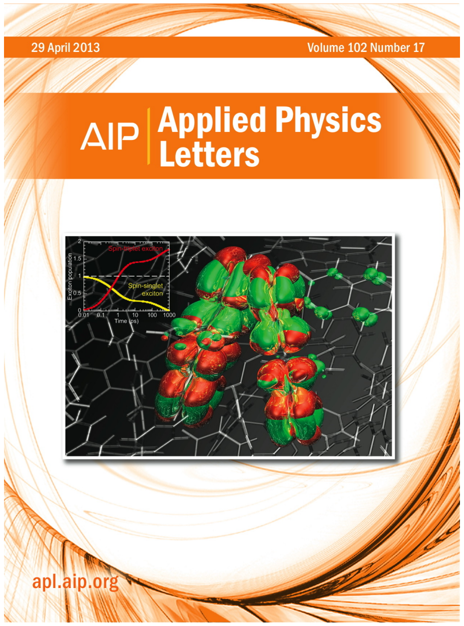

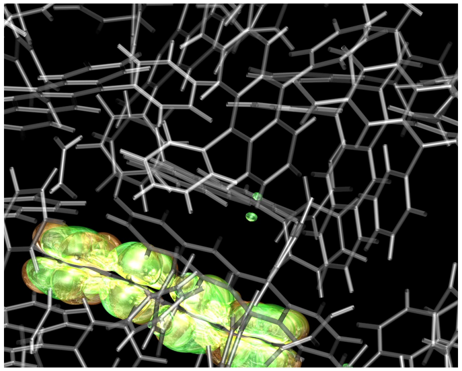

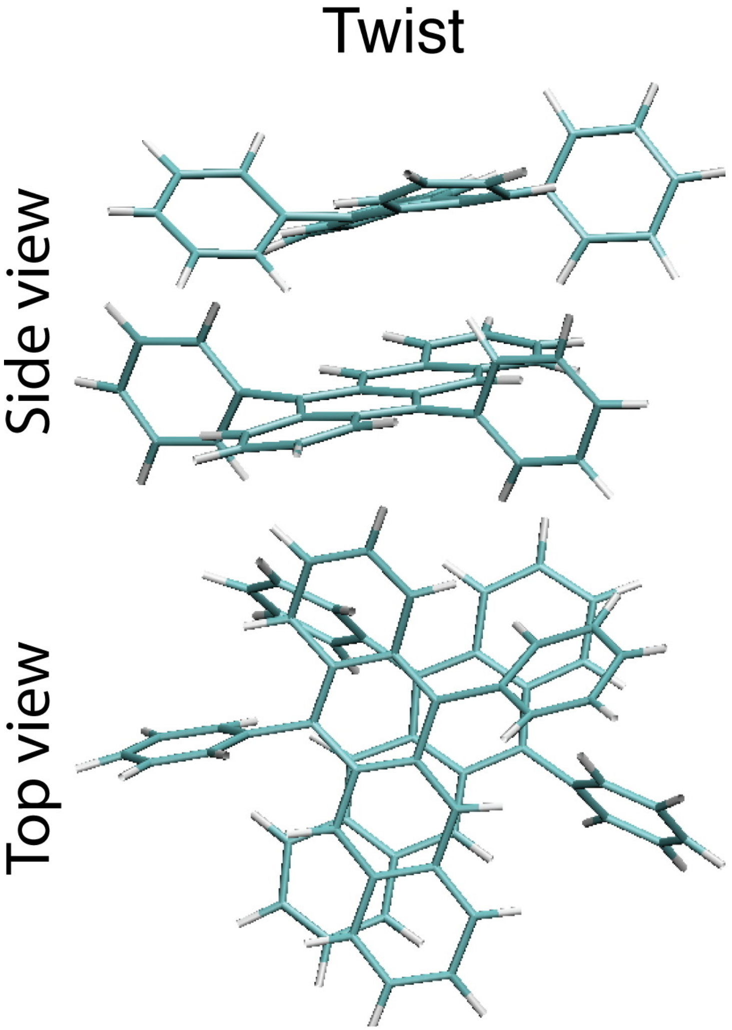

When To Use LR-TDDFT in QXMD

- **QXMD code can excite many independent electron-hole pairs to study high-fluence laser excitation (*e.g.*, laser-induced phase transition) — above the Mott-transition density of electron-hole pairs, they indeed dissociate into free electrons & holes** [Lin *et al*., *Nature Commun*. 8, 1745 ('17)]

Linker *et al., Science Adv.* **8**, eabk2625 ('22)

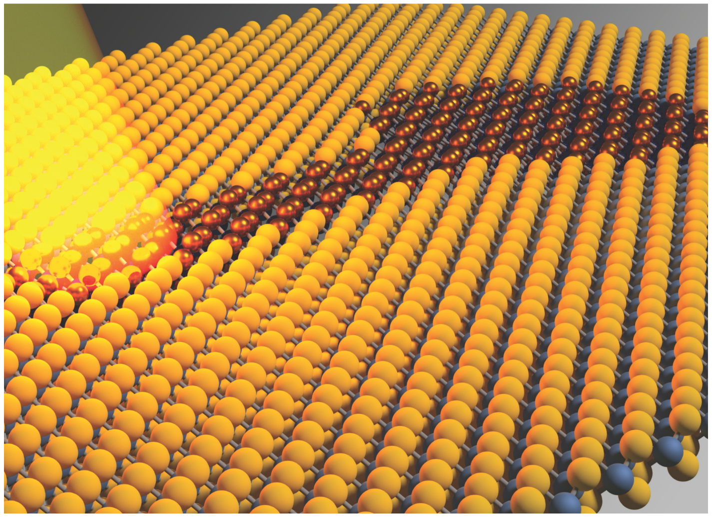

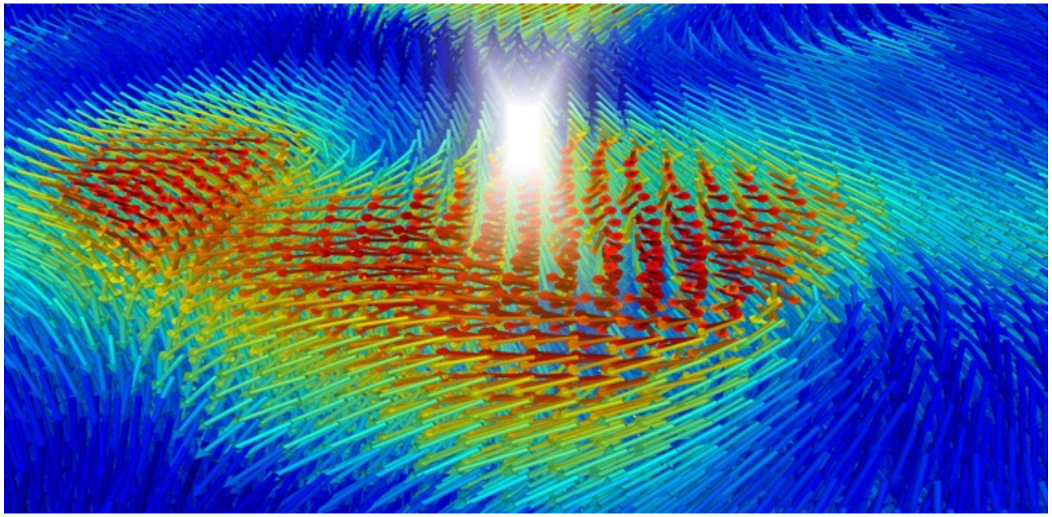

A. Krishnamoorthy *et al*., *Nanoscale* **10**, 2742 ('18); journal cover

- **QXMD uses LR-TDDFT to study excitonic effects for one electron-hole pair (divide-conquer-recombine approach to simulate many interacting electron-hole pairs is under construction)*** [Mou et al., *Appl. Phys. Lett*. **102**, 173301 ('13)]

* Higher-order correlations in xc kernels can describe exciton-exciton interactions [Nakano *et al*., *Phys. Rev. B* **39**, 4930 ('89); Turkowsky *et al*., *Phys. Rev. B* **89**, 075309 ('14)]

Caveat

- **Most TDDFT xc functionals cannot adequately describe certain phenomena like conical intersection**

Levine *et al*., *Mol. Phys*. **104**, 1039 ('06); Yang *et al*., *J. Phys. Chem. Lett*. **7**, 2407 ('16)

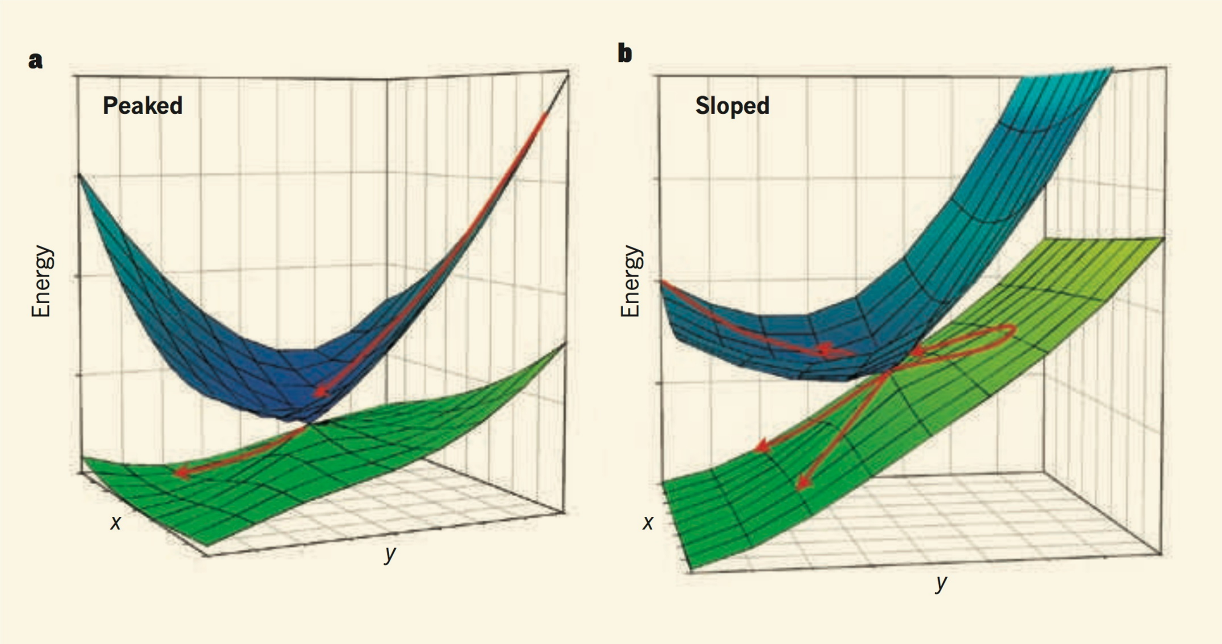

Martinez, *Nature* **467**, 412 ('10)